

**A First-Principles Investigation
on Substitutions in the Carbon
Allotropes Glitter and
Graphene**

GAEL BALDISSIN

A THESIS SUBMITTED IN PARTIAL FULFILLMENT OF THE REQUIREMENTS
OF THE DEGREE OF DOCTOR OF PHILOSOPHY

MATERIALS & PHYSICS RESEARCH CENTRE
SCHOOL OF COMPUTING, SCIENCE AND ENGINEERING
UNIVERSITY OF SALFORD

June 2013

To Prof. Igor L. Shabalin,
for his knowledge and creativity
in Materials Science.

Contents

1	Introduction	1
1.1	Carbon-based nets	2
1.2	Aim of this work	4
1.3	Overview of the thesis	4
2	Carbon-based materials	6
2.1	Heteroatom substitutions on selected nets	7
2.2	n-Diamond	9
2.2.1	Glitter	11
2.3	Graphene	14
2.3.1	Opening a bandgap	15
3	Theoretical background	19
3.1	Density functional theory	20
3.1.1	Electron density	22
3.1.2	Kohn-Sham equations	24
3.1.3	Exchange-correlation functional	25
3.1.4	Spin-dependent DFT	29
3.1.5	Plane-waves, pseudopotentials, and projector augmented waves	30
3.2	Cluster Expansion Hamiltonian: an Ising-like parametrisation	35
3.2.1	The Ising model	36
3.2.2	Lattice gas model	38
3.2.3	Original Connolly-Williams method	39
3.2.4	Cluster Expansion ansatz for multicomponent multi-sublattice systems	43
3.2.5	Validating the Cluster Expansion	44
3.2.6	Implementations	47

3.3	Lattice dynamics and structural stability	50
3.3.1	The harmonic approximation	50
3.3.2	Implementations of lattice dynamics	52
3.3.3	Structural stability	53
4	Glitter: a possible metastable carbon phase	57
4.1	Computational details	58
4.2	Instability of c-diamond-based structures	59
4.2.1	Models based on translation of the sublattice P1 to general position	60
4.2.2	Models with vacancies	61
4.2.3	Models with hydrogen inclusions	64
4.2.4	Summary of c-diamond-based structures: coordina- tion and hybridisation	68
4.3	Dynamical stability of glitter	68
4.4	Metallic nature of glitter	70
4.5	Bulk modulus of glitter	71
4.6	Isoglitter, hexagonite and trigo-hexagonite	72
4.7	Chapter conclusions	75
5	Boron, nitrogen, silicon substituted glitter	76
5.1	Computational details	77
5.2	Binary systems: C-B, C-N and C-Si glitter	77
5.3	Ground states of multi-substitutional system	81
5.3.1	Mechanical and electronic properties	87
5.4	Chapter conclusions	93
6	Boron-substituted graphene	95
6.1	Computational details	96
6.2	Boron doping in the low concentration limit	97
6.3	Graphene: stoichiometric boron substitutions	99
6.3.1	Determination of the Cluster Expansion	99

6.3.2	Electronic properties	106
6.4	Double-layered boron-substituted graphene	110
6.5	Chapter conclusions	115
7	General discussion and conclusions	117
7.1	On the methodology	118
7.2	Outlook	119
	List of Publications	119
	Bibliography	126

List of Figures

2.1	1,4-Cyclohexadiene	11
2.2	Glitter structure	12
2.3	Glitter supercell	13
2.4	Graphical representation of graphene	14
2.5	Band structure around the k point in graphene	15
3.1	Schematic illustration of the pseudopotential idea	32
3.2	Lattice gas model	39
3.3	Cluster figures on a fcc lattice	41
3.4	Schematic ground state representation	46
3.5	Representation of stable, unstable, indifferent equilibrium	54
3.6	Illustration of stable, metastable and unstable atomic arrangements	55
4.1	Conventional representation of cubic diamond	59
4.2	Atomic force modulus calculated for Wen's model and Hirai's models	61
4.3	Phonon dispersion of fcc model and defective diamond	63
4.4	Defective diamond model	64
4.5	Hydrogen-doped model	66
4.6	Phonon partial density of states of H-diamond	67
4.7	Phonon dispersion of glitter	69
4.8	Electronic structure of glitter	71
4.9	Comparison of compressibility of diamond and glitter	72
4.10	Isoglitter, exagonite, trigoexagonite	73
4.11	Phonon density of states of isoglitter, hexagonite, trigohexagonite	74
5.1	Formation energy for binary glitter systems	79

LIST OF FIGURES

5.2	Parent lattices for multisubstitutional systems	82
5.3	Tetragonal representation of CBN ground state	85
5.4	SiCN ₂ B ₂ ground state	87
5.5	Phonon dispersion of CBN ground state	89
5.6	Phonon dispersion of SiBN ground state	90
5.7	Phonon dispersion of SiCN ₂ B ₂ ground state	91
5.8	Band structure of CNB ground state	92
6.1	Energy of a cell containing 2 boron atoms in a honeycomb lattice of 200 atoms	98
6.2	Convex hull of B-C honeycomb layer	102
6.3	Boron graphene: low energy structures	103
6.4	Phonon dispersion and electronic band structure of BC ₃ -II . .	109
6.5	Phonon dispersion and electronic band structure of BC ₅ -I . . .	109
6.6	Double layer B-graphene: dl-BC ₃ -I	111
6.7	Phonon dispersion and electronic band structure of dl-BC ₃ -I .	114

List of Tables

3.1	Density functional theory: number of publications	20
3.2	Cluster correlation functions	42
4.1	Carbon glitter: lattice parameters and formation energy	70
5.1	Formation energies of substituted glitter ground states	84
5.2	Cell parameters of low energy glitter-like structures	86
5.3	Atomic positions in CBN, SiBN and CSiB ₂ N ₂	86
5.4	Bulk modulus and mass density of substituted glitter ground states	88
5.5	Bandgap energies of substituted glitter ground states	88
6.1	Formation energy of low energy structures of the B-graphene system	105
6.2	Bandgap of single-layer and bi-layer B-graphene compounds	106

Acknowledgements

Funding from UK EPSRC for provision of Doctoral Training Award is gratefully acknowledged.

UK Car-Parinello Consortium (UKCP) and the computational facility High End Computing Terascale Resources (HECToR) are kindly acknowledged for the computational time, employed for calculations on B-Graphene.

Prof. Keith Ross, Prof. Alan Oates, Prof. Ian Morrison and Prof. Neil Boag are acknowledged for useful discussions. I am grateful to Prof. Igor Shabalin for sharing with me his ideas. A special thank to Dr. Daniel Bull for his supervision on this work and on Li-N-H materials.

I thank the other members of the research group at Salford University for their support.

Declaration

The work here presented is the original research of the author. This thesis is based on the research carried out under the supervision of Dr. Daniel J. Bull, in the Materials & Physics Research Centre, University of Salford, United Kingdom. No part of this thesis has been submitted for any other degree or qualification.

Abstract

In the literature, a number of syntheses of carbon materials under extreme condition exhibit the presence of a carbon phase, called n-diamond, whose crystal structure remains unclear. Several crystallographic arrangements have been proposed, which are critically assessed in this work with regards to dynamical stability. It is shown that tetragonal carbon (glitter) is the only structure that satisfies this criterion. Glitter is a metallic 3-, 4-connected allotrope containing 1,4-cyclohexadieneoid units, giving a high energy metastable phase. Applying a fully first principles approach, which couples density functional theory (DFT) calculations and Ising-like parameterisation, the possibility of stabilising the structure with nitrogen, boron and silicon substitutions has been investigated, finding that there are arrangements with negative formation energy. These novel arrangements have been tested for vibrational stability, whereby it has been proven that they are dynamically stable. Moreover a bandgap opens, leading to semiconductor bulk materials based on Si, C, B and N.

Graphene, a carbon allotrope having the so-called chicken-net structure, is a zero-bandgap semiconductor, which make it promising for nano-electronic applications. However tuning and modifying the bandgap would expand the range of possible applications, in particular for post-silicon transistors. The effect of B substitutions in the graphene lattice has been studied, in terms of stability and electronic structure. The doping at low B concentration has been studied with a direct DFT approach while the effect at higher concentration has been studied with the above-mentioned coupled approach. Novel arrangements, that have semiconductor behaviour, have been proven to be dynamically stable at 0 K. The effect of a second B-C layer has also been investigated, finding that is effective on bandgap tuning.

Chapter 1

Introduction

In computational materials science, first principles methods allow the calculation of physical properties of materials without the aid of experimental inputs [1]. The advances in algorithms, increased computational power and improvements in the fundamental understanding of condensed-matter physics have made computing based on first principles a powerful tool for crystal structure prediction [2]. The lack of connection with any specific experiment is the intrinsic strength of this approach, which guaranties flexibility and generality in its applications.

Advances in materials science are severely limited by the available materials. Design, synthesis and mass-production of a novel material can be a costly and lengthy process. Identifying the appropriate material for a specific purpose and finding the synthesis route are usually the bottleneck of this process. Computational materials science can help, both in driving the search and in gaining a better understanding on how materials form and react.

In an excellent review, Ceder showed the contribution of *in silico* methods to the design of Li battery materials [3], indicating in the scalability the main advantage of first principles approach. The study of many other systems has been positively affected by the impact of computational methods where predictions have been confirmed experimentally, for instance high pressure phases of Si [4], oxygen ordering in $\text{YBa}_2\text{Cu}_3\text{O}_{6+x}$ [5], surface ordering of III-IV semiconductors [6].

The work presented in this thesis is an attempt to predict the stability

and properties of metastable carbon phases and substituted carbon nets. The theoretical foundations of this work lie in parametrisation of the Hamiltonian employed for structural prediction and on lattice dynamics, as a theoretical tool to test structural stability.

1.1 Carbon-based nets

Carbon is at the cutting edge of technological innovation, driven by its propensity to form different allotropes and to form compounds with many elements.

At ambient conditions, graphite and diamond have comparable formation energies: hexagonal graphite is more stable by ~ 0.03 eV/atom. Having the capability to form various types of chemical bonds with comparable formation energies, carbon can potentially form various allotropes.

The two best-known allotropes, diamond and graphite, have bulk mechanical and electrical properties that could hardly be more different: diamond is the hardest known natural material and is an electrical insulator (or wide band gap semiconductor depending on the crystallographic defects) whilst graphite is an important dry lubricant exhibiting metallic behaviour.

Diamond and graphite are distinguished by the electron hybridisation of carbon atoms: sp^3 and sp^2 , respectively. If carbon is hybridised sp^1 , it is suggested to form linear acetylenic carbon, also called carbyne, whose existence is still controversial [7].

The discovery and synthesis of fullerenes [8], nanotubes [9] and graphene [10] have revolutionised the material science of carbon. Back in 1947, Wallace predicted that graphene would have extraordinary electronic properties, if isolated [11]. Graphene is a carbon allotrope having atoms arranged in a 2-dimensional honeycomb lattice. For years, graphene was considered an academic oddity that existed only in theory and presumed not to exist as a free standing material. Since Novoselov et al. reported the effect of an electric field on synthesised samples of graphene [12], a wide range of opportunities

opened up for novel applications in nano-electronics and photovoltaics. In 2010, “for groundbreaking experiments regarding the two-dimensional material graphene” Andre Geim and Konstantin Novoselov of the University of Manchester were awarded the Nobel Prize in Physics [13].

Several works focus on the properties of new possible carbon forms with co-existing sp^2 and sp^3 hybridisation, including fullerene polymers, nanotube assemblies, diamond-like crystallites, vacancies in graphite, nanofoams and diamond-graphite hybrids [14, 15, 16, 17, 18, 19, 20]. These novel structural arrangements are reported to be kinetically stabilised and, thus, may have the possibility to be formed experimentally as metastable phases; if this is the case, they are predicted to show a range of interesting properties, both from scientific and technological perspectives. To the author’s knowledge, only nano-forms of diamond-graphite hybrids, namely diamond-graphite nanowires [21] and diamond-graphite nanoflakes [22, 23] have been reported, both forms existing as composite structures with a clear phase separation of the diamond-like and graphite-like regions.

In 1994 Bucknum and Hoffmann [24] proposed “glitter” as a potential allotrope of carbon on the basis of chemical intuition. The carbon network is a graphite-diamond hybrid in terms of connectivity and density. Bucknum et al. [25] proposed that glitter is consistent with n-diamond, a phase related to carbon under extreme conditions [26]. To this day, the crystal structure of n-diamond remains unclear.

Instead of modifying the topology of carbon materials, an alternative approach for tuning and modifying the extreme properties of carbon allotropes is alloying carbon nets with *heteroatoms* with no changes in the topology of the original system. The term “heteroatom” is borrowed from organic chemistry, indicating non-carbon (or hydrogen) atoms that have replaced carbon in a molecular structure; the term “alloying” is improperly but widely used in this field [27].

Because of their affinity to carbon and their richness of chemistry, boron, nitrogen and silicon are the ideal elements with which to form alloys; as

such, they form the main focus in the present work. In these systems, the stable stoichiometric compounds of boron carbide [28], silicon carbide [29] and carbon nitride [30] are known.

1.2 Aim of this work

This work is focused on investigating the effect of substitutions on two carbon nets, namely glitter and graphene, using a fully first principles approach. The effect of substitutions are investigated with regards to structural stability and modification of the electronic properties in order to improve the understanding of carbon-based semiconductors.

The stability of pure carbon glitter has also been compared with the other structures that have been proposed in the literature to describe n-diamond.

1.3 Overview of the thesis

In Chapter 2, a brief introduction regarding the materials that have been studied and the possible applications is reported. Chapter 3 contains an explanation of the theoretical methods that are used in the thesis.

Results are presented and discussed in the following Chapters:

- Chapter 4 - **Glitter: a possible metastable carbon phase.** The stability of the atomic arrangements proposed for explaining the crystallography of n-diamond are studied in term of dynamics at 0 K.
- Chapter 5 - **Boron, nitrogen and silicon substituted glitter.** Novel structures of substituted glitter are proposed with a view to stabilising the glitter structure and opening a bandgap.
- Chapter 6 - **Boron-substituted graphene.** Boron substitution in graphene is investigated with a view to finding novel configuration having semiconducting behaviour.

A general discussion and overall conclusions followed by a review of the open questions and the proposed future work are contained in Chapter 7.

A compact disk, with supplementary material in electronic form, is also included.

Chapter 2

Carbon-based materials

Doping and substitution of heteroatoms in carbon nets have provided a number of fruitful routes for tuning and modifying material properties, with a number of materials having been proposed and synthesised [31, 32, 33, 34, 35].

Due to the contiguity in the Periodic Table, boron, nitrogen and silicon have some similarities with carbon, that make them interesting for substitutions in carbon nets: C, Si, B⁻ and N⁺ are isoelectronic in the valence shell. I would like to underline that, despite some similarities, the variety of the bonding of carbon is unique.

The literature regarding carbon based materials with heteroatom substitutions is extensive, however in the next sections, just the key-points relevant for this work are presented:

- carbon substitutions with heteroatoms, Section 2.1;
- the tantalising case of n-diamond and glitter, along with the idea of stabilising the glitter structure with heteroatom substitutions, Section 2.2;
- graphene allotrope and the technological theme of opening a bandgap in the electronic structure, Section 2.3.

2.1 Heteroatom substitutions on selected nets

Boron. Boron substitutions in carbon materials, have been proven to form metastable phases. Diamond can be contaminated by very few types of impurities, due to the rigidity of its lattice. Boron can be found as a substitutional impurity (up to 1 ppm) in natural diamond [36]. By means of chemical vapour deposition (CVD) and high-pressure high-temperature (HPHT) synthesis, boron was incorporated in diamond films up to 1 at.% for electrode applications [37]. Stoichiometric inclusion of boron in the diamond lattice has been shown to be possible by Solozhenko et al. [38], reporting the synthesis of a diamond-like BC_5 compound. X-ray characterisation showed that boron atoms are randomly distributed throughout the lattice [38]. Zinin et al. [39] reported the synthesis of hetero-nano-diamond, cubic BC_3 , at a pressure of 39 GPa and temperature of 2200 K in a laser-heated diamond anvil cell. High-resolution transmission electron microscopy imaging of c- BC_3 , recorded at ambient conditions, shows that it is a nano-crystalline single phase.

The maximum thermodynamic solubility of B in graphite is 2.35 at.% at ~ 2600 K [40]. Way et al. deposited thin graphite-like films of B_xC_{1-x} , with x up to 0.17 [41]. Kouvetakis et al. [42] reported that interaction of benzene with boron trichloride at ~ 1100 K yields a graphite-like metallic material of composition BC_3 . B atoms are ordered in the graphite-like layers, where carbon benzene-like units are surrounded by the substitutional element [43].

The properties of carbon nanotubes are sensitive to the diameter and the chirality of the tube, which is difficult to control in mass production. Alternatively, electronic properties can be tuned chemically by including boron in the nano-structure. In boron doped nanotubes, the Fermi level is shifted downwards due to the missing π -electrons from the boron atoms while the valence-band structure remains otherwise unaltered. When nanotubes form in a carbon arc, the presence of boron results in long boron-doped carbon nanotubes that are generated as dominant zigzags. A metallic behaviour is observed, in contrast to carbon nanotubes, which are semi-conducting [44]. Highly boron-substituted (up to 15 at.%) single-wall carbon nanotubes have

been reported [45]. Core-level electron energy-loss spectroscopy reveals that boron incorporates into the lattice structure of the tubes. The charge transfer and the calculated Fermi-energy shift in the doped nanotubes offer evidence that charge localisation and doping induced band structure changes play an important role at high boron concentration.

Nitrogen. Nitrogen is the most common impurity in natural diamond [46]. Many different typologies of inclusions are present in diamond, involving both single atom and molecular nitrogen incorporation [47]. Investigating inclusion of nitrogen in diamond nano-particles, expected to be important for use in nano-devices, Barnard and Sternberg [48] predicted with density functional tight binding simulations that nitrogen is likely to be positioned at the nano-diamond surface. Kanda et al. grew diamond on boron nitride with high nitrogen concentrations [49], finding that 1200 to 1900 atomic ppm of nitrogen atoms are incorporated in the crystals. Lian et al. [50] and Yu et al. [51] succeeded in synthesising diamond crystals with 1600-2400 ppm of nitrogen using NaN_3 or $\text{Ba}(\text{N}_3)_2$ as a dopant.

The composition and structure of nitrogen-substituted graphite films produced by CVD were studied by Matsui et al. [52]. X-ray diffraction indicated that the structure of the films is similar to that of graphite. The atomic fraction of incorporated nitrogen was found to be a maximum of 12.4 at.%.

Ghosh et al. [53] reported the highest N-doping level achieved for carbon nitride nanotubes, up to 25.7 at%. The precursor imidazole was used as a dual supplier of carbon and nitrogen in the presence of ferrocene catalyst. It was observed that the abundance of N-substituted graphitic units enhances the electrical conductivity of individual nanotubes by donating additional electrons to the network.

Silicon. Silicon and carbon at 1:1 stoichiometry form silicon carbide (SiC), which exists in about 250 crystalline forms [54]. The beta modification of silicon carbide, β -SiC, is formed at temperatures below 2000 K. This polymorph has the zincblende crystal structure, closely related to diamond [55].

It is still a matter of debate whether alloys with off-1:1 stoichiometry can be formed [56]. DUBY and DURAND [57] proposed that the solubility of C in silicon is ~ 9 ppm. Low concentrations of metastable C defects in Si have been created experimentally using molecular beam epitaxy [58, 59] and CVD [60].

Under ambient conditions, Si strongly prefers sp^3 hybridisation and tetra-coordination, while carbon can form bonds based on both sp^3 and sp^2 hybridisation. The reasons for the apparent immiscibility is centred on the bond lengths: the bond length of C is about $2/3$ that of Si. The presence of Si-Si, C-C and Si-C bonds in the same structure would result in large strains, due to the bond length mismatch.

2.2 n-Diamond

Hirai and Kondo in 1991 [26] identified a new possible allotrope of carbon in materials produced by rapid cooling of shock-compressed graphite. The novel form of carbon was called *n-diamond* (new diamond). Electron diffraction (ED) patterns of n-diamond matched with that of cubic diamond apart from the presence of additional reflections at indices $\{2,0,0\}$, $\{2,2,2\}$, $\{4,2,0\}$, which can be indicative of an fcc structure. This feature has been observed in a number of other experiments involving carbon allotrope synthesis under extreme conditions.

Palatnik et al. [61] earlier reported the observation of a metastable carbon allotrope in low temperature annealed carbon films bombarded with argon ions during growth. Konyashin et al. [62] observed a metallic modification of carbon formed by transformation of a diamond surface during treatment in hydrogen plasma. Yamada et al. characterised, by scanning electron microscopy (SEM), nano-clusters of n-diamond and i-carbon (a metastable phase of carbon related to diamond [63]) found as remnants of detonation of trimethylenetrinitramine and graphite in steel chambers [64]. Fine crystals of n-diamond were produced by Frenklach et al. using plasma CVD [65].

Cowley et al. also obtained n-diamond by CVD on platinum wires in the presence of H_2 [66]. Wen et al. synthesised n-diamond in macroscopic amounts from Fe-catalysed carbon black under atmospheric pressure at high temperature [67]. Thin films have been produced by ion-beam deposition [68] and by radio-frequency plasma decomposition of hydrocarbon gases [69]. Many other methods have been successfully utilised for synthesising n-diamond; for a complete overview see Wen et al. [70].

Interestingly, some “natural” occurrences of n-diamond have been reported, both in crude oil [71] and stratum [72]. The phase has been found in solid asphaltenes precipitated from crude oil of the Sureste basin, Yucatan peninsula, Mexico. The Sureste Basin is located near the Chicxulub crater, formed from the meteoric impact widely believed to have caused the Cretaceous-Paleogene extinction event some 66 Million years ago. Whilst the origin of the n-diamond remains contentious, an intriguing hypothesis is that the meteoric impact, which occurred in the same geological time-frame as the formation of the Sureste basin oil fields, provided the extreme conditions required for the formation of n-diamond. Sediments abundant with nano-diamonds are also present in North America. They are dated to ~ 10000 years ago. Electron diffraction reveals the presence of two diamond allotropes, namely cubic diamond and n-diamond; the formation of both requires extraordinary conditions, outside the range of Earth’s typical superficial processes but common to cosmic impacts. These findings provide strong evidence for Earth’s collision with a rare swarm of carbonaceous chondrites or comets.

Despite the ability to synthesise n-diamond in many different ways and the natural occurrences, the crystal structure of n-diamond is still unclear. In part, this is due to the fact that it is usually produced in small amounts and in a nanoscopic form that does not facilitate the structural identification. Up to now, several models have been proposed for n-diamond, most of which are based on modification of the cubic-diamond structure. In a recent publication, Baldissin and Bull [73], studying the dynamical stability of the

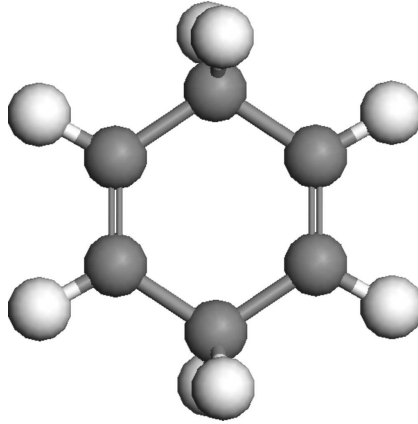


Figure 2.1: Representation of 1,4-cyclohexadiene: carbon (grey), hydrogen (white). The carbon backbone is the building block of the glitter structure.

structures proposed in the literature to describe n-diamond, ruled out the various models based on cubic diamond because of their dynamical instability at 0 K. A further structure, *glitter*, based on a tetragonal lattice, has been shown to be the only structure that is dynamically stable.

2.2.1 Glitter

Glitter has a tetragonal unit cell with space group $P4_2/mmc$ (No. 131) containing 1,4-cyclohexadieneoid unit rings [24], Figure 2.1. Glitter contains both trigonal (3-coordinated) and tetragonal (4-coordinated) C atoms, Figure 2.2. The carbon network can be thought of as a graphite-diamond hybrid in terms of connectivity and density. However according to Well's topological classification [74], it is not strictly a diamond-graphite hybrid. The structure is stabilised by extensive spiroconjugation resonance mechanisms in three dimensions [25, 75].

According to *ab initio* calculations, glitter is less stable than graphite by ~ 0.5 eV/atom [76]. It must be stressed that many widespread carbon forms have high formation energy. For example, Buckminsterfullerenes lie 0.3 eV/atom above the energy level of graphite [63]; this energy deficit does not preclude their existence. Decomposition of graphite and diamond has

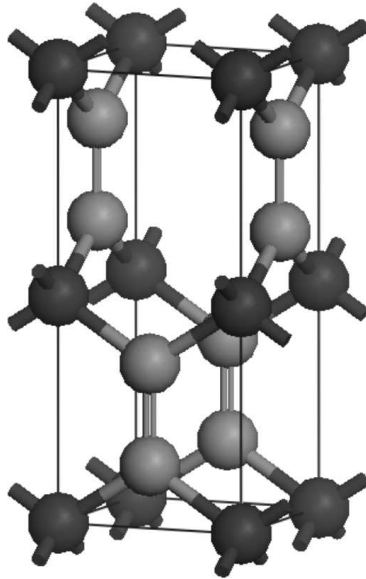


Figure 2.2: Glitter structure: 4-coordinated carbon atoms with sp^3 hybridisation (dark grey) in tetragonal positions and 3-coordinated carbon atoms with sp^2 hybridisation (light grey) in trigonal positions [24].

high activation barrier due to the reconstructive nature of this process in a system characterized by covalent bonding. Similarly, glitter decomposition must be unfavourable because the same kind of interactions is involved. If created, the glitter allotrope would persist, as was argued by Bucknum et al. [25].

Bucknum et al. [25] in 2005 proposed that glitter is consistent with n-diamond on the basis of comparing the experimental diffraction pattern of n-diamond and the simulated diffraction pattern of glitter optimised by density functional theory calculations. In addition to the diffraction evidence, the calculated band structure of glitter [24] shows metallic behaviour, which agrees with the observed electrical behaviour of n-diamond. Glitter can be rationalised as a three-dimensional structure containing ethylenes stacked at a separation of $\sim 2.5 \text{ \AA}$, while the interlayer spacing in graphite is $\sim 3.3 \text{ \AA}$. Figure 2.3 shows an extended view of the glitter structure.

Recently, Bucknum and Castro revised the consistency of the glitter

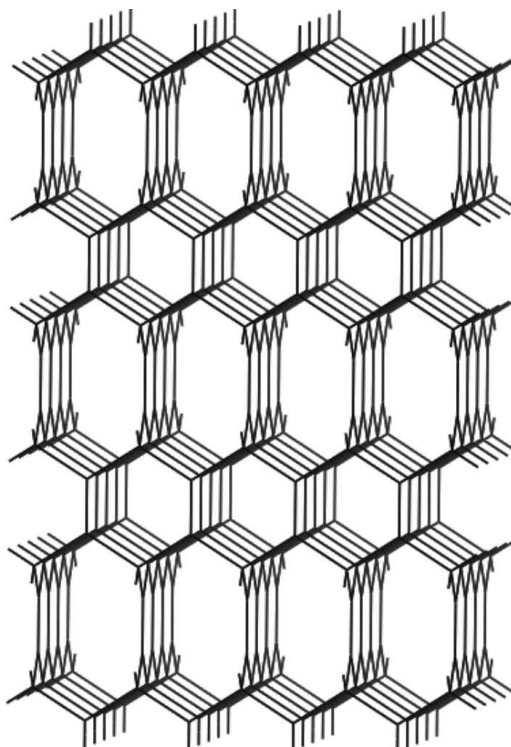


Figure 2.3: Glitter $4 \times 4 \times 3$ supercell: bond order is not considered so as to allow a clearer representation.

model with kinetically stabilised forms of Carbon, stating that tetragonal carbon is a reasonable explanation for both n-diamond and i-carbon [77].

Alloying carbon glitter with heteroatoms, such as boron, nitrogen and silicon, can be of particular interest. Substitution could have effects on the stability and could be used to modulate the properties of the resulting material. However, there is a dearth of information about substituted glitter. Silicon substitutions have been theoretically investigated by Bucknum et al. [78] and more recently by Andrew et al. [56]. Stamatina et al. proposed in 2004 the synthesis of silicon dicarbide, SiC_2 , in a matrix of novolac phenol-formaldehyde resin with silicon powder [79]. SiC_2 is a possible off-1:1 stoichiometry silicon carbon compound. Glitter nets, formed by boron and nitrogen substitutions in trigonal positions, have been investigated by Bucknum and Hoffmann [24]. To the author's knowledge, theoretical papers

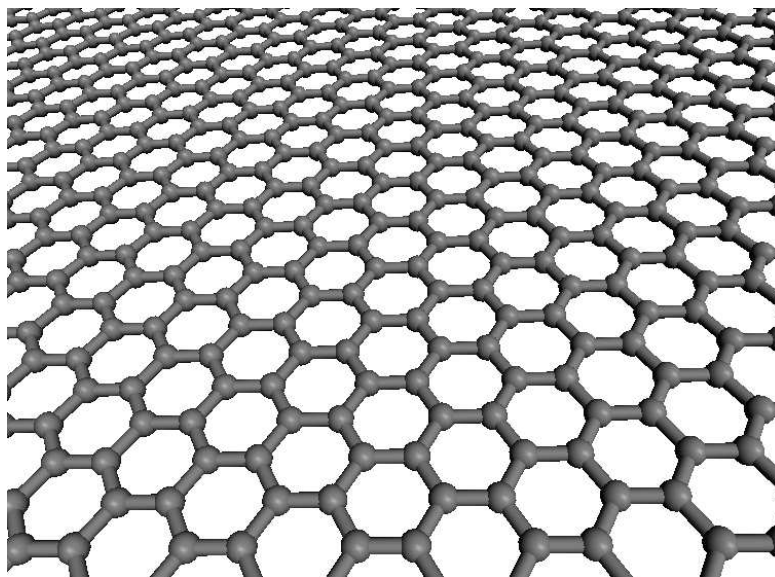


Figure 2.4: Graphical representation of graphene.

on substituted glitter take into account just a few configurations based on chemical intuition; the configurational space has never been extensively investigated. Moreover, the effect of substitutions with more than one type of element has not been considered. Substituted glitter could open a new range of applications as hard light-weight materials in electronics.

2.3 Graphene

Graphene is an allotrope of carbon whose structure is a single planar sheet of sp^2 -bonded carbon atoms. It can be rationalised as an indefinitely large aromatic molecule, the limiting case of the flat polycyclic aromatic hydrocarbons, Figure 2.4. The peculiar atomic arrangement is reflected in its unique electronic structure. Large-area graphene is a zero-bandgap semiconductor presenting massless Dirac-fermion behaviour: conical valence and conduction bands meet at a single point in momentum space [10, 80, 81, 82], see Figure 2.5.

The high carrier mobility at room temperature is one of the main advan-

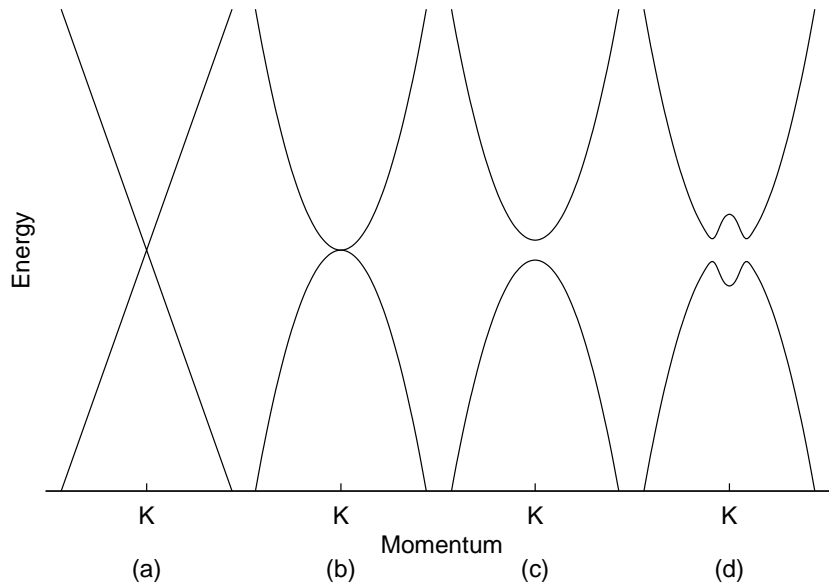


Figure 2.5: Band structure around the k point of (a) large-area graphene, (b) unbiased bilayer graphene, (c) graphene nanoribbons, and (d) bilayer graphene with an applied perpendicular field.

tages ascribed to the application of graphene in electronic devices [83, 84, 85]. The high mobility of large-area graphene [86] comes along with a lack of bandgap at the Fermi level. It is well-known that the mobility decreases for increasing bandgap, as has been shown for related materials, namely carbon nanotubes [87, 88]. However, a bandgap is essential for allowing two important applications:

- the switching on/off processes of transistors for logic application [89];
- the efficient energy conversion in solar cell applications [90].

2.3.1 Opening a bandgap

Regarding graphene-related materials, several approaches have been developed to open a bandgap at the Fermi level:

- lateral confinement forming graphene nanoribbons [91];

- biasing bilayer graphene [92];
- applying strain to graphene [93];
- chemical functionalisation of graphene, [94];
- substitution of graphitic carbon with heteroatoms, in particular B and N [95, 27].

Yang et al. predicted that armchair and zigzag nanoribbons have bandgaps that are approximately inversely-proportional to the nanoribbon width [91]. While theoretical calculations are based on well-defined models, real nanoribbons have rough edges and widths that are not constant along their length [96]. To open a bandgap useful for conventional devices, very narrow nanoribbons with well-defined edges are needed. *Unzipping* carbon nanotubes [97] seems to be the most promising method of producing nanoribbons that are uniform in width and have reduced edge roughness. Edge geometry, edge functionalisation and doping can also affect the bandgap of C-nanoribbons [96, 98].

If an electric field is applied perpendicular to bilayer graphene, a bandgap opens, showing the so-called Mexican-hat shape in the band structure diagram [92, 99], Figure 2.5. The size of the bandgap can be tuned by modulation of the strength of the field. Modest gaps, ~ 250 meV, can be achieved only by applying intense fields, $\sim 3 \times 10^7$ V cm⁻¹ [92, 100].

The effect of uni-axial strain on large-area graphene for opening a bandgap at the Fermi level has been simulated [93]. However the required deformation that is needed to obtain an useful bandgap would be difficult to achieve in practice. To author's knowledge, the effect of biaxial and local strain has never been investigated in detail.

Chemical functionalisation of the graphene surface is a way to manipulate electronic properties of graphene-related materials. The hydrogenation [101, 102, 103, 104] and oxidation [105, 106, 107] of graphene surfaces have been extensively studied, along with other kinds of functionalisations, such

as fluorination and chlorination [108, 109]. The main advantage is that the functionalisation reaction can occur on the graphene substrate, which has recently seen significant advances for mass production [110]. Unfortunately, for covalent functionalisation, a phase separation is likely to take place spontaneously due to the strain associated with the presence of sp^2 and sp^3 carbon atoms in the same layer [104]. The sp^2 hybridisation state is associated with in-plane bonds while covalent functionalisation demands sp^3 hybridisation and therefore tetrahedral coordination.

Alternatively, in-plane substitutions of carbon atoms with heteroatoms, namely B and N, have been proven effective for modifying the electronic structure [95, 27]. The main advantage of in-plane substitution is that the final materials do not exhibit strain effects due to the co-existence of atoms with different coordination in the graphitic layer.

Wang et al. reported the functionalisation of graphene nanoribbons with nitrogen species through high-power electrical joule heating in ammonia gas, leading to n-type electronic doping [111]. Zhao et al. incorporated nitrogen as graphitic dopants in monolayer graphene grown on a copper substrate [112]. Deng et al. [113] developed a novel method for one-pot direct synthesis of N-doped graphene via the reaction of tetrachloromethane with lithium nitride. Nitrogen species can be incorporated into graphene structures with contents in the range 4.5–16.4%. X-ray photoelectron measurements revealed that N-substitutions prevalently occur in the graphitic plane [114]. Using first principles calculation based on Ising-like parametrisation of the Hamiltonian, Xiang et al. [27] found two stable semiconducting structures, C_3N and $C_{12}N$; $C_{12}N$ is a direct semiconductor with 0.98 eV bandgap. The formation of ordered structures is reported to be driven by the repulsive electrostatic interactions between nitrogen atoms.

DFT calculations showed that the electronic properties of triangular graphene with nitrogen and boron substitutions depend on the dopants' positions [115].

Boron doped graphene has been produced by CVD, using different sources of carbon and boron. Cattelan et al. [116] used methane and diborane. Wang et al. used phenylboronic acid as a common source [117]. A BC_3 honeycomb sheet was grown over an NbB_2 (0001) surface [118]. According to first principles calculations, the mono-layer is an indirect bandgap semiconductor [43]. Luo et al. [95] with a Particle Swarm Optimization approach reported that BC_3 is the only semiconducting configuration, a so-called “magic” case, while other compounds at different stoichiometry are metallic.

Chapter 3

Theoretical background

First principles methods assist the understanding of structural, electronic and dynamical properties of materials, allowing quantitative predictions of physical quantities at both microscopic and macroscopic levels. The prediction ability is of fundamental importance for explorative investigations, when direct experimental measurements are time-consuming, costly, technically challenging or not feasible. An elegant example is represented by the works of Pickard and Needs on phases under extreme pressure (order of terapascal) [119, 120].

Much of the information presented in this Chapter is standard knowledge among experts, but as a consequence is rarely discussed. The following sections focus on a few fundamental elements:

- the modelling of the electronics of atomic systems within the framework of the density functional theory (DFT), Section 3.1;
- the Ising-like parametrisation of interatomic energy, that allows one to deal with substitutional systems, Section 3.2;
- the relation between lattice dynamics and structural stability, Section 3.3.

A comprehensive overview of these topics is beyond the scope of this work. The interested reader is referred to a number of excellent publications for DFT [121, 122], for Hamiltonian parametrisation [123, 124, 125], and for lattice dynamics [126, 127].

Year	Number of publications a year
2012	11065
2011	10002
2010	7874
2009	7323
2008	7065

Table 3.1: For the query “Density Functional Theory” the bibliographic database SciVerse Scopus [130] provides ~ 90000 results. The number of publications are increasing in recent years.

3.1 Density functional theory

In computational materials science, the energy and other properties of an arrangement of atoms (bulk solids, molecules, surfaces and so on) can be calculated by solving the quantum many-body problem of electrons and nuclei. The number of involved particles is often vast and the interaction between electrons are quantum-mechanically correlated, rendering an analytical solution impossible.

Many approaches have been attempted to solve this challenge. One of the most successful is the DFT, for which Walter Kohn was awarded the Nobel prize for chemistry in 1998 [128] along with John A. Pople, who shared the award for the development of computational methods. I would like to underline that DFT is not necessarily the best method for any problem involving electrons and nuclei, but its efficiency, accuracy and proficiency are suitable for most purposes. The size of the community of users is convincing evidence of its importance, along with the number of papers published each year, see Table 3.1. Moreover it is among the few quantum mechanical methods that are used in industry, see for instance Wolveton [129].

In principle, solving the Schrödinger equation [131] allows one to understand the properties of materials without using any empirical parameter or

approximation.

In a non-relativistic treatment within the Born-Oppenheimer approximation, which allows the decoupling of the electronic and nuclear degrees of freedom [132], the N -electron Schrödinger equation is written as:

$$H\Psi(\mathbf{r}_1, \sigma_1; \dots \mathbf{r}_N, \sigma_N) = \varepsilon\Psi(\mathbf{r}_1, \sigma_1; \dots \mathbf{r}_N, \sigma_N), \quad (3.1)$$

where H is the Hamiltonian, Ψ the many-electron wave function, \mathbf{r}_i and σ_i the spatial and spin coordinates relative to the i th electron and ε an eigenvalue. Although spin-polarization is relevant in this work, the spin coordinates are now omitted to simplify the notation and focus on other important features. The electronic Hamiltonian, H , is the sum of a one-body term and a two-body term, which contains the electron-electron interactions:

$$H = \sum_{i=1}^N \left[-\frac{\hbar^2}{2m} \nabla_i^2 + V_{ext}(\mathbf{r}_i) \right] + \sum_{i>j} \frac{e^2}{|\mathbf{r}_i - \mathbf{r}_j|}, \quad (3.2)$$

where \hbar is the reduced Plank constant, m and e are the electronic mass and charge, V_{ext} is the external potential. In condensed-matter physics the external potential is due to the interaction with the atomic nuclei. In principle, there is a straightforward method to find the ground state wavefunction: the application of the variational principle. One has to minimise the expectation value $\langle \Psi | H | \Psi \rangle / \langle \Psi | \Psi \rangle$. However, the time-scales involved are so large as to render this approach unfeasible, even for simple molecules.

To overcome this limitation, in most of cases the problem is reformulated as one where the interactions are represented by an effective potential acting on independent electrons, resulting in a set of one-electron Schrödinger-like equations:

$$H\psi_n = \left(-\frac{\hbar^2}{2m} \nabla^2 + V_{ext} + V_{eff} \right) \psi_n = \varepsilon_i \psi_n, \quad (3.3)$$

ψ_n is a set of n one-electron wavefunctions, V_{eff} the effective potential (where the electron-electron interaction is usually written in a mean-field manner) and ε_i are the energy eigenvalues.

Hartree developed an early approach, setting V_{eff} to the average of the Coulomb potential between one electron and all the others [133], neglecting two main features of the physical system: electron-electron interactions depend on the position; fermions, as electrons are, obey the Pauli exclusion principle and, hence, Fermi-Dirac statistics. The Hartree-Fock approach treats the exchange interaction exactly, but it does not include correlation [134].

3.1.1 Electron density

Hohenberg and Kohn showed that the electron density, $n(\mathbf{r})$, is the cornerstone of an exact theory for the solution of the many-body problem [135]: the electron density is the central quantity that allows a description of the complexity of electron interactions.

Knowing the n -electron wavefunction, $\Psi(\mathbf{r}_1, \dots, \mathbf{r}_n)$, the electron density, $n(\mathbf{r})$ can be obtained by integration:

$$n(\mathbf{r}) = \langle \Psi | \sum_{i=1}^N \delta(\mathbf{r} - \mathbf{r}_i) | \Psi \rangle = N \int d^3r_2 \dots \int d^3r_N |\Psi(\mathbf{r}, \mathbf{r}_2, \dots, \mathbf{r}_N)|^2, \quad (3.4)$$

where $\delta(\mathbf{r})$ is the Dirac delta function. In principle, given the external potential one can determine the electron density through the previous determination of the N -electron wavefunction. There is one-to-one relation from the potential to the electron density.

From the Kato theorem [136] one can, in principle, read off all information necessary for determining the Hamiltonian directly from the density distribution of electrons interacting with nuclei. The coordinates of the nuclei, \mathbf{R} , are the coordinates of the cusp singularities of the electron density. The nuclear charge, Z , can be determined by the density derivatives close to the cusps:

$$Z = - \left[\frac{a_0}{2n_0(\mathbf{r})} \frac{\partial n}{\partial r} \right]_{r \rightarrow |\mathbf{R}|} \quad (3.5)$$

where a_0 is the Bohr radius. The external potential is therefore fully defined. Integrating the electron density over space gives the number of electrons,

N . Thus the electronic Hamiltonian is fully defined. There is a one-to-one relation from the electron density to the external potential.

The generalisation of the previous result to a system with a fixed number of electrons, N , and for any arbitrary external potentials was formally given by Hohenberg and Kohn in form of two powerful theorems [135].

Within an additive constant, the electron density determines the external potential. If the statement is true then it immediately follows that the electron density uniquely determines the Hamiltonian operator. This follows as the Hamiltonian is specified by the external potential and the total number of electrons, N , which can be computed from the density simply by integration over all space. Because the Hamiltonian fully describes the system, an additional consequence is that every property of the system is determined by the electron density. This was generalised to include systems with degenerate states by Levy [137]. The energy is a functional of the electron density, $E[n(\mathbf{r})]$.

The density that minimises the energy is the exact ground state density. There exists a universal functional for the energy, which can be uniquely defined, given the external potential. The density that minimises this functional is the ground state density and the energy at the minimum, the ground state energy.

The problem is redefined into a problem that depends only on the electronic density, $n(\mathbf{r})$, rather than the many-body wave function. This is a tremendous advantage since $n(\mathbf{r})$ only depends on one three-dimensional position.

However, whilst Hohenberg-Kohn theorems are extremely important, they do not offer a computational route to calculate the ground-state density of a system. One year later, Kohn and Sham [138] developed a simple method for carrying-out DFT calculations.

3.1.2 Kohn-Sham equations

Kohn and Sham [138] devised a one-electron approach within the framework of the DFT. They showed that the ground-state density of a system, \mathbf{R} , of interacting electrons can be calculated as the ground-state density of an auxiliary system, \mathbf{A} , of non-interacting electrons.

Let us write the relation between the exact kinetic energy of the real system, $T[n]$, and the kinetic energy of \mathbf{A} , $T_s[n]$:

$$T[n] = T_s[n] + T_c[n], \quad (3.6)$$

where $T_c[n]$ is the remainder. If $T_c[n]$ is small, the exact kinetic energy, $T[n]$, is well approximated by $T_s[n]$. Similarly the exact Coulomb functional, $U[n]$, can be written as a sum of a Hartree term, $E_H[n]$, plus a term that takes into account the quantum nature of the interacting electrons $\Delta U[n]$:

$$U[n] = E_H[n] + \Delta U[n]. \quad (3.7)$$

The exact energy functional can be written as:

$$E[n] = T_s[n] + \int d^3r V_{ext}(\mathbf{r})n(\mathbf{r}) + E_H[n] + E_{xc}[n], \quad (3.8)$$

where $E_{xc}[n] = T_c[n] + \Delta U[n]$. This term is called the exchange-correlation energy functional. Variationally, equation 3.8 is as follows:

$$\frac{\delta E[n]}{\delta n(\mathbf{r})} = \frac{\delta T_s[n]}{\delta n(\mathbf{r})} + V_{ext}(\mathbf{r}) + e^2 \int d^3r' \frac{n(\mathbf{r}')}{|\mathbf{r} - \mathbf{r}'|} + \frac{\delta E_{xc}[n]}{\delta n(\mathbf{r})}. \quad (3.9)$$

Let us now consider the auxiliary system, \mathbf{A} , of non-interacting electrons:

$$\frac{\delta E[n]}{\delta n(\mathbf{r})} = \frac{\delta T_A[n]}{\delta n(\mathbf{r})} + V_A(\mathbf{r}). \quad (3.10)$$

The energy is expressed in terms of the kinetic energy of non interacting electrons and a potential $V_A(\mathbf{r})$.

Equations 3.9 and 3.10 are identical if the potential $V_A(\mathbf{r})$ satisfies:

$$V_A(\mathbf{r}) = V_{ext}(\mathbf{r}) + e^2 \int d^3r' \frac{n(\mathbf{r}')}{|\mathbf{r} - \mathbf{r}'|} + V_{xc}(\mathbf{r}; [n]), \quad (3.11)$$

where $V_{xc}(\mathbf{r}; [n])$ is the functional derivative of the exchange-correlation energy, the so-called exchange-correlation potential, which is also a functional of the electronic density. Equation 3.11 is the condition for the existence of the virtual system **A**. If it is satisfied, equations 3.9 and 3.10 must have an identical solution. The N -electron Schrödinger equation can be solved for **A**:

$$\left[-\frac{\hbar^2}{2m}\nabla^2 + V_A(\mathbf{r}) \right] \psi_i(\mathbf{r}) = \varepsilon_i \psi_i(\mathbf{r}), \quad (3.12)$$

the electron density $n_A(\mathbf{r})$ of **A** can be calculated by summing the square moduli of the occupied orbitals:

$$n_A(\mathbf{r}) = \sum_i f_i |\psi_i(\mathbf{r})|^2, \quad (3.13)$$

where f_i is the occupation factor. If Equation 3.11 is satisfied, the electron densities of **R** and **A** are the same: $n_R(\mathbf{r}) = n_A(\mathbf{r})$.

Equations 3.12 and 3.13 must be solved iteratively to self-consistency starting from a trial density. This is the well-known set of equations called Kohn-Sham equations. Equation 3.12 is written here in extended form:

$$\left[-\frac{\hbar^2}{2m}\nabla^2 + V_{ext}(\mathbf{r}) + e^2 \int d^3r' \frac{n(\mathbf{r}')}{|\mathbf{r} - \mathbf{r}'|} + V_{xc}(\mathbf{r}'; [n]) \right] \psi_i(\mathbf{r}) = \varepsilon_i \psi_i(\mathbf{r}). \quad (3.14)$$

The problem is not linear because the third and fourth terms depend on the electron density, which depends on ψ_i , which depends in turn on the effective potential V_A .

3.1.3 Exchange-correlation functional

The success of the Kohn-Sham approach relies on mapping the real system into a system of fictitious non-interacting electrons with the same electron density as the real system. This approach has the advantage that the auxiliary system can be calculated at a relatively low computational cost. The flip-side is that the exchange and correlation functional, introduced in Equation 3.8, hides the difficult part of the physics involved. The complexity of $E[n]$ is displaced to $E_{xc}[n]$ and it is not surprising that the exact form is

unknown. This term takes into account all the quantum effects and, in some cases, the spurious electron self interaction. It does not depend on the external potential so, if it were known in its exact form, it would, in principle, work for any system.

$E_{xc}[n]$ is usually split into the exchange, $E_x[n]$, and the correlation part, $E_c[n]$. The exact mathematical form for the exchange is known but leads to expensive computation, especially for solids. Regarding the correlation, no exact form exists that can be practically used in standard calculations. There are however some specialised calculations, see for instance [139].

Because electrons are fermions, the many-electron wave function is antisymmetric under the exchange of pairs of electrons. The antisymmetry produces a spatial separation of electrons in the same quantum state, which includes the spin state; this is the manifestation of the Pauli exclusion principle. The separation itself decreases the Coulomb energy of the system, the reduction is called the *exchange energy*. Moreover, electrons are dynamically correlated.

The probability of finding an electron in \mathbf{r}' when another is in \mathbf{r} gets much smaller than 1 when $\mathbf{r}' \rightarrow \mathbf{r}$. Along its trajectory the electron sees around itself a depression of density.

The problem of finding effective approximation of E_{xc} is central in DFT. Presently, there are many different kind of exchange-correlation term; they are not based on exact theory, therefore they are validated *a posteriori*.

The standard functionals for molecular system are, so-called, hybrid functionals [140]. For solids they do not constitute the standard choice because they require the evaluation of the Hartree term, which significantly increases the computational cost. For periodic solids, the local density approximation (LDA) and generalised gradient approximation (GGA) are the most frequently used in the solid-state community for total-energy calculations.

Local density approximation and generalised gradient approximation

The simplest approximation for the exchange-correlation functional is the local density approximation (LDA) [138]: E_{xc} is constructed by assuming that the exchange-correlation energy at a point \mathbf{r} per electron in the electron gas, $\epsilon_{xc}(\mathbf{r})$, is equal to the exchange correlation energy per electron in a homogeneous electron gas that has the same electron density, $n(\mathbf{r})$:

$$E_{xc}^{LDA}[n(\mathbf{r})] = \int \epsilon_{xc}^{HOM}[n(\mathbf{r})]n(\mathbf{r})d\mathbf{r}. \quad (3.15)$$

The exchange-correlation energy functional is assumed purely local. Despite its simplicity, the LDA works well for solid systems. This approximation is valid for $n(\mathbf{r})$ varying very slowly in space; it fails in situations where the electronic density undergoes rapid changes, especially in molecules and surfaces. It is characterised by over-binding effects, tending to overestimate the bond strength in solids.

Conversely the GGA has the tendency to over-correct the over-binding inherent in LDA. The GGA introduces a dependence on the local gradient of the electron density, $\nabla n(\mathbf{r})$, in an attempt to include the effects of inhomogeneities. The functional can be written as:

$$E_{xc}^{GGA}[n(\mathbf{r})] = \int n(\mathbf{r})\epsilon_{xc}^{HOM}[n(\mathbf{r})]F_{xc}[n(\mathbf{r}), \nabla n(\mathbf{r})]d\mathbf{r}, \quad (3.16)$$

where $F_{xc}[n(\mathbf{r}), \nabla n(\mathbf{r})]$ is the enhancement factor.

There are several different flavours of GGA functional. The PW91 functional, due to Perdew and Wang [141] has been constructed using Quantum Monte Carlo for the uniform electron gas and exact properties of the exchange-correlation hole. The Perdew-Burke-Ernzerhof (PBE) functional [142] is nowadays the most commonly used functional for solid-state calculations. It was designed to satisfy several conditions that are obeyed by the exact functional and it contains no empirical parameters. In most cases, PBE gives similar results as PW91 [143, 144], but it has a simpler analytical form.

In a few cases, the LDA has better agreement with experiment than GGA, for example in layered materials, such as graphite and hexagonal boron nitride, or molecular crystals where binding is based on weak interactions [145]. The improved performance is a mere artifact due to inherent over-binding and not a better description of the physical system. For this reason, LDA functionals have been excluded for the systems treated in the present thesis, in particular for the layered ones. In this work, GGA functionals have been used for evaluating the energy of the systems based on tetragonal carbon and on graphene, PW91 and PBE respectively.

It is worth highlighting that Luo et al. [95] and Xiang et al. [27] used the LDA approach for B and N substituted graphene respectively. It is well established that the GGA approximation describes more consistently the electronic phenomena of surfaces and molecules, as graphene layered materials should be considered. This choice is supported by Sluiter and Kawazoe [104] and Pujari et al. [146], who used the GGA approximation for the study of graphene hydrogenation.

Hybrid functionals

It is widely accepted that the LDA and GGA functionals are not appropriate for bandgap calculations [147, 148, 149]. An emblematic case is that of La_2CuO_4 , an important material for high temperature superconductors: despite having a 2 eV bandgap, it is predicted to be metallic by LDA, PBE and PW91 functionals [150].

Hybrid functionals, which are characterised by mixing non-local Hartree Fock exchange with semi-local exchange in certain proportions, have been shown to improve the calculation of bandgaps [151, 152, 153, 154]. This is done because the two different approaches (local and non-local) sometimes have complementary deficiencies that in some way tend cancel one another [147].

The most popular hybrid functional is the B3LYP [155]:

$$E_{xc}^{B3LYP} = 0.8E_x^{LDA} + 0.2E_x^{HF} + 0.72\Delta E_x^{B88} + 0.19E_c^{VWN} + 0.81E_c^{LYP}, \quad (3.17)$$

where E_x^{LDA} is the LDA exchange, E_x^{HF} the Hartree Fock exchange, ΔE_x^{B88} Becke's correction [156], E_c^{VWN} Vosko-Wilk-Nusair correlation functional [157] and E_c^{LYP} Lee-Yang-Par correlation [158]. The mixing coefficients have been determined by a fitting on a set of molecules.

Under periodic boundary conditions, calculation of the HF exchange is computationally taxing because of the slow decay of the exchange interaction with distance.

Heyd et al. [159] overcame this problem, proposing to screen the Coulombic potential. This is accomplished by splitting the exchange contribution (E_x) into short-range (SR) and long-range (LR) parts:

$$E_{xc}^{HSE} = \alpha E_x^{HF,SR}(\mu) + (1 - \alpha) E_x^{PBE,SR}(\mu) + E_x^{PBE,LR}(\mu) + E_c^{PBE}, \quad (3.18)$$

the mixing coefficient α is set to $1/4$, the screening parameter, μ , is typically used in the range $0.2-0.3 \text{ \AA}^{-1}$. The HSE06 functional, used in this work, has $\mu = 0.2 \text{ \AA}^{-1}$ [160]. The truncation of the long-range part has little impact on the calculated properties of finite system [161], however it has the undeniable advantage of lowering the computational cost.

Barone et al. revised the quantitative accuracy of bandgap calculation of low dimensional graphene derivatives using screened hybrid functionals [162]. They have been also used to study doped nanotubes [163] and N-substituted graphene [27].

3.1.4 Spin-dependent DFT

Isolated atoms are usually magnetic, however most solid state systems are non-magnetic. Magnetism arises by the competition between exchange and kinetic energy effects: the gain in exchange energy is connected to the loss in kinetic energy, that is related to delocalisation of the valence electrons (in a solid). If valence electrons are sufficiently localised, magnetism occurs. Iron is a typical example [164].

In low-dimensional systems (surfaces and interfaces, single- and multi-layers, ultra-thin films and wires, deposited clusters and so on), the tendency

toward magnetism is considerably enhanced.

In standard Kohn-Sham theory (Section 3.1.2) there is no spin component, therefore magnetic systems cannot be described. Spin-dependent DFT is a generalisation of the standard Kohn-Sham formalism that allows one to deal more realistically with systems characterised by spin polarisation. The term that contains the quantum nature of the electron interaction is the exchange-correlation functional. Therefore, this is the term from which spin polarisation emerges. The LDA, for instance, must be extended to the local spin density approximation (LSDA) [165].

Complex forms of magnetism, such the non-collinear magnetism, are not relevant to the present work.

3.1.5 Plane-waves, pseudopotentials, and projector augmented waves

When modelling an arrangement of atoms, it is convenient to impose periodic boundary conditions, even if the system does not have a three-dimensional periodicity. The main advantage of this approach is that in a periodic system the electronic wave function can be written as a product of a cell-periodic part and a wavelike part [166]. Symbolically written as:

$$\psi_i(\mathbf{r}) = \exp[i\mathbf{k} \cdot \mathbf{r}]f_i(\mathbf{r}). \quad (3.19)$$

The cell-periodic part, $f_i(\mathbf{r})$, can be expanded using a convenient discrete basis set consisting of plane waves. Therefore the electronic wave function can be written as a sum of plane waves:

$$\psi_i(\mathbf{r}) = \sum_{\mathbf{G}} c_{i,\mathbf{k}+\mathbf{G}} \exp[i(\mathbf{k} + \mathbf{G}) \cdot \mathbf{r}], \quad (3.20)$$

where \mathbf{G} are the reciprocal lattice vectors, defined by $\mathbf{G} \cdot \mathbf{l} = 2\pi m$ for all \mathbf{l} lattice vector of the crystal, and m is an integer. The coefficient $c_{i,\mathbf{k}+\mathbf{G}}$ for plane waves with small kinetic energy are more important than those with large kinetic energy, allowing truncation of the basis set of plane waves at some particular cutoff.

Among the many advantages of using a plane-wave basis set, it is worth mentioning that the basis set is spatially unbiased and complete; it does not depend on atomic positions. Moreover plane waves and their derivatives in k -space have simple mathematical expressions. The drawback is that an additional approximation must be introduced: “the pseudopotential approximation”.

Pseudopotentials

In general, plane waves are a very poor basis set to expand electronic wave functions because a very large number are needed to expand core orbitals and to replicate the rapid oscillations of the wave function in the core region. Fortunately, chemical properties depend on the valence electrons much more than on core ones. Core electrons, tend to be chemically inert, while valence electrons are available for bonding. For many elements, valence electrons can only occupy the outermost electron shell. A simple example is that of methane molecules (CH_4), comprising 4 C-H covalent bonds, each formed by atoms sharing a pair of electrons. The two electrons in the inner shell of carbon are so tightly bound that they do not directly participate in the bonds.

When modelling atomic systems, a good approximation is replacing the core region with an effective potential, called a pseudopotential. This approximation helps in reducing the number of electrons that must be taken into account for the solution of the quantum many-body problem, but more importantly it allows the complicated effects related to the motion of electrons close to the nucleus, to be hidden into the overall pseudopotential effect. Figure 3.1 shows a graphical representation of the pseudopotential concept. The corresponding pseudo-wavefunctions are identical to the real wavefunctions outside the core region, but are smoother and node-less within the core region [167]. Thus, they can be expanded using a much smaller basis set of plane waves.

Although accuracy and smoothness have improved over the years [168],

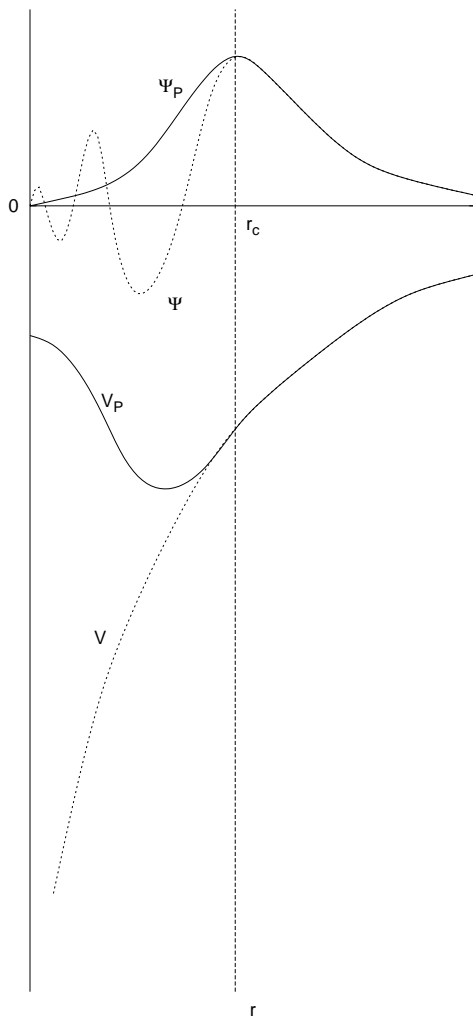


Figure 3.1: Schematic illustration of the pseudopotential idea. The dashed lines show the all-electron wavefunction, Ψ , and ionic potential, V ; the solid lines show the corresponding pseudo-wavefunction, Ψ_P , given by the pseudopotential, V_P . All quantities are shown as a function of distance, r , from the atomic nucleus. All-electron wavefunction and pseudo-wavefunction are identical beyond the cutoff radius r_c .

the norm-conservation constraints, typical of the so-called norm-conserving pseudopotential [169, 170], prevent localised electronic orbitals from being represented by very smooth pseudo wavefunctions. For first row elements and transition metals, characterised by strongly localised $2p$ and $3d$ orbitals, the resulting pseudopotentials require a large plane-wave basis set. To overcome this limitation the cut-off radius could be increased, but this adversely affects transferability.

In order to obtain maximally smooth pseudo wavefunctions, Vanderbilt [171] introduced ultrasoft pseudopotentials (USPP), relaxing the norm-conservation constraint. As with norm-conserving approach, the all-electron and pseudo wave functions are required to be equal outside the cutoff radius r_c , but inside r_c they are allowed to be as soft as possible. The consequence is that the pseudo wave functions are not normalised inside r_c , resulting in a charge deficit. This problem can be overcome by introducing localised atom-centered augmentation charges.

USPPs allow multiple reference states for each angular momentum channel leading to an improved transferability over an extended region of energy [172]. Consequently the construction of pseudopotentials is rather difficult due to the fact that many parameters must be considered.

The *ab initio* code CASTEP [173] implements density functional theory using plane wave basis sets and the pseudopotential approximation. It plays a central role in this work, having been employed to perform most of the calculations presented. The *ab initio* code VASP, which also uses plane wave basis sets, implements, in addition to pseudopotentials, the projector augmented wave (PAW) method. This has been employed in a limited number of cases. The background theory is briefly introduced in the following section.

Projector augmented wave

The drawback of the plane wave pseudopotential method is that all information on the full wave function close to the nuclei is lost. Blöchl [174] introduced the projector augmented wave method that allows calculations

to be performed with great computational efficiency whilst working directly with the all-electron valence wave function and all-electron valence potentials.

The projector augmented wave method [174] combines the versatility of the linear augmented-plane-wave (LAPW) [175] method and the formal simplicity of the plane wave pseudopotential approach. The plane-waves have the flexibility to describe the bonding and tail regions of the wave functions. Atomic orbitals can, on the other hand, describe correctly the nodal structure of the wave function near the nucleus.

The PAW method provides full access to the wave function, dividing it into two parts: partial wave expansions in a sphere around the atom (augmentation region) and envelope functions outside the spheres (interstitial region). The envelope functions and partial wave expansions are then matched at the sphere radius of the augmentation region.

The method is based on a linear transformation of the pseudo wave function, $\tilde{\Psi}$, to the all-electron wave function Ψ :

$$|\Psi\rangle = \mathcal{T}|\tilde{\Psi}\rangle, \quad (3.21)$$

$\tilde{\Psi}$ and Ψ differ near the ion core region, thus the linear transformation is assumed to be a sum of non-overlapping atom-centred contributions:

$$\mathcal{T} = 1 + \sum_R \hat{\mathcal{T}}_R, \quad (3.22)$$

$\hat{\mathcal{T}}_R$ is localised to sphere denoted Ω_R that encloses the atom R . Within Ω_R , it can be expanded into convenient functions such spherical harmonics:

$$|\tilde{\Psi}\rangle = \sum_i |\tilde{\phi}_i\rangle c_i. \quad (3.23)$$

Despite the complex formalism [176], the expression for the total energy, forces and stress are closely related to the ultrasoft approach, differing in the choice of the auxiliary functions and technical aspects.

3.2 Cluster Expansion Hamiltonian: an Ising-like parametrisation

In this section, the basic concepts that have been applied for studying the energetics of substitutional systems in this work are outlined. It is often convenient to map substitutional systems onto an Ising-like model [177] where atoms can be identified on the basis of the occupation of well-defined topological positions on an underlying lattice [125]. The Hamiltonian can be parametrised as a function of the configurational variables using a Cluster Expansion (CE) approach [178, 179].

When combined with *ab initio* total energy calculations, usually based on DFT, the CE method relies completely on first principles. The accuracy is affected only by the truncation of the expansion and by the approximations of the *ab initio* method.

In particular the cluster expansion (CE) method [178, 179] has been successfully used to describe configurational properties of stable and metastable phases of alloys, intermetallics, semiconductors and ceramics [123, 124, 180, 181, 182, 183]. Applications to graphene have also been presented in the literature [104, 27].

The main advantage of the cluster expansion method is that the energy can generally be written as a rapidly converging sum over cluster contributions, where interactions of larger clusters become negligible. A practical example of this idea is common in organic chemistry: the formation enthalpy of a molecule can be expressed as a sum of nearest neighbour contributions, namely bonds. Contributions from longer-range interactions usually provide only minor corrections. This is the essence of the Ising model.

An approach based on systematic total energy calculations would treat each configuration independently, failing to take advantage of any similarities. Conversely, the CE approach uses a parametrisation built on a relatively small set of structural energies to predict the total energy of different configurations. This approach allows one to investigate a wide portion of the

configurational space at a relatively low computational cost.

I do not hesitate to underline the importance of this powerful idea, which allows a treatment of substitutional systems from first principles.

The works of Ising [177] and of Connolly and Williams [178] are briefly described to set the framework of the problem.

3.2.1 The Ising model

Ising, in his doctoral thesis [177], proposed a model for handling configurational properties of ferromagnetic systems that involve phase transition related to ordering/disordering phenomena. The model was actually suggested by the physicist Lenz, supervisor of Ising, but it was named after the student, who provided its solution.

Whilst it is striking in its simplicity, the Ising model remains one of the most successful models in statistical mechanics. It shows two main advantages: firstly, the problem is formulated into a general probabilistic setting and, secondly, it allows one to relate local properties, which depend on local configurations and on system topology, to the properties of the extended system.

The first formulation can be described as follows: consider a linear arrangement of $n + 1$ atoms, each interacting only with the two neighbouring atoms in the atomic chain; consider a local property that is associated with any atom; the property is described by a discrete variable, called *spin*, that at any instant, can be in one of the two states, either *up* or *down*.

Let us now consider a sequence, ω , of atoms:

$$\omega = (\omega_0, \omega_1, \dots, \omega_n), \quad (3.24)$$

where ω_j represents the discrete variable describing the local status, namely spin up, \uparrow , or a spin down, \downarrow . Let us define a *spin function*, σ_j :

$$\sigma_j = \begin{cases} -1 & \text{for } \omega_j = \downarrow \\ 1 & \text{for } \omega_j = \uparrow \end{cases} \quad (3.25)$$

It is possible to calculate the energy, U , associated with the configuration ω using the following:

$$U(\omega) = -J \sum_{i,j} \sigma_i(\omega) \sigma_j(\omega) - m H_m \sum_i \sigma_i(\omega). \quad (3.26)$$

The first sum represents the energy due to the spin interactions; it runs over the pair i, j of nearest neighbours; J is the interaction parameter (for $J > 0$, the interaction tends to keep the spins aligned, for $J < 0$, spins have opposite orientations), the second term represents the effect of an external magnetic field of intensity H_m , the positive constant m is a property of the material. The contribution to the energy is minimum when all spin are in the same direction as the external field.

In the canonical ensemble, the probability of occurrence, P of a configuration, ω can be defined as follow:

$$P(\omega) = \frac{e^{-\beta U(\omega)}}{Z} \quad (3.27)$$

where β is the thermodynamic factor and Z is the canonical partition function:

$$Z = \sum_{\omega} e^{-\beta U(\omega)}. \quad (3.28)$$

Let us define an energy U_i associated with each point i , as:

$$U_i(\omega) = -\frac{J}{2} \sum_{|j-i|=1} \sigma_i(\omega) \sigma_j(\omega) - n H \sigma_i(\omega). \quad (3.29)$$

The relative probability of a configuration is simply obtained by taking a product over all the points using the energy at each point to determine the statistical weight. The one dimensional Ising model, which shows no phase transition, was solved by Ising himself [184].

The model is easily extended to more dimensions. The square lattice Ising model was given an analytic description by Onsager in 1944 [185]. Remarkably, the latter is one of the simplest statistical models to show a phase transition. The Ising model has been incredibly successful, having

been applied to a broad range of physical and non-physical problems. For an example of the latter, the reader is referred to the model proposed by Weidlich on social polarisation [186].

3.2.2 Lattice gas model

In computational materials science, disordered condensed-matter systems are among the most difficult to treat. There are many degrees of complexity of ordering/disordering phenomena. It is, however, possible to identify two distinct classes of system:

- structurally disordered systems, where atomic positions cannot be associated with any underlying lattice, for instance, amorphous and liquid systems;
- configurationally disordered systems, where atomic positions are topologically fixed by the underlying lattice, but the distribution of atoms in the lattice can have many different degrees of ordering.

The second class, which can be treated with Ising-like parametrisation methods, is the one of interest here. It must be noted that the atoms can exhibit atomic displacements from the ideal lattice positions, either due to lattice vibrations or local atomic relaxations. The key point is that they have to possess topological translational symmetry and they can be mapped according to the geometry of the underlying lattice. The ideal underlying lattice is called the *parent lattice*. Figure 3.2 shows on the left side a particular configuration of a binary system on an underlying 2-dimensional square lattice while on the right side there is a representation of the relaxed lattice. In the relaxed lattice atoms move from the ideal position however they can be mapped univocally onto the parent lattice. Having n atoms in the lattice, a full description can be achieved using n positional vectors.

A usual way to describe the atomic configuration on the lattice is using the so-called *pseudospin*, σ_i , which is a discrete variable. The variable is named after the original work of Ising, but in general they are not related

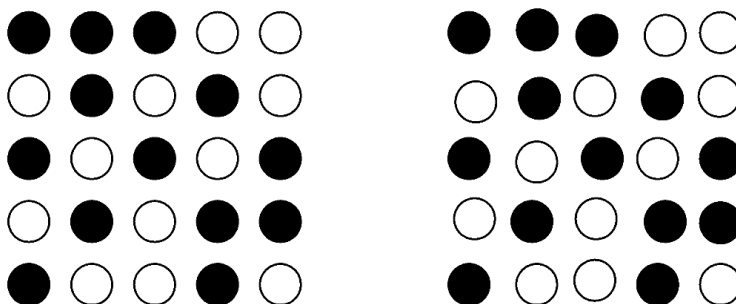


Figure 3.2: Representation of a binary substitutional system, the two different elements are distinguished by different colour (black and white). On the left is shown a particular configuration on an underlying parent lattice, 5×5 , while the right side represents the relaxed system. The lattice gas model allows a description of the system with a vector of occupational variable with 25 elements.

with any magnetic property. For binary systems, the variable usually takes the values $+1$ or -1 , depending on whether atom A or B occupies site i . If there are N sites in the system, the configuration is uniquely specified by a N -dimensional vector $\sigma = \{\sigma_1, \sigma_2, \dots, \sigma_N\}$.

It is reasonable that the local relaxation strongly depends on the local environment and finally just from the local distribution of atoms. Mapping the real system into a lattice gas model is a convenient way to reduce the number of variables without losing too much information about the system.

I would like to stress again that the association of an atom with a lattice site in any given atomic configuration is merely topological, without prescribing its exact position.

3.2.3 Original Connolly-Williams method

Connolly and Williams [178] calculated interaction energies using an expansion of the total energy obtained by *ab initio* calculations of an alloy system mapped onto a lattice gas model. The technique was used to predict energies

of random alloys of 4d transition metals.

The idea is representing the energy, $E(\sigma)$, of an arbitrary configuration, σ , on a given underlying lattice as a sum of interaction energies of geometric figures (cluster figures). The energy of each configuration can be expressed by an Ising-like expansion:

$$E(\sigma) = J_0 + \sum_i J_i \sigma_i + \sum_{j < i} J_{ij} \sigma_i \sigma_j + \sum_{k < j < i} J_{ijk} \sigma_i \sigma_j \sigma_k + \dots \quad (3.30)$$

where the J is an interaction energy. The first two terms on the right, Equation (3.30), define the energy of the random alloy with no mutual interactions, the third term contains all pair interactions, the fourth all three-body interactions, and so on.

Equation (3.30) can be written in a compact form by introducing a correlation function ξ_F for each class of symmetrically equivalent figures F :

$$\xi_F(\sigma) = \frac{1}{ND_F} \sum_f \sigma_{i_1} \sigma_{i_2} \dots \sigma_{i_m}, \quad (3.31)$$

D_F represents the number of figures of class F per site and N the number of sites in the structure. The index f runs over the ND_F figures in class F and m denotes the number of sites of figure f . Equation (3.30) becomes:

$$E(\sigma) = N \sum_F D_F \xi_F(\sigma) J_F. \quad (3.32)$$

The original application of Connolly and Williams for $A_xB_{(1-x)}$ system can be described as follow: choosing arbitrarily 5 different configuration on an underlying fcc lattice (fcc A, $L1_2$ A_3B , $L1_0$ AB, $L1_2$ AB_3 and fcc B) and 5 cluster figures, see Figure 3.3, it is possible to calculate 5 distinct expansion coefficients, namely $\mathbf{J} = \{J_0, J_1, J_2, J_3, J_4\}$, from the calculated total energies of the 5 different chosen configurations, $\mathbf{E}_s = \{E_0, E_1, E_2, E_3, E_4\}$.

A cluster figure (or simply cluster), α , is described by a vector of elements α_i of discrete variables.

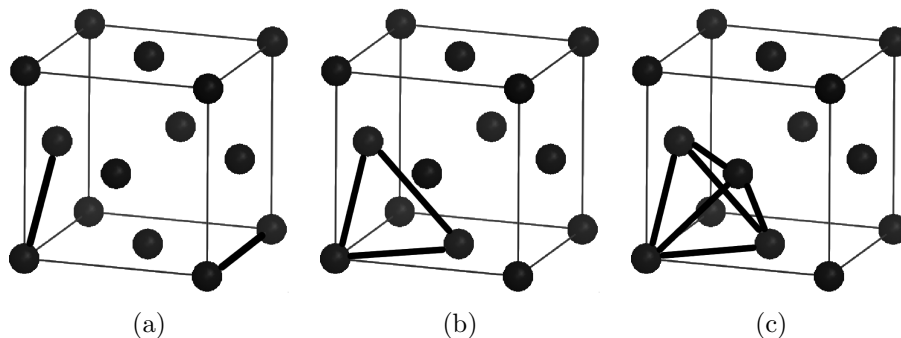


Figure 3.3: Cluster figures on an fcc lattice: (a) pair clusters (first and second nearest neighbour); (b) first nearest neighbour triangular cluster; (c) first nearest neighbour tetragonal cluster.

Let us write explicitly the energies in terms of effective Hamiltonian:

$$\begin{aligned}
 E_0 &= \xi_0(\sigma_0)J_0 + \xi_1(\sigma_0)J_1 + \cdots + \xi_4(\sigma_0)J_4, \\
 E_1 &= \xi_0(\sigma_1)J_0 + \xi_1(\sigma_1)J_1 + \cdots + \xi_4(\sigma_1)J_4, \\
 &\vdots \qquad \qquad \qquad \vdots \qquad \qquad \qquad \vdots \\
 E_5 &= \xi_0(\sigma_5)J_0 + \xi_1(\sigma_5)J_1 + \cdots + \xi_4(\sigma_5)J_4.
 \end{aligned} \tag{3.33}$$

In matrix form:

$$\mathbf{E}_s = \xi \mathbf{J}. \tag{3.34}$$

The determination of the vector of the expansion parameters, \mathbf{J} , is reduced to a matrix inversion task:

$$\mathbf{J} = \xi^{-1} \mathbf{E}_s. \tag{3.35}$$

Considering a binary substitutional system with an fcc parent lattice, cluster functions are shown in Table 3.2. This is a system of 5 equations having 5 variables, that can be solved analytically. In the Connolly-Willimas method a systematic inversion of the expansion is performed determining explicitly the parameters of the effective Hamiltonin. The number of calculated structural energies is exactly the same as the expansion parameters to be determined in the expansion.

Given any particular configuration, the energy of the configuration itself can be calculated within the accuracy of the method, using the expansion

Formula	Structure	ξ_0	ξ_1	ξ_2	ξ_3	ξ_4
A	fcc	1	1	1	1	1
A ₃ B	L1 ₂	1	0.5	0	-0.5	-1
AB	L1 ₀	1	0	-1/3	0	1
AB ₃	L1 ₂	1	-0.5	0	0.5	-1
B	fcc	1	-1	1	-1	1

Table 3.2: Cluster correlation functions for the 5 configurations on an fcc parent lattice [178].

parameters that have been calculated analytically.

For sake of clarity, correlation functions related to single and pair clusters for fcc A, L1₂ A₃B, L1₀ AB are here explicitly calculated. In the conventional representation, Figure 3.3, the fcc-based structures has 4 atoms in the unit cell, each atom having 12 near neighbors, leading to 4 single clusters and 48 pair clusters. Atomic species A and B are represented by the occupational variables (+1) and (-1) respectively. Considering the fcc A structure, the correlation functions for the single-atom and pair clusters of fcc A, ξ_1^A and ξ_2^A , are as follow:

$$\xi_1^A = \frac{1}{4}[4(+1)] = 1; \quad (3.36)$$

$$\xi_2^A = \frac{1}{48}[48(+1)(+1)] = 1; \quad (3.37)$$

for the fcc B structure the occupational variables invert. The correlation functions of L1₂ A₃B are calculated as follow:

$$\xi_1^{A_3B} = \frac{1}{4}[3(+1) + (-1)] = 0.5; \quad (3.38)$$

$$\xi_2^{A_3B} = \frac{1}{48}[24(+1)(+1) + 24(+1)(-1)] = 1; \quad (3.39)$$

for L1₂ AB₃, occupational variables invert. At composition 1:1 A:B, the correlation functions of L1₀ are:

$$\xi_1^{AB} = \frac{1}{4}[2(+1) + 2(-1)] = 0; \quad (3.40)$$

$$\xi_2^{AB} = \frac{1}{48}[8(+1)(+1) + 32(+1)(-1) + 8(-1)(-1)] = -\frac{1}{3}. \quad (3.41)$$

Regarding the understanding of correlation functions related to clusters having more complex geometry (triplets and quartets), the interested reader is advised to refer to relevant literature [178, 187].

3.2.4 Cluster Expansion ansatz for multicomponent multisublattice systems

According to the lattice gas model, a configuration, σ , can be represented by a vector of discrete variables, σ_i , called pseudospin, which indicates the type of element occupying site i . A scalar intensive quantity, q , can be expressed as a function of σ using as a basis set the cluster figures. Usually, the property that is expanded is the total energy, E . Multicomponent systems, namely alloys, have been covered since the first applications of the cluster expansion. Tepech et al. extended the multisublattice system approach from alloys to ionic systems [188]. In the general form of multicomponent multisublattice systems, the cluster expansion is formalised as follows:

$$E(\sigma) = \sum_{\alpha} m_{\alpha} J_{\alpha} \langle \xi_{\alpha'}(\sigma) \rangle, \quad (3.42)$$

where the symbols have the following definitions:

- α is a cluster figure (or cluster), see section 3.2.3;
- the sum runs over the clusters α that are not equivalent by symmetry operations of the space group of the parent lattice and it is averaged over all clusters α' that are equivalent to α by symmetry;
- m_{α} is the multiplicity of the *cluster*, α , which represents a set of sites in the parent lattice;
- $\xi_{\alpha'}$ are the *cluster functions*, which depend on the particular configuration;

- J_α are the expansion coefficients, also known as effective cluster interactions (ECIs).

The ECIs are determined by fitting to the calculated energies of a set of structures, where the number of ECIs is less than the number of structural energies. This method is generally referred as the Structure Inversion Method.

3.2.5 Validating the Cluster Expansion

In essence the Structure Inversion Method (SIM) is nothing more than a fitting method. The main complication is that the number of unknown parameters is, in principle, infinite. A finite number of ECIs related to a discrete number of cluster figures cannot provide an exact description of any substitutional system. For practical applications, total energy calculations can be performed only on a limited set of crystal structures, implying that an exact expansion can never be achieved, since there is the need to truncate the expansion at some point. Determining the optimal number of fitting terms along with the best set of cluster figures is the central problem. This process is carried out according to the criterion of maximising the forecasting proficiency. The main conditions to do so are presented here: minimisation of the Cross Validation (CV) score, which measures the predictive power of the parametrisation, and identification of the correct ground states.

Cross validation score

In structural prediction, a model is judged by its ability to reproduce the data on which it is based and more importantly by its predictive power. The predictive power of the CE is usually estimated by the cross validation (CV) score [189]. This is analogous to the root mean square error, except that it is specifically designed to estimate the error made in predicting the energy

for structures not included in the fit:

$$(CV)^2 = n^{-1} \sum_{s=1}^n \left(E_s - \hat{E}_{(s)} \right)^2, \quad (3.43)$$

where E_s is the calculated energy of the structure, s , by *ab initio* methods, while $\hat{E}_{(s)}$ is the predicted value from fitting (n-1) other structural energies [190, 191]. The CV score is a statistic tool, whose formal proof was reported by Li [192].

The strongest feature is that the predictive power of a CE is estimated simply removing one point at time. This property relies on the assumption that the errors in the calculated energies are statistically independent. The CV score gives a measure of the predictive power of the fit obtained with all structures included [189, 192].

Ground states

For binary systems, plotting the formation energy of the structures as a function of the molar concentration, χ , is a convenient way to display the results, Figure 3.4. A particular structure contributes to the ground-state line if its formation energy is lower than the linear interpolation of the energies of the two ground state structures that bracket it. Using the example in Figure 3.4, the three structures $S0$, $S1$ and $S2$ with $\chi_{(S0)} < \chi_{(S1)} < \chi_{(S2)}$ are the lowest in energy at their individual concentrations, the structure $S1$ has to fulfill the condition:

$$\Delta E_f(S1) < \frac{\chi_{(S1)} - \chi_{(S2)}}{\chi_{(S0)} - \chi_{(S2)}} \Delta E_f(S0) + \frac{\chi_{(S1)} - \chi_{(S0)}}{\chi_{(S2)} - \chi_{(S0)}} \Delta E_f(S2) \quad (3.44)$$

to be a ground state at $\chi_{(S1)}$. If Equation 3.44 holds, a mixture of the phases $S0$ and $S2$ would be higher in energy than the structure $S1$. When the ground-state line is constructed, it is possible to check for structures that lie on or very close to it, the so called *configurationally excited states*.

The most important criterion that must be satisfied in validating the accuracy of a CE is the prediction of the correct ground states. The CV

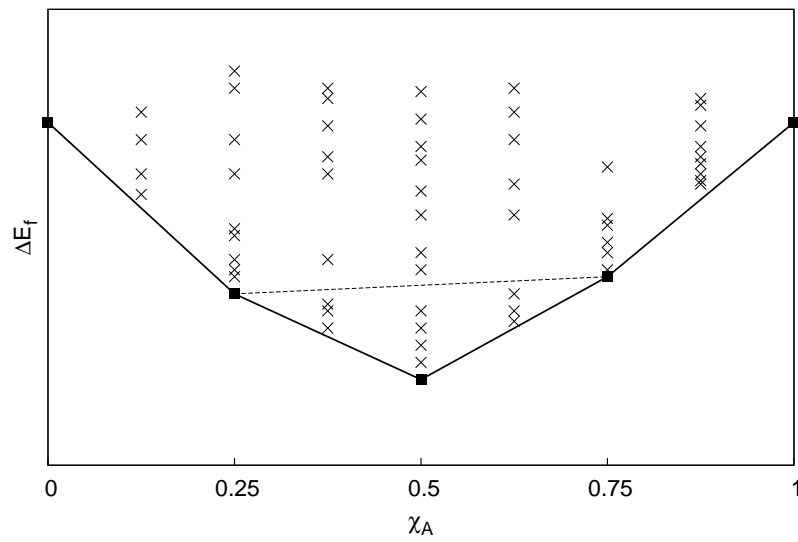


Figure 3.4: Schematic ground state representation of a binary system A_xB_{1-x} . Besides the pure elemental crystals, the ground state line is formed by three structure at concentration $\chi_A = 0.25, 0.50, 0.75$, namely $S0, S1$ and $S2$.

score criterion is focused on the optimisation of the absolute energy value. The ground states are determined by ranking of energies at constant concentration. A low CV score does not necessarily lead to the prediction of the correct ground state. The CE algorithm gives absolute preference to the set of clusters for the expansion that predicts the ground states according to the calculated energies. If no set of clusters predict the correct ground states for the set of structural energies provided, the common praxis is adding an extra weight, w , to chosen structures in order to predict the correct ground states. The weighted cross validation score is defined as follow:

$$(WCV)^2 = n^{-1} \sum_{s=1}^n \left(w_i (E_s - \hat{E}_{(s)}) \right)^2. \quad (3.45)$$

3.2.6 Implementations

Among the many implementations of the configurational thermodynamics packages, based on CE approach, there are some codes freely available, such the UNiversal CLuster Expansion (UNCLE) [193] and the Alloy Theoretical Automated Toolkit (ATAT) [194, 190, 191]. The author's choice fell on the `maps` code of the ATAT package because of its recent application on related substituted-carbon system, namely N-graphene [27].

The CE algorithm usually starts by computing the energies of a small set of structures. A convenient initial set is usually formed by structures with small unit cells, which make the calculation rapid. For the initial set of structural information and related energies, it is possible to calculate the ECIs, and then to use them for exploration of the configurational space to predict new ground states. The total energy of the newly predicted ground states are computed. Again the fitting process is performed and the process is repeated until the convergence criteria are satisfied. Any new cycle includes a new structural energy. As a consequence the expansion becomes progressively more accurate. An alternative approach is to start from a wide database of selected structures. In both cases the CE code needs to be interfaced to the code that performs the total energy calculations.

The MIT Ab-initio Phase Stability (**maps**) code included in the **ATAT** package implements a fitting process of ECIs to a set of structural energies. It is interfaced with many codes for total energy calculation, either based on first principles (**VASP** [147] and **ABINIT** [195]) or on semi-empirical approaches (**GULP** [196]). Chakraborty et al. [197] devised the interface between the all-electron density functional theory code **WIEN2k** [198] and the *maps* code. Among the outputs of the work contributing to this thesis is the extension of the **maps** code to the use with **CASTEP**, described in the next section.

Interfacing MAPS with CASTEP

The input parameters for the **maps** code describe the geometry of the parent lattice. Lattice parameters, atomic topological positions and occupancies are defined in the input file `lat.in`. **maps** automatically computes all the other pieces of information needed for the fitting. The parametrisation is an iterative process that gradually increases the number of structural energies in the fit and the accuracy of the fit itself. The algorithm of **maps** automatically determines the most appropriate structure and cluster to add to the fit, the structural information of which is written to the file `str.out` and subsequently used to generate the input for the total energy calculation.

In this work a script, named `runstruct_Castep`, has been developed. The script, by reading the file `str.out`, creates the appropriate input files for the **CASTEP** code and runs the calculation. In the case that the calculation is successful, it extracts the total energy to a file called `energy`. If not, an error message is written and provided to the user.

Two files are needed by the interface: `cell.wrap` and `param.wrap`. These files follow the syntax of the `.cell` and `.param` input files of **CASTEP**, respectively. The `cell.wrap` file contains cell constraints and pseudopotentials whilst the `param.wrap` file contains the parameters for the calculations. In addition to the existing **CASTEP** keyword, the file `cell.wrap` can contain two extra ones: `KPPRA` and `ASE-SYM`. The former defines the number of *k*-points per reciprocal atom. A utility enables the automatic construction of

k -point meshes from this single parameter defining the k -point density. If the `ASE-SYM` keyword is active, a Python script based on the ASE [199] package determines the space group of the initial structure; this is written into a file called `spacegroup` and a Crystallographic Information File (CIF) [200] is created inside the same folder where the calculation runs. The Python extension for ASE is required, namely the `spglib` module, which implements the space-group search algorithm of Grosse-Kunstleve [201]. The structural information (lattice parameters and atomic positions) must not be included directly in `cell.wrap` as the interface extrapolates this information from the `str.out` file to create a `.cell` file for CASTEP.

3.3 Lattice dynamics and structural stability

A significant part of the work presented in this thesis is based in the ab initio calculation of lattice dynamics. In general, phonon modes are calculated from first principles as a means to obtain other physical properties of a material, such as the thermodynamics of solids, or to compare with the spectroscopic measurements from Raman or neutron scattering. In this work, however, attention is focused on the phonon modes themselves as an indicator of the dynamic stability of particular arrangements of atoms. Material properties, either spectroscopic or thermodynamic, are outside the scope of this work and, therefore, are not taken into consideration.

3.3.1 The harmonic approximation

In the harmonic approximation, phonon modes are calculated under the fundamental assumption that atoms vibrate in a harmonic potential. The amplitude of atomic displacement is small compared to the interatomic spacings. Within the theory of lattice dynamics, the potential energy of a crystal, E , is assumed to be a function of the atomic positions.

Within the Born-Oppenheimer approximation [132], electrons are always in their ground state for any particular arrangement of atoms. Therefore the energy of the crystal can be expressed as a Taylor expansion of atomic displacements from equilibrium:

$$\begin{aligned}
 E = E_0 + \sum_{l\kappa\alpha} E'_\alpha(l\kappa)u_\alpha(l\kappa) + \frac{1}{2} \sum_{l\kappa\alpha} \sum_{l'\kappa'\alpha'} E''_{\alpha\beta}(l\kappa; l'\kappa')u_\alpha(l\kappa)u_\beta(l'\kappa') \\
 + \frac{1}{6} \sum_{l\kappa\alpha} \sum_{l'\kappa'\alpha'} \sum_{l''\kappa''\alpha''} E'''_{\alpha\beta\gamma}(l\kappa; l'\kappa'; l''\kappa'')u_\alpha(l\kappa)u_\beta(l'\kappa')u_\gamma(l''\kappa'') + \dots,
 \end{aligned} \tag{3.46}$$

E_0 is the energy at equilibrium; $u_\alpha(l\kappa)$ the displacement of atom κ in the l 'th unit cell in the direction α ; $E'_\alpha(l\kappa)$, $E''_{\alpha\beta}(l\kappa; l'\kappa')$ and $E'''_{\alpha\beta\gamma}(l\kappa; l'\kappa'; l''\kappa'')$ are the derivative of the energy with respect to atomic displacement evaluated at equilibrium. When the expansion of Equation 3.46 is truncated at second

order, it is called the *harmonic approximation*. The first derivative is zero for the equilibrium condition, where the net force on the atoms is zero:

$$E'_\alpha(l\kappa) = \left. \frac{\partial E}{\partial u(l\kappa)} \right|_0 = 0. \quad (3.47)$$

The second order derivatives are commonly known as the interatomic force constants:

$$E''_{\alpha\beta}(l\kappa; l'\kappa') = \left. \frac{\partial^2 E}{\partial u(l\kappa) \partial u(l'\kappa')} \right|_0. \quad (3.48)$$

It is a measure of the negative force in the α direction on atom l per unit length, when atom l' is moved in the β direction, and all other atoms are at equilibrium positions.

The harmonic approximation is used to obtain information about the phonon modes of a crystal. The accuracy is sufficient to describe most of the lattice dynamical effect of interest. However, further terms in the summation are required if anharmonic terms play a dominant role. This is often the case at elevated temperatures, manifest most notably in the lattice expansion.

The equations of motion for the lattice can be derived by calculating the forces on each atom within the harmonic approximation, then substituting those forces into Newton's second law:

$$F_\alpha(l\kappa) = m_{l\kappa} \frac{\partial^2 u_\alpha(l\kappa)}{\partial t^2} = - \sum_{\alpha\beta\gamma} E''_{\alpha\beta}(l\kappa; l'\kappa') u_\beta(l'\kappa'). \quad (3.49)$$

Assuming Born-von Kármán periodic boundary conditions [126] and, hence, a periodic plane-wave solution:

$$u_\alpha(l\kappa) = \frac{1}{\sqrt{m_\kappa}} e_\alpha(\kappa) e^{i(\mathbf{q}\cdot\mathbf{r}-\omega t)}. \quad (3.50)$$

That leads to:

$$\omega^2 e_\alpha(\mathbf{q}; \kappa) = \sum_{\alpha,\beta} D_{\alpha,\beta}(\mathbf{q}; \kappa\kappa') e_\beta(\mathbf{q}; \kappa') \quad (3.51)$$

$e_\alpha(\mathbf{q}; \kappa)$ represents the eigenvectors, which describe the relative motion of atom κ in a phonon with wavevector \mathbf{q} .

The dynamical matrix is the mass-reduced Fourier transform of the force constant matrix:

$$D_{\alpha,\beta}(\mathbf{q}; \kappa\kappa') = \frac{1}{\sqrt{m_\kappa m_{\kappa'}}} \sum_{l'} E_{\alpha\beta}(l\kappa; l'\kappa') e^{i\mathbf{q}\cdot\mathbf{x}(l')} \quad (3.52)$$

The sum runs over l' only, because the force constant matrix depends on the difference between cell indices and not on each cell index individually.

3.3.2 Implementations of lattice dynamics

In the harmonic approximation, the central problem is obtaining the second derivatives of the energy that represents the interatomic force constants. There are a number of methods for achieving this. Within first principles energy models, the two most widely used are the linear response [202] and the, so called, finite-displacement supercell method [203].

The linear response method allows one to evaluate the derivatives of the energy in relation to a perturbation, namely atomic displacement. First-order derivatives of the wavefunction and charge density are directly calculated. According to the “2n+1 theorem”, the knowledge of the derivatives of the wave functions up to order n allows one to calculate the derivatives of the energy up to order 2n+1. In this context, its usefulness derives from the fact that the second-order derivatives of the total energy can be obtained directly from the first-order derivatives of the wave functions. In principle, the third order derivatives can also be calculated, in the case that anharmonic effects are of interest. One of the most significant advantages of the linear response method is that responses to perturbations of different wavelengths are decoupled. This allows the calculation of normal-mode frequencies at arbitrary wave vectors, thus avoiding the use of supercells.

In the supercell method, the frequencies of selected phonon modes can be calculated from the forces acting on atoms produced by finite, periodic, displacements of a few atoms in an otherwise perfect crystal at equilibrium. The supercell method is based on the direct evaluation of Equations 3.48 and 3.49. By considering many such displacements, one creates a linear set

of equations in unknown force constants and atomic forces. The force acting on an atom is related to the displacement of all other atoms. The values of the force constant matrices are obtained through a least-squares Born-von Kármán fit [126].

The linear response method is more accurate than the supercell method for pointwise calculations of phonon dispersion curves. Performing pointwise phonon calculations with the linear response method, the dynamical matrix is calculated directly without missing any force constants. In contrast, the supercell method always truncate the force constant range.

The supercell method can include spurious anharmonic terms and mirror image effects that introduce errors into force constant fitting. However, the main advantage of the supercell method is its relative simplicity; it can be straightforwardly implemented within any total energy method that calculates forces on atoms. This enables the use of ultrasoft pseudopotentials, which are of fundamental importance for the systems that are studied in the present work. By contrast, the linear response method, as implemented in CASTEP, is currently limited to the use of norm-conserving pseudopotentials.

Despite its drawbacks, the supercell method has been proven to give accurate results. Furthermore, phonon calculations based on both the linear response and supercell methods have often been demonstrated to give a similar quality of result [204]. In the literature, the vibrational modes of carbon-based materials have, by-and-large, been investigated with the supercell method, see for instance [95, 27].

3.3.3 Structural stability

In this section, strategies for obtaining information about the structural stability of crystalline materials within the theory of computational lattice dynamics is reviewed. The subject is introduced with the well-known case of static equilibrium in classical mechanics, which is determined, for a given system of particles, by the condition that the net force on each particle is permanently zero.

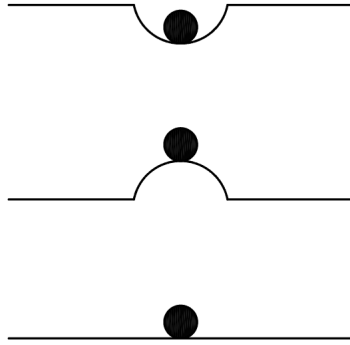


Figure 3.5: Graphical representation of stable (top), unstable (center), indifferent (bottom) equilibrium of a ball on a surface.

Conservative forces, F , can be expressed as the gradient of a scalar function, called potential energy. At equilibrium, the first derivative of the potential energy along any direction must be zero, indicating that no net force is present. Further information on the equilibrium stability can be determined by examining the second derivatives. For a mono-dimensional system, the following three cases can be distinguished:

- positive second derivative: the equilibrium is defined “stable”; for a small perturbation, the system restores the equilibrium;
- null second derivative: the equilibrium is “indifferent”; if perturbed, the system will stay in the new state that is characterized by constant energy;
- negative second derivative: “unstable” equilibrium; if the system is perturbed, the resulting forces cause it to move even farther away from equilibrium.

For 2- or 3-dimensional systems, different directions can have different deriva-

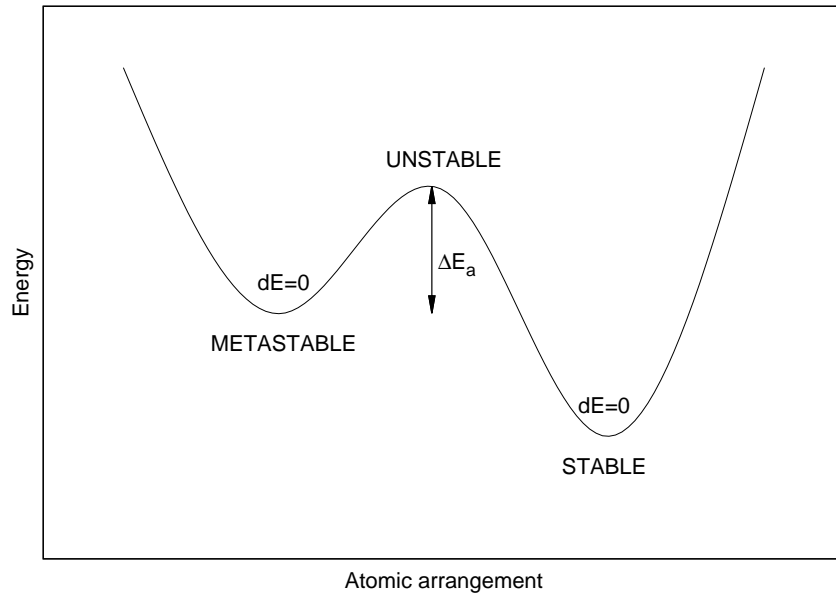


Figure 3.6: Illustration of stable, metastable and unstable states of equilibrium using energy against atomic arrangement. ΔE_a is the activation barrier.

tive of the potential energy, for instance the so-called saddle-point can be present.

Metastability

Many phenomena, common in life, are characterised by metastability, which is the behaviour of certain physical systems that can exist in long lived states that are not the system's most stable state in term of energy. Typical examples are avalanches and sparkling water. In materials science, diamond and the Martensitic phase of steel [205] are probably the most famous cases. The metastable state must be characterised by local stable equilibrium for the long-lived state to be allowed.

From the atomistic point of view, the equilibrium state of an arrangement of atoms (bulk solids, surfaces, nano-forms, molecules) have typologies similar to the classical mechanic case.

Atomistic calculations: equilibrium stability

Within the remit of atomistic calculations, a crystal structure can be considered to be in equilibrium when the net force on each atom is negligible.

Further information on the local potential energy landscape (therefore on the nature of the stability of the equilibrium structure) can be obtained by calculating the phonon dispersion spectrum. Essentially, this involves calculating the dynamical matrix, diagonalisation of which yields the eigenvalues, the square-roots of which are the mode frequencies. An imaginary frequency is indicative of an unstable equilibrium. If phonon modes have positive eigenvalues, the equilibrium is stable: the structure lies on a local minimum of the potential energy and therefore the structure can be considered a possible metastable phase, regardless of the magnitude of the formation energy.

Conventionally the imaginary frequencies are plotted as a negative number (of equal modulus) in the phonon dispersion spectrum. This number gives the rate of exponential growth of the instability [126].

An additional application of the phonon approach that must be mentioned, in spite of it not being employed in this thesis, is the *ab initio* determination of transition states [206]. A stable or metastable atomic system lies on a local minimum, meaning that the energy increases as atoms are displaced from their equilibrium positions; a transition state lies at a saddle-point in the energy landscape, therefore all vibrational frequency are positive except for the vibrational normal mode that corresponds to the reaction coordinate.

In summary, phonon mode calculations are an invaluable method for evaluating locally the potential energy. The criterion that is applied in this work for phase stability is the absolute absence of phonon modes with negative eigenvalues.

Chapter 4

Glitter: a possible metastable carbon phase

Despite the ability to synthesise n-diamond in many different ways (Section 2.2), the crystal structure of n-diamond remains unclear. The structural identification has been challenging, because usually small amounts of nanoforms are produced. Nanoclusters and films are the most common form of n-diamond. The only synthesis known to produce n-diamond in macroscopic amounts is a solid state synthesis involving solid catalysts [67]. Until now, several models have been proposed for the structure of n-diamond, but none is completely convincing.

The work reported in this Chapter focuses on the comparison of the dynamical stability of tetragonal carbon, known as glitter, with other structures that have been proposed in the literature for n-diamond. The results reported are mainly based on recent article by Baldissin and Bull [73].

The investigation of the dynamical stability of the crystallographic arrangements proposed for n-diamond have been performed in the pressure range 0-30 GPa. A number of authors have investigated the stability of proposed n-diamond structures in terms of mechanical stability [207, 208], expressed in terms of violation of Born conditions [209]. Mechanical instability represents a long wavelength limit of the more general instability related to the occurrence of phonon modes with negative eigenvalues [210]. Whilst the mechanical stability has largely been calculated at ambient pressures,

in this work wide a range of pressure has been taken into account. Not limiting the investigation to standard pressure is important because many diamond-like materials are synthesised under high pressure conditions [64]. It is important to underline that pressure can have a dramatic effect on the vibrational properties of a crystal structure.

Many other 3-dimensional carbon allotropes have been theoretically predicted in the last decades. Bucknum and co-workers proposed other 3,4-connected carbon nets, namely isoglitter [211], hexanogite [212] and trigohexagonite [213]. Although these structures are not directly related to n-diamond, a study of their dynamical stability at $P = 0$ GPa is presented in this work.

The aim of the current Chapter is to shed some light on the stability of the structures that have been proposed in the literature and, therefore, the possibility of them existing as free-standing materials.

4.1 Computational details

The stability of the proposed structures has been evaluated in relation to both atomic forces and phonon eigenvalues, calculated using the *ab initio* code CASTEP [173], as described in Section 3.3.3. The exchange-correlation functional of Perdew and Wang (PW91) with generalized-gradient corrections is employed [141].

The electron-ion interactions are described using ultrasoft pseudopotentials [171]. The pseudo-wave functions are expanded on a plane wave basis set using a 500 eV kinetic energy cut-off. The Brillouin zone is sampled by Monkhorst-Pack k -point grids [214] assuring 0.04 \AA^{-1} k -point separation in the Brillouin zone. A BFGS algorithm [215] is used to optimise atomic positions and lattice parameters simultaneously until the *ab initio* forces and stresses, calculated by the Hellmann-Feynman theorem [216], become negligible (forces are below 0.001 eV/\AA and stresses below 0.01 eV/\AA^3). Geometry optimisations are performed at 0 K for a given pressure. Phonon dispersion

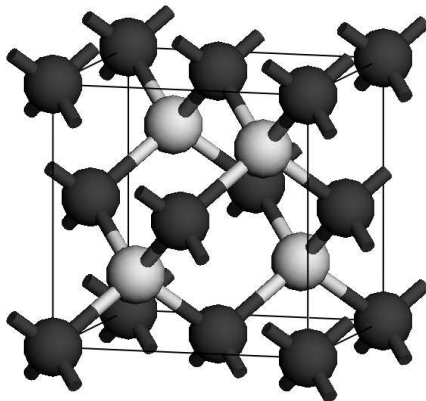


Figure 4.1: Conventional representation of cubic diamond: atoms in sublattice P0 (0,0,0) are represented by dark grey spheres, atoms in position P1 ($1/4, 1/4, 1/4$) are represented by light grey spheres. Most of the crystallographic models, that have been proposed, include a modified sublattice, P1, retaining pristine sublattice P0.

is calculated using the supercell method [203, 217].

4.2 Instability of c-diamond-based structures

The main source of structural information for n-diamond in the literature is from X-ray or electron diffraction. The patterns that have been recorded match with the one of cubic diamond apart from the presence of additional reflections, see Section 2.2. In an attempt to match the Bragg reflections of cubic diamond and the otherwise forbidden reflections, crystallographic arrangements based on modifications of the cubic diamond structure have been proposed.

The cubic diamond structure can be rationalised as being formed by two distinct sublattices. Figure 4.1 shows the two sublattices, here called P1 and P0. The modifications that have been proposed include either a translation of sublattice P1 away from high symmetry positions (Section 4.2.1), or the introduction of vacancies (Section 4.2.2), or hydrogen substitutions (Section

4.2.3). A further model based on cubic diamond but having a modification of both sublattices [218] is also included. This stratagem allows the overall cubic symmetry to be maintained whilst introducing the extra reflections that are the fingerprint of n-diamond.

It is demonstrated that, on the basis of the current methodology, all these models are dynamically unstable and, therefore, must be ruled out as possible metastable phases.

4.2.1 Models based on translation of the sublattice P1 to general position

On the basis of transmission electron microscopy (TEM) patterns, Hirai and Kondo [26], proposed that n-diamond is a modified form of cubic diamond composed by distorted hexagonal-ring-planes. Three rhombohedral structures in space group $R3$, have been proposed with lattice parameter $a = 3.57 \text{ \AA}$, $\gamma = 90^\circ$ and internal coordinates of $(0,0,0)$, $(0.5,0.5,0)$, (x,x,x) , $(0.5+x, 0.5+x, x)$, with $x=\{0.333, 0.4, 0.416\}$. The three rhombohedral structures are called here H1, H2 and H3. On the basis of Hirai's models, Wen et al. [67] proposed a further model with $x=0.355$. This new arrangement was suggested because it produced a better match with the experimental data from X-ray diffraction (XRD). According to this model, n-diamond would have an interlayer distance between hexagonal ring planes of 2.07 \AA . These models are all variations of the cubic diamond structure where a C sublattice has been rigidly translated to general position. In these models, the crystal cell is forced to be cubic to match the diffraction pattern of n-diamond.

In the present work, for hydrostatic pressures in the range 0-100 GPa, the degree of freedom has been relaxed to find the minimum energy geometry and atomic forces. Figure 4.2 shows the absolute value of the atomic force as a function of pressure. It can be seen that increasing the pressure does not stabilise the structures. For pressures higher than 15 GPa, Wen's structure

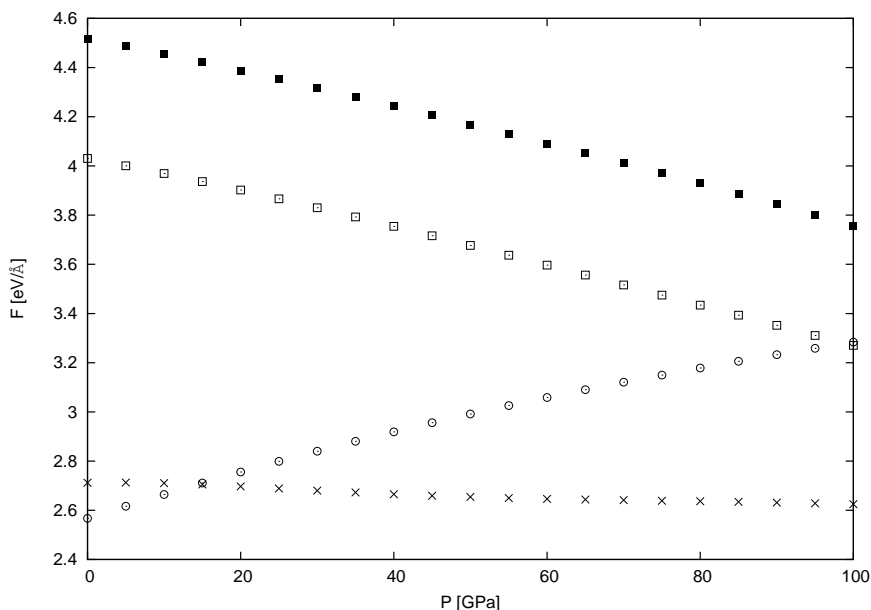


Figure 4.2: Atomic force modulus calculated in the present work for Wen's model (crosses) [67], and for Hirai's models, H1 (open circles), H2 (open squares), H3 (solid squares) [26].

has atomic forces with smaller moduli than Hirai's models. Nevertheless, it can not be considered as a possible metastable phase, because forces are far from being negligible indicating the tendency of atoms to move from the assigned position to a lower energy configuration. For symmetry, atomic forces have the same modulus and lie in the same direction, pushing the atoms of the translated sublattice (P1) back to the cubic diamond arrangements.

4.2.2 Models with vacancies

In order to produce the extra reflections to the diffraction pattern of cubic diamond, models with the P1 sublattice completely (fcc model) or partially (defective diamond model) substituted by vacancies, have been proposed.

fcc-carbon

The fcc-carbon model was proposed by Jarkov et al. [219], who observed the consistency with Bragg reflections from transmission electron microscopy (TEM). This model was also proposed by Konyashin et al. [220], comparing the lattice parameter of the fcc carbon computed by linear combination of atomic orbitals (LCAO) with those measured by TEM of the new carbon modification found while treating the surface of diamond in a hydrogen plasma. The fcc model is derived from the cubic diamond structure by introducing vacancies in the P1 sublattice whilst retaining atoms in the P0 sublattice. Using density functional theory calculations, however, Pickard et al. [76] showed that the calculated lattice parameter is not consistent with the experimentally measured one at ambient pressure.

According to phonon calculations reported here, for the fcc model there are phonon modes whose calculated frequencies have negative eigenvalues at $P = 0, 10, 20,$ and 30 GPa, clearly indicating that the structure is unstable at any pressure that has been considered. One can conclude that this model represents an unstable arrangement of atoms and therefore does not represent a possible local minimum in the energy landscape. Figure 4.3 shows the phonon dispersion from the fcc model at 0 GPa.

Defective diamond

The defective diamond model was proposed to explain the ageing of n-diamond samples synthesised according to Wen et al. [67]. The proposed structure can be derived from cubic diamond by imposing a fractional occupancy, χ , on C atoms in the P1 sublattice ($0 < \chi_{C(P1)} \leq 0.25$) [221]. During ageing (up to 180 days), the observed XRD intensities of all the peaks associated with n-diamond significantly weakened, indicating that n-diamond is a metastable phase. According to this model, the structure of n-diamond is suggested to change from fcc-like to diamond-like through an increase of carbon occupancy in P1.

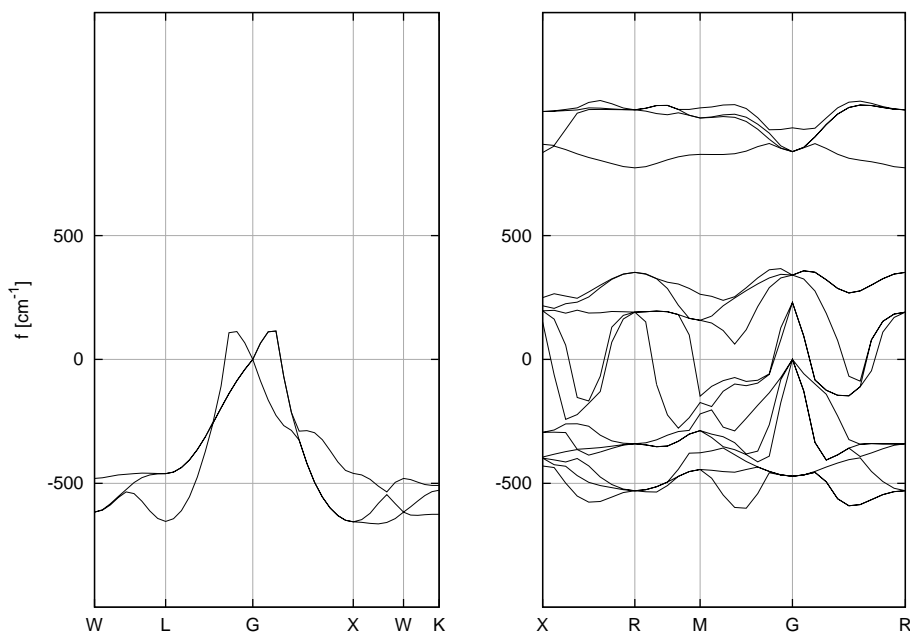


Figure 4.3: Phonon dispersion of fcc model (on the left) and defective diamond with SG P-43M (on the right) at 0 GPa: modes with negative eigenvalues clearly indicate the structure instability.

This model is not represented by an ordered structure, as in the previous case; instead it is characterised by substitutional disorder. For the investigation of vibrational properties in such systems, a common approach is to map the disordered system onto a supercell with a similar stoichiometric composition. Using as a parent lattice the $2 \times 2 \times 2$ supercell of the primitive cell of cubic diamond, an arrangement was built to maximize both the symmetry and the distance between carbon atoms in the P1 sublattice. For the calculation reported here, the possible configurations have been generated using a structure enumeration algorithm [222] and the resulting symmetry has been calculated using the tools of the ASE package [199] with a space-group search algorithm extension [201]. The structure displayed in Figure 4.4 represents the one in which the vibrational investigation has been performed. According to the calculations presented in the present work, the defective diamond model is unstable at any considered pressure. Figure 4.3 shows the phonon

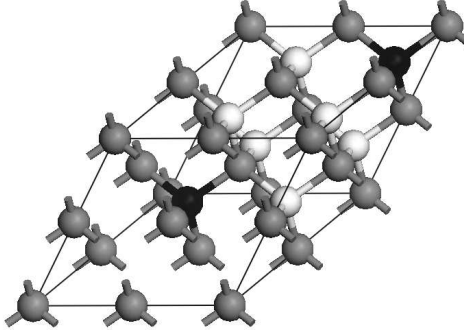


Figure 4.4: The defective diamond model used for phonon calculations (SG P-43M): C in P0 (grey), C in P1 (black), vacancy in P1 (white). Concentration of C atoms in P1 is 25 at.% as the upper limit suggested in Ref. [221].

dispersion calculated at 0 GPa. Phonon modes whose calculated frequencies have negative eigenvalues are present.

4.2.3 Models with hydrogen inclusions

To generate the extra reflections characteristic of the n-diamond structure, an alternative way to vacancy inclusion is hydrogen inclusion. Due to the small scattering cross-section relative to heavier elements, hydrogen is generally undetectable with conventional X-ray diffraction techniques [223]. Therefore, its effect on diffraction patterns would be similar to the inclusion of vacancies. To this end, two models have been proposed: a hydrogen-doped cubic diamond model [218] and a carbon-hydrogen zincblende compound [66].

Hydrogen-doped cubic diamond

Wen et al. [218] proposed that hydrogen can substitute carbon in both the P0 and P1 positions. DFT calculations based on the virtual crystal approximation (VCA) [224] were compared with the experimental XRD pattern of Fe-catalysed n-diamond [67]. According to Wen et al. [218], at H concentrations less than 19 at.%, H-doped diamond is mechanically stable and at

4 at.% the optimised XRD pattern matches the experimental data.

This model is characterised by substitutional disorder, therefore the same approach as in Section 4.2.2 has been employed. Using as a parent lattice the $2\times 2\times 2$ supercell of the primitive cell of cubic diamond, an arrangement at concentration $\chi_H=0.0625$ was built to maximize both the symmetry and the distance between defects, see Figure 4.5. The model presents hydrogen substitution in the (0,0,0) position. This model has 15 carbon atoms and one hydrogen atom in the unit cell. The $4\times 4\times 4$ supercell at $\chi_H=1/128$ has also been investigated, in which there are 127 carbon and 1 hydrogen atom. The dimension of this model makes phonon calculations computationally expensive, therefore the investigation has been limited to pressures of 0 and 40 GPa.

In the present work no phonon calculations without negative eigenvalues have been found. Figure 4.6 displays the Phonon PDOS of the $2\times 2\times 2$ and $4\times 4\times 4$ supercells. It is clearly shown that instability is mainly due to hydrogen atoms. At the lower H concentration ($4\times 4\times 4$ supercell) the backbone of carbon atoms is stable; conversely at $\chi_H=0.0625$ it is unstable. For the $4\times 4\times 4$ supercell the presence of populated states related to unstable phonon modes which involve carbon atoms is minimal.

It is well-known that diamond films produced by chemical vapour deposition (CVD) techniques in a hydrogen-rich atmosphere have both a high hydrogen content and lattice vacancies [225]. In addition, natural Argyle diamonds have high a hydrogen content [226]. In hydrogen-doped diamond, much of the hydrogen is located at the boundaries between diamond grains, or in non-diamond carbon inclusions, although within the diamond lattice itself, hydrogen-vacancy complexes are present, whereby a hydrogen atom is bonded to one of the carbon atoms in the vicinity of the vacancy [225, 227]. It is concluded here that, if there are hydrogen inclusions in the diamond structure, dopant atoms do not occupy carbon positions.

Some words must be spent on the possible application of the Virtual Crystal Approximation (VCA) to carbon-hydrogen system as an alternative

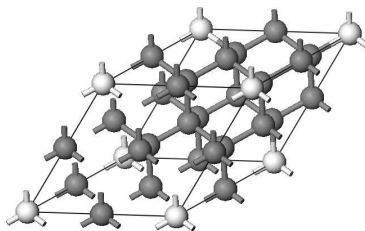


Figure 4.5: Structure used for phonon calculations in hydrogen-doped carbon: C (gray), H (white); the model is based on a $2 \times 2 \times 2$ supercell of c-diamond (SG F-43M), $\chi_H=1/16$. A further model based on a $4 \times 4 \times 4$ supercell of c-diamond (SG F-43M) has also been employed, $\chi_H=1/128$.

to the approach adopted here. The VCA allows one to handle configurationally disordered systems at relatively low computational cost [228]. The potentials, which represent atoms of two or more elements, are averaged into a composite atomic potential, having the advantage that a single configuration with a small unit cell represents the disordered system. However some properties that depend on the local environment cannot be reproduced. The VCA ignores any possible local distortion and assumes that on each potentially disordered site there is a virtual atom that interpolates between the behaviour of the actual components. This approach cannot be expected to reproduce the finer details of the disordered structures.

In hydrogen-substituted carbon systems, the size mismatch between carbon and hydrogen causes local distortions that cannot be captured by the VCA approach, as an averaged potential is applied. By contrast, the instability due to the local environment is evidenced by the approach applied in this work, coupling symmetry analysis and phonon calculations.

Carbon-hydrogen zincblende compound

Studying the intensity ratio of forbidden and allowed diamond reflections in XRD patterns of n-diamond produced by CVD, Cowley et al. [66] proposed that n-diamond includes hydrogen atoms in the P1 sublattice. Experimental observations were supported by total energy calculations performed within

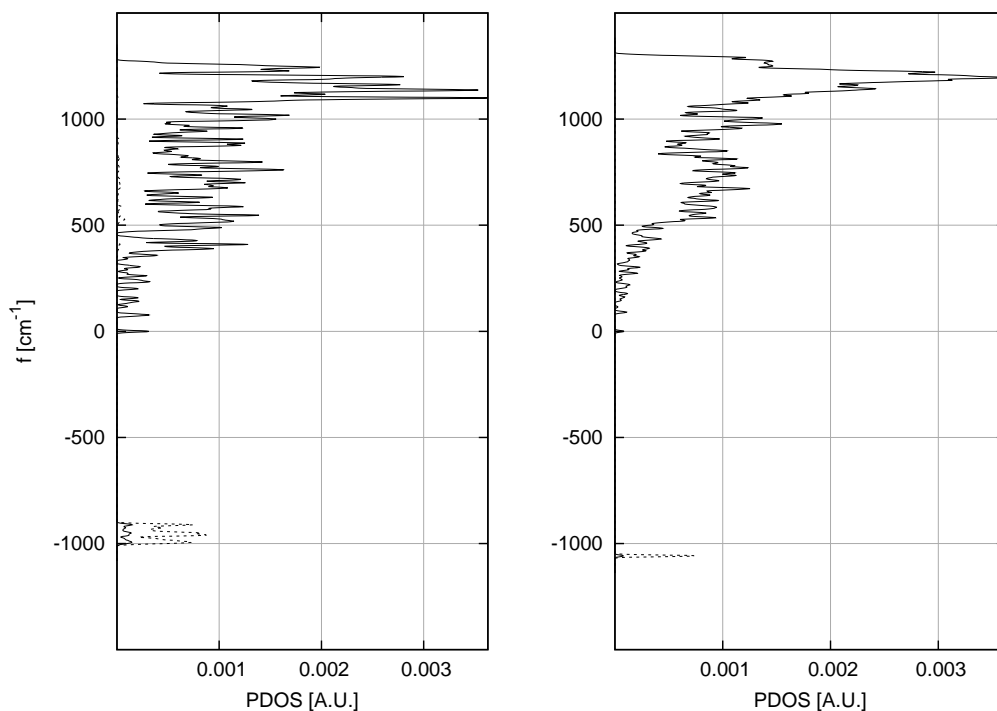


Figure 4.6: Phonon partial density of states (PDOS) of H-diamond: carbon atoms (continuous line), hydrogen atoms (short dashes): on the left, model with $\chi_H=1/16$; on the right, model with $\chi_H=1/128$. For both computational models, it is clearly shown that modes with negative eigenvalues are mainly related to hydrogen. For the model at lower hydrogen concentration the carbon backbone is much more stable.

the projector augmented wave (PAW) method in the framework of DFT. This model can be considered a limiting case of the previous one where one carbon sublattice is completely substituted by hydrogen.

According to the present work, this model has phonon modes with negative eigenvalues at any considered pressure, denoting structural instability.

4.2.4 Summary of c-diamond-based structures: coordination and hybridisation

The consistency of coordination and hybridisation plays an important role for a proper overlap of the atomic orbitals; this concept is central in both organic and inorganic chemistry. A proper overlap allows the formation of strong bonds, leading to stable structures.

Interestingly, this feature is lacking for any structure derived from modification of cubic diamond. Excluding *a priori* Hirai's and Wen's models that are not equilibrium structures, the proposed models considered up to this point are characterised by *exotic* coordination numbers: in fcc carbon C is 12-coordinated, in defective diamond many sp^3 carbon are not 4-coordinated; in hydrogen-doped and H-zincblende model hydrogen is 4-coordinated.

These models are clearly built-up to satisfy the matching of the simulated diffraction pattern with the experimental ones. However they do not take into account a key-point in condensed matter physics and chemistry: the chemical bonding.

4.3 Dynamical stability of glitter

Bucknum and Hoffman proposed a 3,4-connected hybrid structure [24], that respects the consistency between hybridisation and coordination, as discussed in Section 2.2.

In this work, the phonon modes have been calculated at pressures of 0, 10, 20 and 30 GPa. For all but the highest pressure, the eigenvalues have positive values throughout the Brillouin zone, giving real frequencies and indicating the dynamical stability. Figure 4.7 display the phonon dispersion of glitter at 0 GPa. At 30 GPa, negative eigenvalues are observed, resulting in the frequency of one of the acoustic bands becoming imaginary. Examination of the modes indicates that both the sp^2 and sp^3 atoms are involved in the instability.

The stability of glitter lies in the fact that the structure does not have

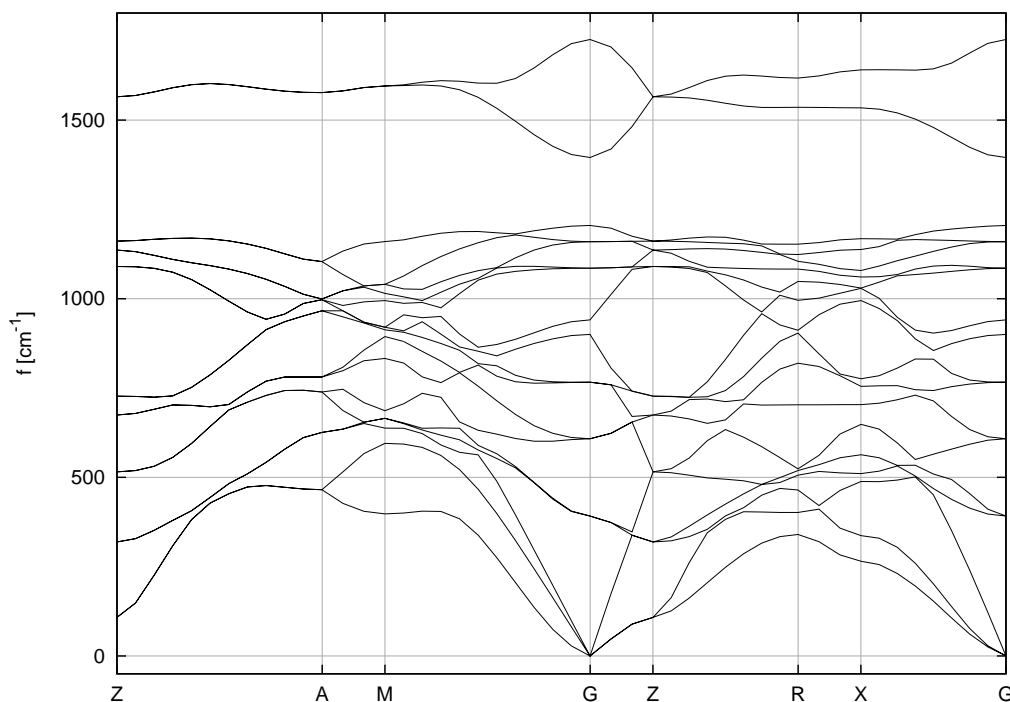


Figure 4.7: Phonon dispersion of glitter at 0 GPa: it is clearly shown that modes with negative eigenvalues are not present.

exotic coordinations: atoms having a geometry due to sp^3 hybridisation are tetra-coordinated and those having a geometry due to sp^2 hybridisation have triple coordination. However glitter presents high formation energies: Table 4.1 lists the formation energy of the glitter structure with zero point energy (ZPE) corrections. They are broadly in agreement with previously reported values based on LDA functional with no ZPE corrections [76].

A high formation energy is usually an indicator of internal stress. Although the glitter unit cell is not very distorted under isotropic compression (at $P = 0$ GPa, $c/a = 2.301$, and at $P = 30$ GPa $c/a = 2.336$, Table 4.1), distortion affects the chemical bonding: at 30 GPa, the tetragonal-trigonal-tetragonal angle is compressed to 114.54° , very far from the ideal sp^2 geome-

Table 4.1: Carbon glitter: lattice parameters, vibrational corrections, formation energy and resume of dynamical stability. Formation energy include vibrational corrections. The reference state is cubic diamond (SG Fd-3m). The vibrational energy contribution, ΔE_{vib} , has a positive effect on stabilizing the structure with respect to c-diamond.

	Pressure			
	0 Gpa	10 GPa	20 GPa	30 GPa
a [\AA]	2.6025	2.5710	2.5436	2.5194
c [\AA]	5.9872	5.9507	5.9172	5.8863
Dynamics	Stable	Stable	Stable	Unstable
ΔE_{vib} [eV/atom]	-0.021	-0.022	-0.023	—
ΔE_f [eV/atom]	0.432	0.433	0.438	—

try, which implies an angle of 120° . It is likely that the extra bond strain due to high pressure, forces the atomic arrangement beyond its breaking-point.

4.4 Metallic nature of glitter

Bucknum and Hoffman calculated the electronic structure of glitter using the extended Hückel method [24]. The interaction of the π -orbital of carbon in trigonal positions separated by $\sim 2.5 \text{ \AA}$ leads to a substantial dispersion of the highest occupied and the lowest unoccupied band. In the present work, the electronic band structure has been calculated with the modern B3LYP exchange correlation functional [155] and norm-conserving PPs [229]. The system is metallic, exhibiting band overlap at the Fermi level, see Figure 4.8. The PDOS highlights that states at the Fermi level are due to the p orbitals of trigonal carbon atoms, confirming the metallic nature of the structure due to overlap of stacking ethylene units [230].

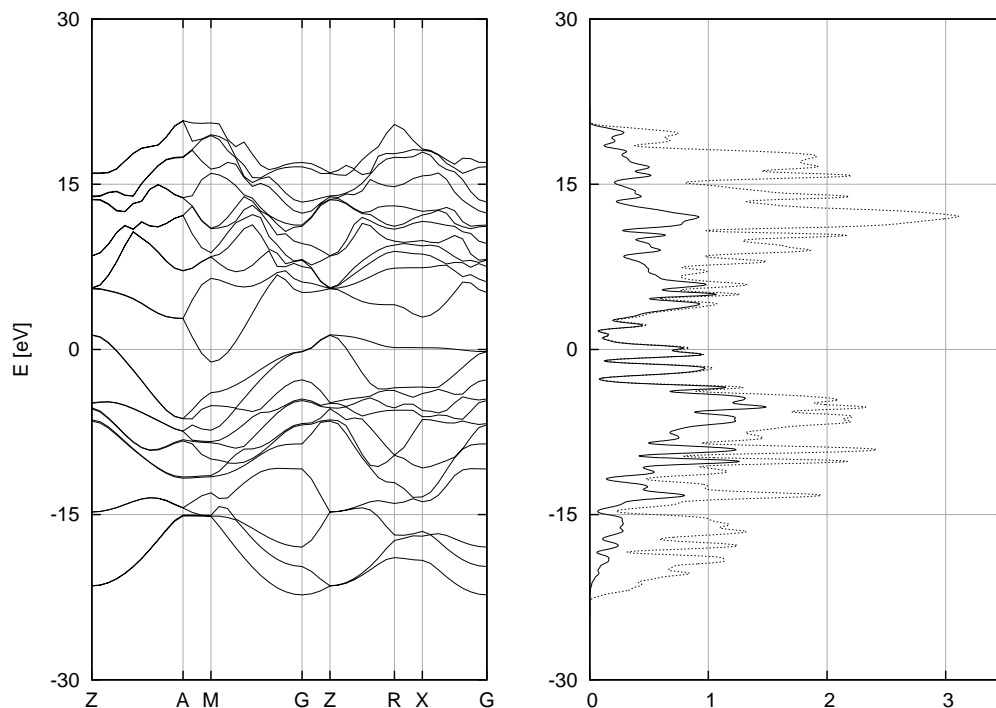


Figure 4.8: Electronic structure of glitter calculated with B3LYP functional: band structure on the left and electronic DOS on the right. The states of p orbitals of trigonal carbon atoms are displayed with a continuous line, the full DOS by short dashes line.

4.5 Bulk modulus of glitter

In order to compute the bulk modulus of glitter, total energies were calculated using the PAW [231, 232] method as implemented in the VASP code [147] and parameterised in terms of the equation-of-state proposed by Alchagirov et al. [233], as implemented in the Atomic Simulation Environment (ASE) [199].

According to the calculations presented here, glitter would be a mechanically stiff material: the fitted bulk modulus is 350 GPa, see Figure 4.9. Although the bulk modulus does not necessarily correspond to the practical hardness of the material, it reflects the ideal stiffness near equilibrium positions under isotropic compression. According to Cohen semi-empirical

theory, glitter was expected to surpass cubic diamond in its intrinsic strength [24]. It is however counter-intuitive that a structure containing ethylene unites stacked at a separation of $\sim 2.5 \text{ \AA}$ would be stiffer than diamond that has all atoms tetra-coordinated.

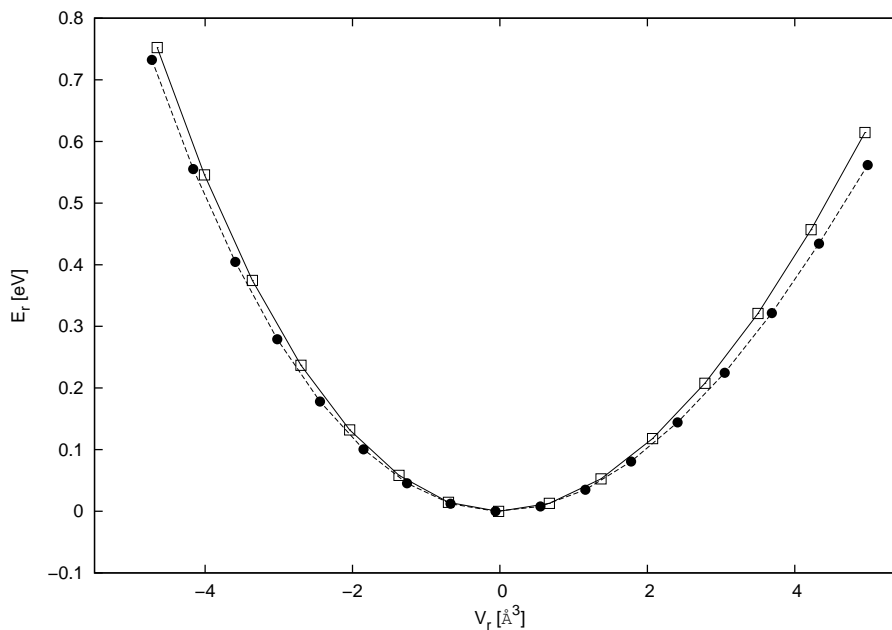


Figure 4.9: Comparison of compressibility of diamond (open squares) and glitter (solid circles): the fitted bulk modulus is 431 GPa for diamond and 350 GPa for glitter. The plot has as reference the equilibrium volume and equilibrium energy of the relative structure: $V_r = V - V_{eq}$ and $E_r = E - E_{eq}$, where V_{eq} and E_{eq} are respectively the volume and the energy at equilibrium.

4.6 Isoglitter, hexagonite and trigohexagonite

Among the many possible novel carbon arrangements that have been theoretically predicted in the last decades, three other structures in particular attracted author's attention. Bucknum and co-workers proposed three carbon structures having 3-connected and 4-connected carbon atoms: isoglitter [211], hexanogite [212] and trigohexagonite [213], Figure 4.10.

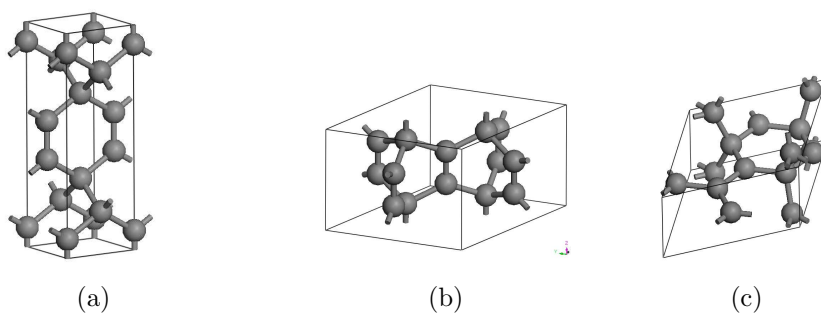


Figure 4.10: (a) Isoglitter; (b) Exagonite; (c) Trigoexagonite.

Isoglitter is a structural relative of tetragonal glitter, built upon the 1,4-cyclohexadieneoid motif. Building blocks are coordinated in a parallel fashion, while in glitter they are coordinated orthogonally to each other.

Hexagonite was proposed as a hypothetical organic zeolite. This structure presents hexagonal channels of $\sim 5 \text{ \AA}$. The structure was produced by elaborating the molecule bicyclo[2.2.2]-2,5,7-octatriene (barrelene) in three dimensions.

Trigoexagonite is a complex structure having cyclopropane-like substructures of the lattice, arranged in a triad, and 1,3,5-trimethylene-cyclohexane-like and trimethylene-methane-like units.

For a detailed description these structures, the reader is referred to the relevant literature [211, 212, 213].

In this work the three structure have been investigated, testing the vibrational stability at 0 K and 0 GPa. As shown in Figure 4.11, they can not be considered possible carbon allotrope because of the presence of modes with negative eigenvalues.

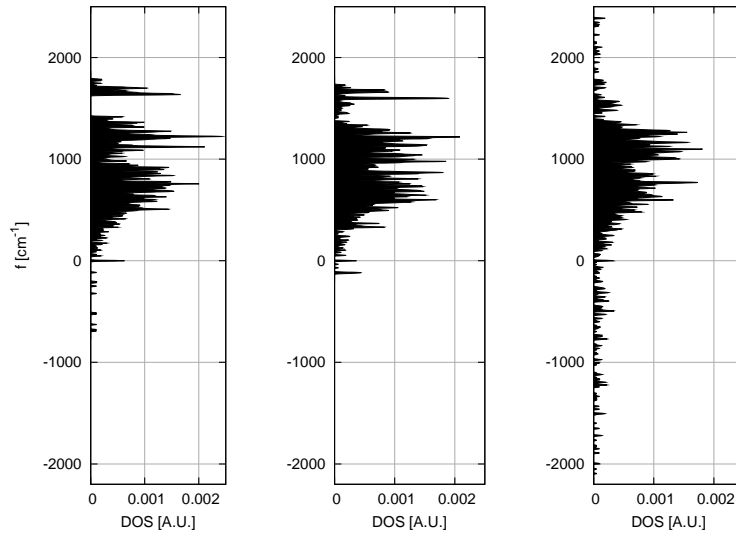


Figure 4.11: Phonon density of states (DOS) of isoglitter (on the left), hexagonite (center), trigohexagonite (on the right) at 0 GPa: modes with negative eigenvalues are present for each proposed crystallographic arrangement.

4.7 Chapter conclusions

Among the arrangements proposed for n-diamond, glitter is the only one that is stable with regards to the dynamics at 0, 10 and 20 GPa, whereby phonon modes with negative eigenvalues are not present.

Moreover glitter presents the following three characteristics:

- it is metallic;
- it is a stiff material;
- its diffraction pattern is consistent with the experimental one of n-diamond [77].

Glitter seems to be the ideal candidate for n-diamond. However, it has high formation energy, Table 4.1, and there has been much speculation on its kinetic stability [25].

Wen et al [67] reported that n-diamond synthesised from Fe-catalysed carbon black gradually transformed to other structural phases during the ageing process (90-180 days), implying that n-diamond is a metastable phase. Supposing that n-diamond has the glitter structure, it is possible that in the presence of defects or poorly crystallised grains, it will gradually decompose to more stable phases.

It must be underlined that many structures that have been proposed in the literature until now for carbon phases are deficient in terms of stability: the structures based on cubic-diamond and other 3-,4-connected structure proposed by Bucknum and co-workers are not stable. In the author's opinion, an extended investigation on the stability of the structures proposed in the carbon literature would lead to ruling-out many arrangements that have been suggested purely on the basis of chemical intuition. This would be not just an exercise of application of theoretical tools but would guide experimental researchers toward the synthesis of novel carbon allotropes, with novel and exciting properties.

Chapter 5

Boron, nitrogen, silicon substituted glitter

In Chapter 4, it was argued that the tetragonal glitter structure is the most likely candidate for the interpretation of n-diamond, given that structures based on c-diamond were shown to be dynamically unstable. The calculations indicate that glitter has a relatively high formation energy with respect to diamond, which would make its synthesis difficult under moderate conditions. It is therefore of interest to examine the effect of alloying carbon-glitter with boron, nitrogen and silicon. Whilst the main objective is to gain an insight into the effects of substitution on the material's stability, determining whether there are any significant changes to the metallic nature of the basic glitter structure is also of interest.

Three compounds with heteroatom inclusions have been proposed in the literature, on the basis of chemical intuition, first principles calculation and synthetic methods SiC_2 [79, 78, 56, 234], and B_2C and CN_2 [24].

To the author's knowledge, inclusion of more than one type of element in the glitter structure has not been investigated. The aim of the work presented is to find the most stable structures of B, N, Si-substituted glitter by performing a ground state search based purely on first principles. The most technologically relevant structures are analysed and discussed in detail.

The Chapter is outlined as follow:

- computational details in Section 5.1;

- investigations on binary systems in Section 5.2;
- multi-element systems in Section 5.3;
- conclusions of the Chapter in Section 5.4.

5.1 Computational details

The MIT Ab-initio Phase Stability (`maps`) code of the Alloy Theoretic Automated Toolkit (ATAT) [194, 190, 191] was employed to parametrise the Hamiltonian. DFT [138, 135] total energy calculations were performed using the projector augmented wave (PAW) [231, 232] method as implemented in the VASP code [147]. The Perdew-Wang-91 (PW91) generalized gradient approximation has been employed for the exchange-correlation functional [141]. The tetrahedron method with Blöchl's corrections has been used for accurate calculation of total energies [235]. The Brillouin zone was sampled by Monkhorst-Pack k -point grids [214]. The cut-off energy for plane wave basis set is set to 520 eV. This guarantees that the absolute energies are converged to 1 meV/atom.

The following reference states have been used for the calculation of the formation energy: diatomic nitrogen molecule in a $10 \times 10 \times 10$ Å box; cubic diamond; cubic silicon; α -boron.

Some properties, namely vibrational and electronic, of ground states were calculated using CASTEP [173]. Details of these calculations are provided along the text.

5.2 Binary systems: C-B, C-N and C-Si glitter

This section focusses on the effect of substitution of carbon-glitter with a single atomic species; the substitutional binary systems of C-B glitter, C-N glitter and C-Si glitter are considered. As discussed previously, the crystal

structure of carbon glitter presents distinct crystallographic positions with distinct local chemical environments: the tetragonally coordinated sites with sp^3 hybridisation and the trigonally coordinated sites with sp^2 hybridisation. The naming convention adopted here for these two sites is T for tetragonal and t for trigonal.

In the present work, the configurational space of substituted binary glitter was investigated up to 12 atoms per unit cell. The six positions (2 T and 4 t) in the parent lattice can be occupied either by C or X, where X is alternatively boron, nitrogen or silicon. Considering permutations and symmetry, there are 2466 possible combinations for any considered C-X system. I wish to underline that 2466 structures are a daunting number for a direct DFT investigation because each structure must be structurally optimised.

Figure 5.1 summarises the main results of the calculations on the binary systems, where the formation energy of the ground states is plotted as a function of the molar fraction of C, χ_C .

In the heteroatom rich part of the configurational space, structures are characterised by a large relaxation and distortion because of forcing many B, N atoms into tetragonal positions, or Si into trigonal positions. In order to avoid these situations, the CE calculation for the C-B glitter system has been performed in the range $\chi_C \geq 1/3$, for the C-N glitter system $\chi_C \geq 0.5$ and for the C-Si glitter system $\chi_C \geq 0.5$. The resulting set of fitting parameters (ECIs) have been used to predict the energy of structures at lower carbon concentrations, extrapolating outside of its true range of validity; this affords a reasonable indication of the trends in the formation energies.

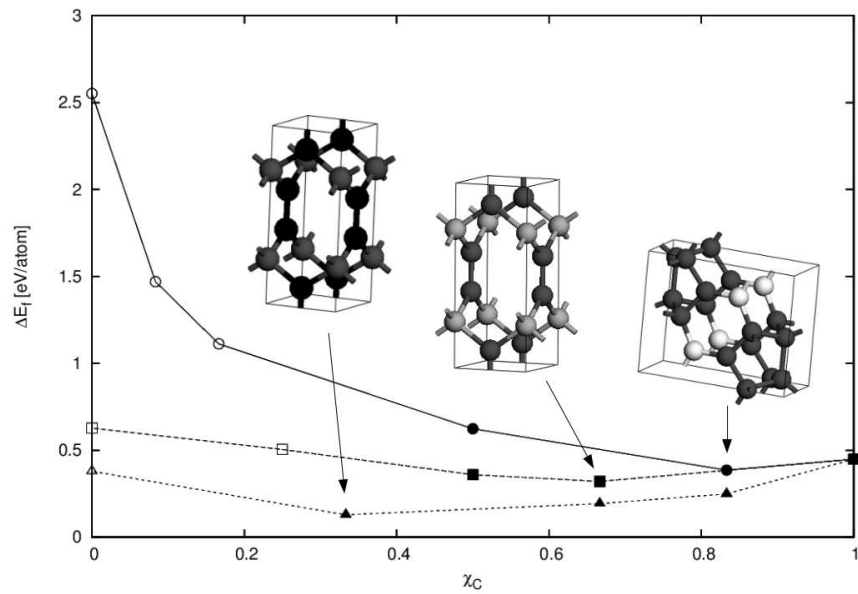


Figure 5.1: Formation energy per atom for C-N glitter (circle), C-Si glitter (square), and C-B glitter (triangle). Solid symbols represent ground states calculated within the range of concentration adopted in the CE calculation; open symbols are either end-compounds or points extrapolated at low C concentration. Carbon atoms are represented by dark grey spheres, silicon by light grey, nitrogen by white and boron by black ones. For the B-C system the structure with minimum formation energy is B_2C [24], for the Si-C system is SiC_2 [56], for the N-C system a structure with formula unit C_5N .

C-B system. Starting from the end-compound, pure C glitter, the substitution of carbon by boron stabilises the intermediate structures as long the substitution can occur in the trigonal positions. The minimum in the formation energy is reached for the compound B_2C , where all the trigonal positions are occupied by boron. As chemical intuition suggests, forcing B to the tetragonal positions, leads to an increase of the formation energy.

C-Si system. The C-Si system shows the opposite behaviour: Si substitution is preferred in T. The formation energy minimum occurs with tetragonal silicon dicarbide (silicon atoms in T and carbon atoms in t). If silicon is forced into trigonal position, the formation energy increases.

C-N system. From the point of view of the chemical bonding, the case of the C-N system is the most interesting. At low nitrogen concentration, the substitution of opposite trigonal C with N in the 1,4-cyclohexadieneoid unit ring stabilises the system. This is probably due to the formation of a ring sharing 6 electrons in an aromatic-like fashion, see the C-N glitter compound in Figure 5.1. Substitution of carbon with nitrogen in the glitter structure generally leads to a destabilisation of the structure. For the configuration with coupled nitrogen atoms in the trigonal positions and a N in the closest tetragonal position, the distance between nearest neighbours trigonal-N gets closer to a triple N-N bond, showing a strong tendency to decompose the glitter arrangement, forming N_2 . Additional selection rules of the novel structures to introduce in the CE calculation, implemented with a *csH* script, has been added to avoid these configurations.

The forecasting reliability of a CE calculation is tested with a CV score (usually less than 15 meV/atom for metal alloy systems). Here, the CV scores are high, particular for Si-C glitter: $CV = 0.013$ eV for the C-B system, $CV = 0.066$ eV for the C-N system and $CV = 0.100$ eV for the Si-C system. In the case of covalent bonding involving carbon, the bond energy is much higher than the those typically involved in ordering of alloys, which are typically in the range 0.10-0.01 eV/atom. The difference in formation energy between different configurations at the same concentration is much higher

and consequently, in the author’s opinion, it is possible to accept higher CV scores in predicting the formation energy itself. In light of this, the CE value is “acceptable” for B-system, while for N and Si, they are still on the high side. In these cases, the CE calculation shows just an indication of the possible relevant configurations, and they must be interpreted with care.

The dynamical stability of the structures having the minimum formation energy for the three systems (B_2C , SiC_2 , C_5N), along with CN_2 early proposed by Bucknum et al. [24], have been investigated with the tool of *ab initio* lattice dynamics. Structures with B and N substitution are found to be dynamically unstable. SiC_2 is found to be stable, in agreement with Andrew et al. [56].

Summarising, boron and nitrogen preferentially substitute carbon in trigonal positions while silicon in the tetragonal, in accordance with chemical intuition. The tendency of nitrogen to adopt a pyramidal rather than trigonal configuration leads generally to a destabilization of the structures. By considering up to 12 atoms per unit cell, no configurations have been identified that energetically stabilise the structures with respect to the elemental reference states. Binary substitutions are likely to make the glitter structure dynamically unstable, with the exception of the particular case of SiC_2 .

5.3 Ground states of multi-substitutional system

Studying the configurational space of a multi-substitutional systems is a very challenging task: considering 4 different atomic species sharing any crystallographic position in the glitter parent lattice is hard even using Ising-like parametrisation methods. Observations from the respective binary systems, Section 5.2, lead to simplified models, whereby tetragonal positions are occupied by C or Si and trigonal positions are shared by C, N, B.

Three computational models, based on three different parent lattices, have been designed:

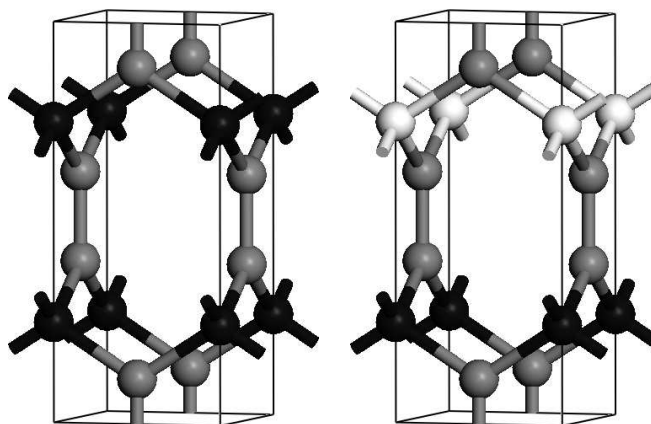


Figure 5.2: Parent lattices for multi-substitutional systems: on the left side the topology of the parent lattice used in Model-A and Model-B, black spheres represent the tetragonal position T , while grey ones the trigonal position t ; on the right side the topology used in Model-C, tetragonal positions are distinguished in $T_{(1)}$, black spheres, and $T_{(2)}$, white spheres.

- Model-A: C in T and C,N,B in t ;
- Model-B: Si in T and C,N,B in t ;
- Model-C: C in $T_{(1)}$ Si in $T_{(2)}$ and C,N,B in t ;

Figure 5.2 shows the topology of the Models. Model-C is the simplest model having C and Si sharing tetragonal position.

Considering crystallographic cells of up to 12 atoms per unit cell, the systems based on Model-A and Model-B includes 3933 different structures, that based on Model-C includes 7569 different structures. The increased number of structures for Model-C is an effect of populating the $T_{(1)}$ and $T_{(2)}$ position with different elements, leading generally to symmetry lowering.

According to CE terminology, in each of these models, atoms in the tetragonal positions act as spectator atoms while those occupying the t sites are considered as active atoms. The former do not explicitly enter the expression of CE because the configuration of the respective sublattice can not change. However, the total energy includes the contribution of the spectator species

so that the ECIs coupling two sites also includes the indirect interaction between these sites mediated through the spectator species [188].

Parametrisation has been performed with the condition that the concentrations of B and N in \mathbf{t} are above a certain limit ($\chi_{X(\mathbf{t})} \geq 1/12$, where $X=B,N$) to restrict the field of the investigation and to avoid structures already investigated as binary systems. For each Model ~ 200 structures have been employed in the fitting process, giving CV scores in the range 44-53 meV. Remarkably ground states with negative formation energy are found.

The representation of the formation energy of multicomponent system is graphically complex: results are therefore reported in tabular form, Table 5.1. Moreover the focus of this work is on the identification of structures with low formation energy and it is not to give a detailed representation of the configurational space of these system.

Model-A. At a composition B:C:N 1:1:1, a ground state with the lowest formation energy has been found. It shows a negative formation energy, $\Delta H_f = -0.133$ eV/atom. Views of the tetragonal representation of the CBN ground state are displayed in Figure 5.3. The structure lies within the space group $I4_122$. It is interesting to note that boron and nitrogen couple in trigonal position with complete substitution of C. B-N groups are located in the structure to minimise electrostatic interaction.

At the same composition, the expansion algorithm suggested a possible competitive structure, belonging to the space group $Pnna$. The structure is 6 meV higher in energy than the CBN ground state. The arrangement of B-N groups in the carbon framework, is similar to the one of the CBN ground state, but with a lower symmetry .

Model-B. For Model-B, the structures having the lower energies are similar to those ones found for Model-A. The ground state structure at composition Si:C:N 1:1:1 belongs to the space group $I4_122$ having formation energy $\Delta H_f = -0.322$ eV/atom. The structure with the successively higher formation energy belongs to the space group $Pnna$, $\Delta H_f = -0.315$ eV/atom. They are the homologous of the structures found for Model-A, having Si instead

Table 5.1: Formation energies of ground states of substituted glitter having negative values: Model-A having C in the tetragonal sublattice and C,B,N sharing the trigonal sublattice; Model-B having Si in the tetragonal sublattice and C,B,N sharing the trigonal sublattice; Model-C having C in $T_{(1)}$, Si in $T_{(2)}$ and C,B,N sharing the trigonal sublattice; Structures, that combine boron and nitrogen in trigonal position, have low formation energies.

Formula	$\chi_{C(\tau)}$	$\chi_{C(t)}$	χ_{Si}	χ_B	χ_N	ΔE_f [eV/atom]
Model-A						
CBN	1/3	0	0	1/3	1/3	-0.133
Model-B						
C ₄ Si ₄ BN ₃	0	1/3	1/3	1/12	1/4	-0.037
CSi ₂ BN ₂	0	1/6	1/3	1/6	1/3	-0.210
Si ₂ BN ₃	0	0	1/3	1/6	1/2	-0.218
SiBN	0	0	1/3	1/3	1/3	-0.322
Model-C						
C ₃ SiBN	1/6	1/3	1/6	1/6	1/6	-0.039
CSiBN ₃	1/6	0	1/6	1/6	1/2	-0.041
C ₅ Si ₂ B ₁ N ₄	1/6	1/4	1/6	1/12	1/3	-0.105
C ₅ Si ₂ B ₃ N ₂	1/6	1/4	1/6	1/4	1/6	-0.150
C ₃ Si ₂ BN ₆	1/6	1/12	1/6	1/12	1/2	-0.441
CSiB ₂ N ₂	1/6	0	1/6	1/3	1/3	-0.598

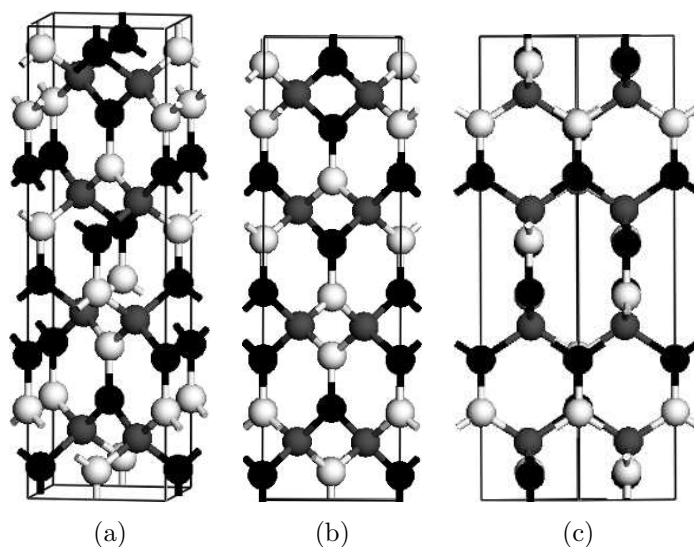


Figure 5.3: Tetragonal representation of CBN ground state: boron (black spheres), nitrogen (white) and carbon (dark gray).

of C in tetragonal position.

Model-C. A structure with very low formation energy, $\Delta H_f = -0.598$ eV/atom, has been predicted by the CE algorithm and verified by DFT calculation. The structure exhibits coupling of N and B in trigonal position, Figure 5.4. While in the CBN and SiBN structures, the substitutional groups are placed in order to minimize electrostatic interactions, in the SiCN_2B_2 ground state the B-N are placed in order to favour the strongest bonds, Si-N and C-B.

Vibrational analysis, performed with the *ab initio* code **CASTEP**, shows that all the structures reported here are dynamically stable. Systems are characterised by strong optic modes, due to the vibration of B-N group, at high frequency, $\sim 1200 - 1400 \text{ cm}^{-1}$. Figure 5.5 on Page 89, Figure 5.6 on Page 90 and Figure 5.7 on Page 91 display the phonon dispersion of CBN, SiBN and CSiB_2N_2 , respectively.

Table 5.2 and Table 5.3 report the lattice parameters of low-energy structures.

Table 5.2: Cell parameters (a,b,c) and distance between ethilene-like units (d) of low energy glitter-like structures. A ground state compound is indicated by “g.s.”, a *first excited configurational state* by “f.e.c.s”

Compound	Space Group	a [Å]	b [Å]	c [Å]	d [Å]
CBN g.s.	$I4_122$ (No. 98)	3.668	3.668	12.430	2.595
CBN f.e.c.s	$Pnna$ (No. 52)	6.220	3.660	3.676	2.596
SiBN g.s.	$I4_122$ (No. 98)	4.516	4.516	14.120	3.210
SiBN f.e.c.s	$Pnna$ (No. 52)	7.062	4.525	4.512	3.212
CSiB ₂ N ₂	$P - 4m2$ (No. 115)	2.856	2.856	6.467	2.856

Table 5.3: Fractional atomic positions (x, y, z) in CBN, SiBN and CSiB₂N₂.

Element	Wyckoff Position	x	y	z
CBN: a=b=3.668 Å, c=12.430 Å				
C	8f	0.2658	0.2500	0.6250
B	8c	0.0000	0.0000	0.6974
N	8c	0.0000	0.0000	0.8111
SiBN: a=b=4.516 Å, c=14.120 Å				
Si	8f	0.2632	0.2500	0.6250
B	8c	0.0000	0.0000	0.7113
N	8c	0.0000	0.0000	0.8117
CSiB ₂ N ₂ : a=b=2.856 Å, c=6.467 Å				
C	1d	0.0000	0.0000	0.0000
Si	1a	0.0000	0.0000	0.0000
B	2g	0.0000	0.5000	0.6261
N	2g	0.0000	0.5000	0.8482

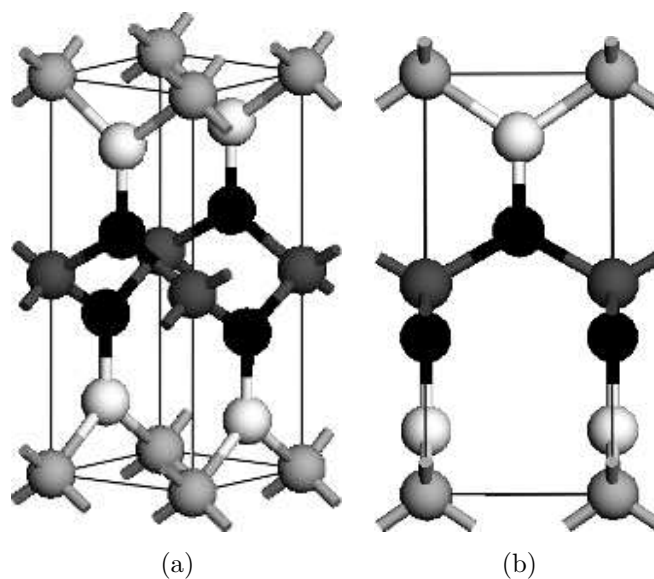


Figure 5.4: SiCN₂B₂ ground state: boron (black spheres), nitrogen (white), silicon (light gray) and carbon (dark gray).

5.3.1 Mechanical and electronic properties

The bulk modulus, B , was computed using the equation of state proposed by Alchagirov et al. [233] and implemented in Atomic Simulation Environment (ASE) [199], see Section 4.5. The CBN ground state would be a stiff material: the calculated bulk modulus is 310 GPa. For compounds with silicon substitutions, the bulk modulus decreases, Table 5.4. The calculated density, ρ , shows that the compounds would be light weight materials, see Table 5.4.

The electronic band structures have been calculated both with PW91 and B3LYP functional, Table 5.5. The compounds are indirect bandgap semiconductors, confirming the author's hypothesis of the effectiveness of heteroatom substitutions for tailoring the bandgap. Figure 5.8 on Page 92 displays the electronic band structure of CBN-glitter ground state calculated with the GGA and B3LYP hybrid functionals. Despite the similar shape of the calculated band structure, it is interesting to note the solid shift in energy of the bands, due to the non-local Hartree-Fock contribution.

Table 5.4: Calculated bulk moduli, B , and mass densities, ρ , for ground-state substituted glitter compounds.

Compound	Bulk Modulus	Density
	B [GPa]	ρ [g/cm ³]
CNB	310	2.93
SiCN ₂ B ₂	169	2.82
SiNB	250	2.44

Table 5.5: Bandgap energies, E_{BG} , of substituted glitter ground states calculated with the PW91 and B3LYP functionals.

Compound	PW91	B3LYP
	E_{BG} /[eV]	E_{BG} /[eV]
CBN	2.20	3.70
SiCN ₂ B ₂	0.38	1.40
SiBN	0.87	2.50

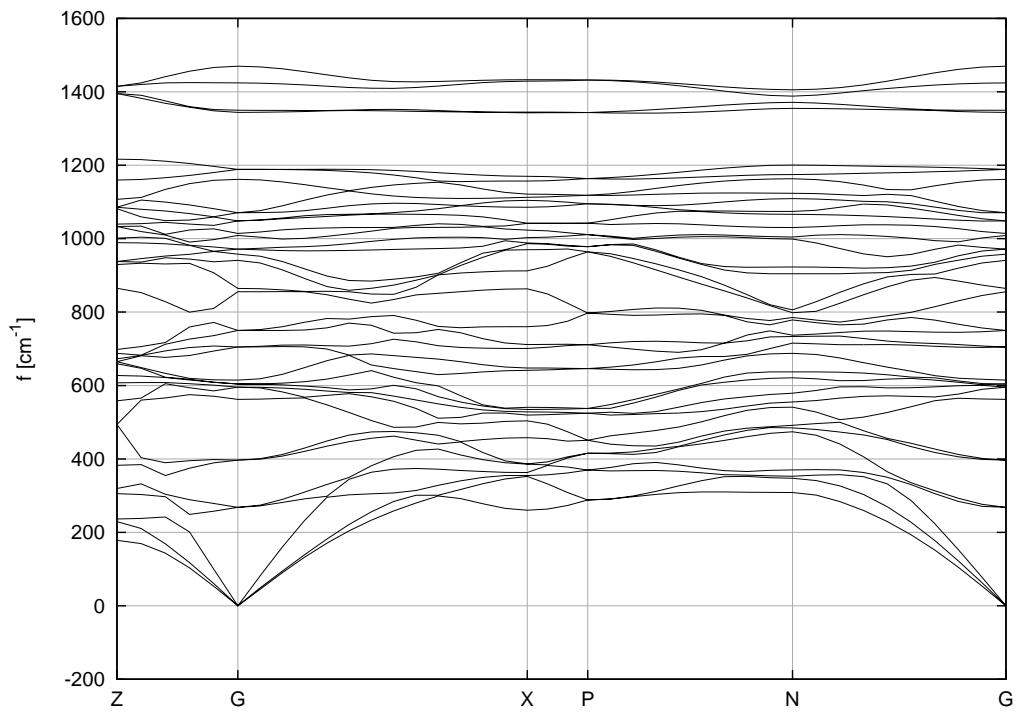


Figure 5.5: Phonon dispersion of CBN ground state.

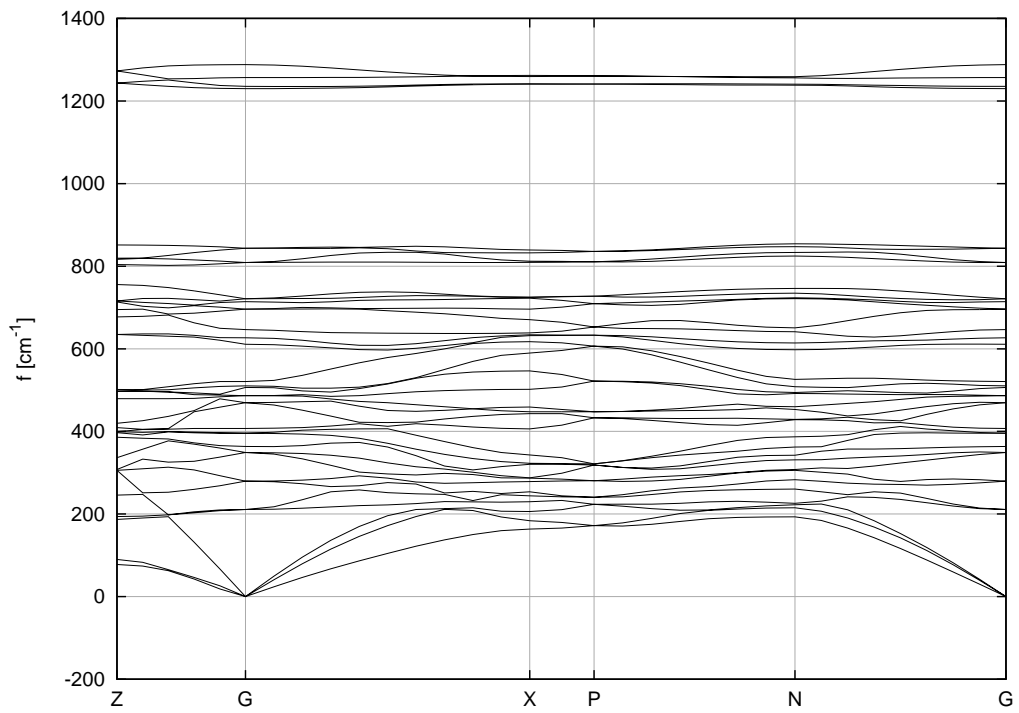


Figure 5.6: Phonon dispersion of SiBN ground state.

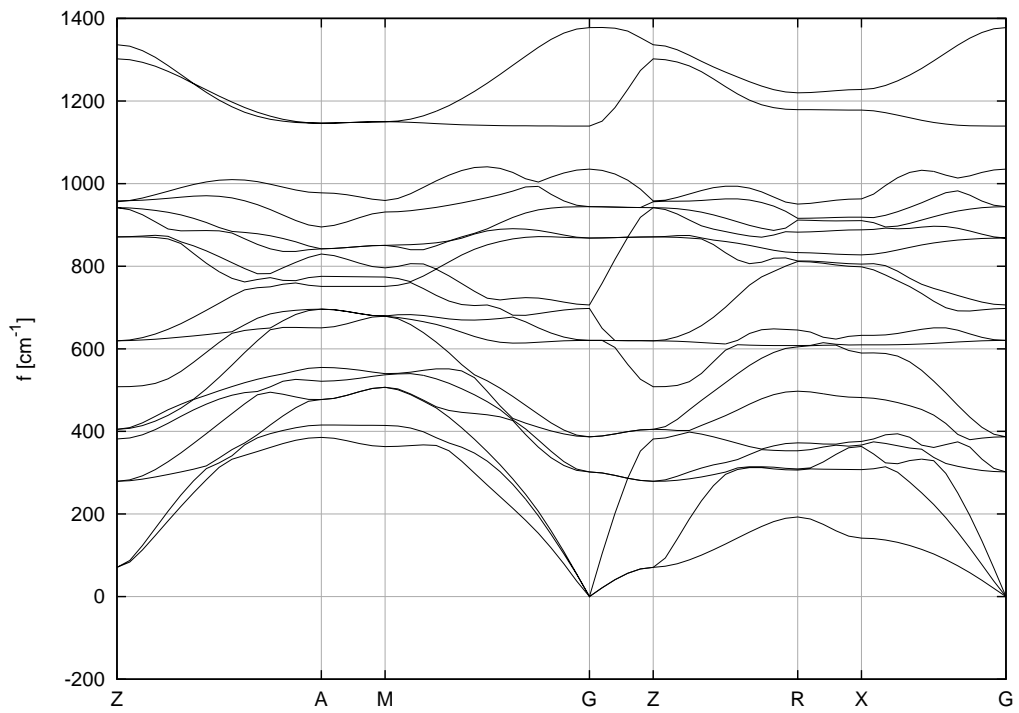


Figure 5.7: Phonon dispersion of SiCN₂B₂ ground state.

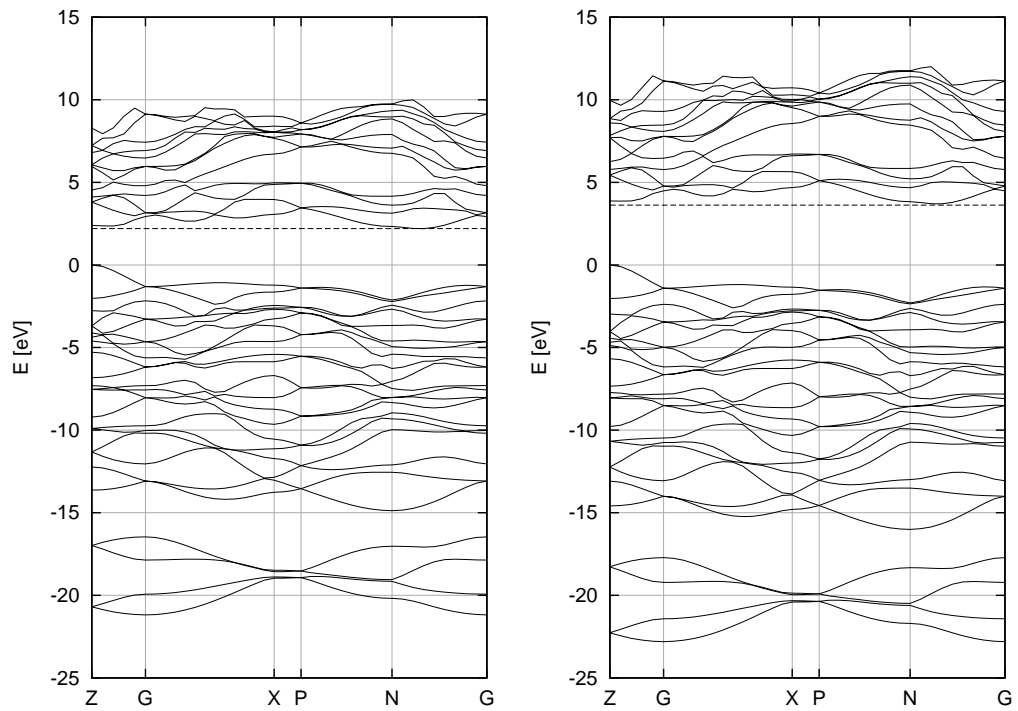


Figure 5.8: Band structure of CBN ground state calculated with PW91 (on the left) and B3LYP functional (on the right). The short dashes lines are references to highlight the band shift.

5.4 Chapter conclusions

Substitution of carbon atoms in the glitter structure with a single atomic species, namely boron, nitrogen or silicon, does not lead to strong stabilisation. However, several particular arrangements, deriving from multi-element substitution, show a dramatic stabilisation effect. The configurational space explored here is limited, so it is entirely possible that there are other structures with lower formation energies. For the models that have been taken into account, structures with low formation energies exhibit coupling of B and N in the trigonal positions. This result could have important implication in finding a synthetic route to bulk glitter-like structures.

Regarding the comparison of the stability with other B-N, C-N, C-B phases, similar comments to the ones about the stability of glitter can be proposed. It is likely that a reaction path from glitter-like structures to more thermodynamically stable phases would have high activation barriers due to the reconstructive nature of this process in systems characterized mainly by covalent bonding [25].

Many other metastable phases in the B-C-N system have been already synthesized, such as the ternary graphite-like BC_xN and ternary diamond-like BC_xN [236, 237]. Moreover Marwitz et al. [238] recently synthesised the aromatic compound 1,2-dihydro-1,2-azaborine, presenting adjacent sp^2 boron and sp^2 nitrogen substituting carbon atoms in a benzene-like ring.

Interestingly, the calculated bandgaps span a wide range, some 2 eV. It is likely that the bandgap could be modulated by controlling the concentration in tetragonal positions of C and Si, having an effect on the distance of the ethylene-like unit, Table 5.2, and the orientation of the B-N groups. A detailed understanding of these phases is essential for the design of novel hard light-weight semiconductors with adjustable bandgap based on common, cheap and non-toxic elements.

Group theory analysis, performed with the software VIBRATE! [239], suggests that some vibrational modes are Raman active, most notably some of the high-energy optic modes. It is entirely possible that this could constitute

a spectroscopic fingerprint of this class of compounds. Comparison of the calculated Raman spectra with experimental ones could lead to the identification of glitter-like structures. This is the subject of an on-going research programme with Dr. Vladimir M. Vishnyakov (Dalton Research Institute, Manchester Metropolitan University, Manchester, UK) for the possible identification of the structure of boron silicon carbo-nitride thin films, whose crystal structure is still unclear [240].

Chapter 6

Boron-substituted graphene

The main advantage of modifying the electronic properties of graphene-related materials by the substitution of carbon atoms with heteroatoms, namely B and N [95, 27], have been reviewed in Section 2.3.1: in-plane substitutions are not likely to lead to phase separation, because of the absence of strain effects due to the presence of atoms with sp^3 hybridisation in the graphitic layer [104]. The B-C honeycomb system has been investigated by Luo et al. [95] in the framework of first principles calculations, who predicted two-dimensional boron-carbon nano-structures through a particle-swarm optimisation (PSO) algorithm [241]. Single-layer B-C honeycomb compounds have been predicted at various boron concentrations, $\chi_B = \{1/6, 1/4, 1/3\}$. According to band structure calculations, the predicted compounds were found to be metallic, except for the ground state compound at composition BC_3 , which is a semiconductor. The predicted metallic arrangements were mostly characterised by isolated chains of boron atoms (as an example see Figure 6.3d on Page 103). The boron substructures were called 1D zigzag boron chains. In the BC_3 ground state compound, boron is uniformly distributed in the plane: six-membered rings of carbon atoms are surrounded by 6 boron atoms, leading to a structure with isolated carbon rings, see Figure 6.3e on Page 103. For its particular structure and electronic behaviour, BC_3 ground state has been defined a “magic case” [95].

In the present Chapter, the effect of boron substitution in graphene is investigated in more detail than previously. As a result, some rather different

conclusions are arrived at compared to those presented by Luo et al. [95], in particular the statement regarding the absence of semiconductor arrangements other than BC_3 .

In the present work, doping at low concentration has been investigated with systematic DFT calculations on different configurations having boron dopants at increasing distance. The direct DFT approach is possible because of the limited number of possible combinations at low boron concentration. For stoichiometric compositions, the number of possible configurations dramatically increases. Therefore, the cooperative effect of substitutions at higher boron concentrations has been investigated with Cluster Expansion [178, 179] coupled with *ab initio* calculations. The bi-layered system has been also investigated, showing that interlayer interactions can affect the electronic structure.

Computational details are reported in Section 6.1, conclusions of the Chapter in Section 6.5. Results, along with the relevant discussion, are reported in the following Sections:

- B-doping of graphene, Section 6.2;
- effect of boron substitution in single layer graphene, Section 6.3;
- effect of a second honeycomb layer, Section 6.4.

6.1 Computational details

Spin-polarized total-energy calculations were performed using the *ab initio* code CASTEP [173], employing the Perdew–Burke–Ernzerhof (PBE) exchange-correlation functional [142] and ultra-soft PPs [171]. The wave functions of the valence electrons are expanded using a 650 eV (550 eV for CE structures database) kinetic energy cut-off. For optimised structures, force magnitudes are less than 0.02 eV/Å (0.04 eV/Å for CE structures database).

The package Alloy Theoretic Automated Toolkit (ATAT) was employed to parametrise the Hamiltonian as a polynomial in the occupational variables

[190, 191, 194]. Structure are built on the graphene primitive cell expanded in the planar directions. The `runstruct_Castep` script, written by the author, has been employed to interface the CE code with the *ab initio* code. The vibrational stability of selected structures was investigated using the finite displacement method [203, 217]. Electronic band structures have been calculated using both the B3LYP and HSE06 [242, 159] functionals with norm-conserving PPs [229], for which an energy cut-off of 900 eV has been employed.

6.2 Boron doping in the low concentration limit

The interaction between two substitutional boron atoms and the carbon substrate has been investigated using a cell based on 10×10 primitive cells of graphene. The cell contains 198 C atoms and 2 dopant B atoms, giving a boron concentration $\chi_B = 0.01$. The DFT calculations are performed on a 3D periodic lattice. In order to mimic the 2D nature of graphene, a large interlayer distance of 11 Å is used, which guaranties no contamination of the electronics with spurious interlayer contributions. The volume of the supercell is $\sim 5800 \text{ \AA}^3$.

In Figure 6.1, the total energy of the different configurations is displayed as a function of the dopants' distance. The reference state is the configuration having the longest B-B pair distance.

For the first nearest neighbour (NN) substitution, the system has the highest energy. This configuration is characterised by a direct B-B bond and the lowest number of C-B bonds (4 C-B bonds while all the other configurations have 6 C-B bonds).

An energy minimum occurs for the third NN substitution, which corresponds to a 1,4-substitution in 6-membered ring, see insert in Figure 6.1.

According to this set of calculations, the boron-carbon honeycomb system differs fundamentally from the nitrogen-carbon substituted system [27] and

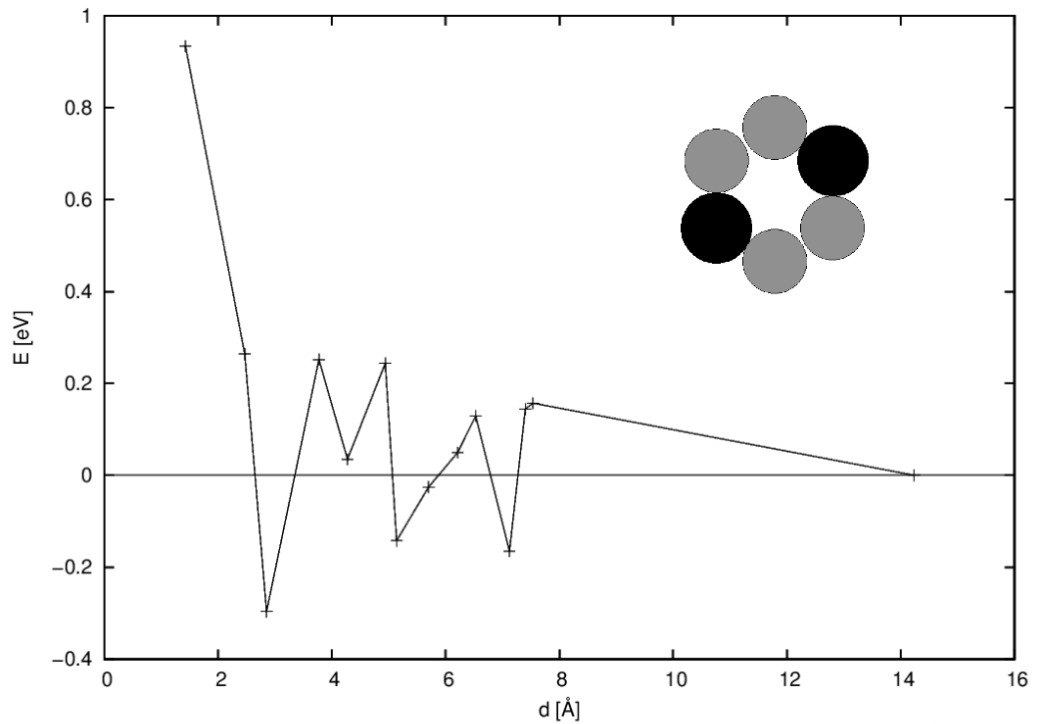


Figure 6.1: Energy, E , of a cell containing 2 boron atoms in a lattice of 200 atoms as a function of distance, d , of boron substitutions. The reference state is the configuration having dopants at the longest distance (14.24 Å). The distance is merely a topological reference related to the unrelaxed structures, while E is referred to relaxed structures. It is interesting to note the minima at the 3rd, 7th and 11th NN. The insert shows a graphical representation of 1,4 substitution in a six-membered ring, corresponding to the 3rd NN. Boron is represented by black spheres, carbon by grey ones.

hydrogen/oxygen/fluorine functionalised systems [104, 106, 108]:

- in the nitrogen-carbon system, the repulsive interaction between in-plane nitrogen atoms are dominant, forcing dopant atoms to spread into the honeycomb layer; this effect prevents the phase separation in the nitrogen-doped graphene into one region of undoped graphene and a region of highly substituted graphene;
- in systems with covalent out-of plane functionalisation (typical cases are hydrogenation, oxidation, fluorination), the groups involved in the functionalisation tend to stay close to each other in order to decrease the strain related to the coexistence of sp^2 and sp^3 carbon atoms in the same layer; this phenomenon is likely to lead to phase separation between fully functionalised and bare graphene;
- in boron-substituted graphene, boron atoms tend neither to cluster nor stay isolated; ordering on the short-range seams to be favoured, at least at low concentration.

This observation suggests that the structures with 1D zigzag boron chains, as identified by Luo et al. [95] are unlikely to be the lowest energy configurations. In fact, configurations that do not have direct boron-boron bonds are likely to be favoured, in accordance with the tendency of carbon and boron to form stable compounds.

6.3 Graphene: stoichiometric boron substitutions

6.3.1 Determination of the Cluster Expansion

As discussed above, the collective behaviour of stoichiometric substitutions can not be realistically investigated by a direct DFT search, owing the size of the configurational space. In the present work, structures up to 16 atoms per

unit cell has been investigated in the concentration range $0 \leq \chi_B \leq 0.5$. The system includes $\sim 10^4$ possible configurations. A CE approach has therefore been employed, for exploration of the configurational space at a relatively low computational cost. The geometry and total energy of 74 structural arrangements have been used as input to the CE algorithm. The cluster expansion converged with a CV score of 35 meV using 11 pair interactions, 7 triple interactions and 4 quad-interactions.

Taking into account structures up to 16 atoms per unit cell, the CE approach allows the consideration of many different stoichiometries: $\chi_B = \{ 0.0000, 0.0625, 0.0714, 0.0833, 0.1000, 0.1250, 0.1429, 0.1667, 0.1875, 0.2000, 0.2143, 0.2500, 0.2857, 0.3000, 0.3125, 0.3333, 0.3571, 0.3750, 0.4000, 0.4167, 0.4286, 0.4375, 0.5000 \}$. However many of these stoichiometries do not lead to structures close to the convex hull and therefore are not considered in the following discussion. Arbitrarily, a limit of 50 meV/atom above the convex hull has been used. This limit is a reasonable energy gap for evaluating energetic competition among different arrangements, considering that it corresponds to a Boltzmann temperature of about 580 K. The reference states for calculation of the formation energy are α -boron [243] and pure graphene.

Figure 6.2 shows the convex hull for $0.0 \leq \chi_B \leq 0.5$. Following the notation of Luo et al. [95], the structure with the lowest formation energy for a particular composition is denoted B_mC_n -I. Structures with successively higher energies then have the suffix II, III etc. An important point is that additional structures have been identified here to those presented in literature. Therefore, there is not necessarily a direct correspondence between the structure names used herein and in the previous literature.

From Figure 6.2, it is clear that B substitutions increase the formation energy. For $\chi_B = 0.4$, corresponding to the stoichiometry B_2C_3 , the formation energy is ~ 0.4 eV/atom. Structures for $\chi_B > 0.4$ are not considered in the following discussion because of the high formation energy. Moreover pure boron mono-layers are not based on the honeycomb layered lattice, but are suggested to adopt structures with trigonal and hexagonal motifs

[244, 245, 246]. Luo et al. [95] found that other topologies, different from the honeycomb lattice, are prevalent at high boron concentration. The cluster expansion method works on a fixed topology and it does not allow the investigation of topological disorder, Section 3.2.2. Therefore it is not a suitable method for investigation of the B-rich part of the configurational space.

According to the above-mentioned criteria, structures with formula unit BC_7 , BC_5 , BC_3 , BC_2 and B_2C_3 (corresponding to $\chi_B=0.125$, 0.167, 0.250, 0.333 and 0.4, respectively) are found to be energetically favoured.

Description of low-energy structures

In the following discussion of the low-energy structures, the concentration $\chi_B=0.250$ is considered first, since it corresponds to the stoichiometry where Luo et al. [95] identified the semiconducting configuration ($\text{BC}_3\text{-I}$).

At $\chi_B = 0.250$, the ground state $\text{BC}_3\text{-I}$ is found, Figure 6.3e, in agreement with PSO method proposed by Luo et al. [95] and early considerations based on chemical intuition [43]. $\text{BC}_3\text{-I}$ is characterised by the presence of isolated benzene-like units, which are defined by arrangements of the 1,4-B-substituted 6-membered unit that was discussed in Section 6.2.

In this work, an entirely novel arrangement is found as the *first excited configurational state*; $\text{BC}_3\text{-II}$, shown in Figure 6.3f, is 10 meV lower in energy than $\text{BC}_3\text{-III}$, that was identified as the *first excited configurational state* by Luo et al. [95]. The $\text{BC}_3\text{-II}$ compound presented here has a complex structure with ethylene-like and naphthalene-like isolated units, which both contain the 1,4-B-substituted 6-membered rings. $\text{BC}_3\text{-III}$ (the same structure as Luo's $\text{BC}_3\text{-II}$ compound) is a 1D zigzag boron-chain structure, that does not contain the 1,4-B-substituted 6-membered rings.

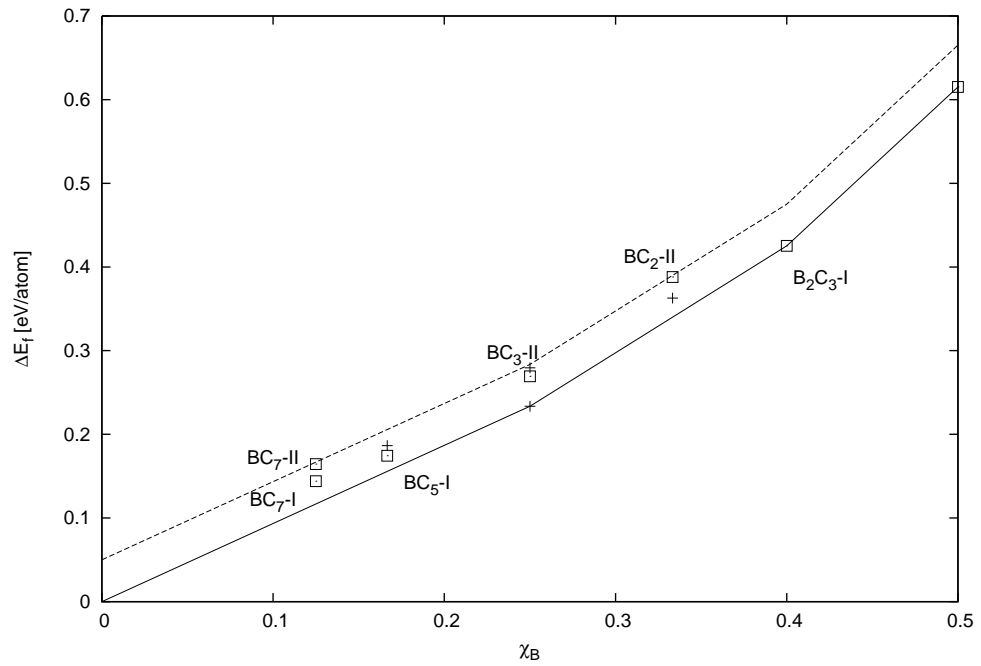


Figure 6.2: Convex hull of B-C honeycomb layer, with $\chi_B \leq 0.5$: structures predicted in the previous work (cross) [95], structures predicted in this work (open square). The latter are associated with the relevant nomenclature. For ease of reference, a dashed line lies 50 meV/atom above the convex-hull (solid line). Formation energy, ΔE_f , is referred to graphene and α -boron.

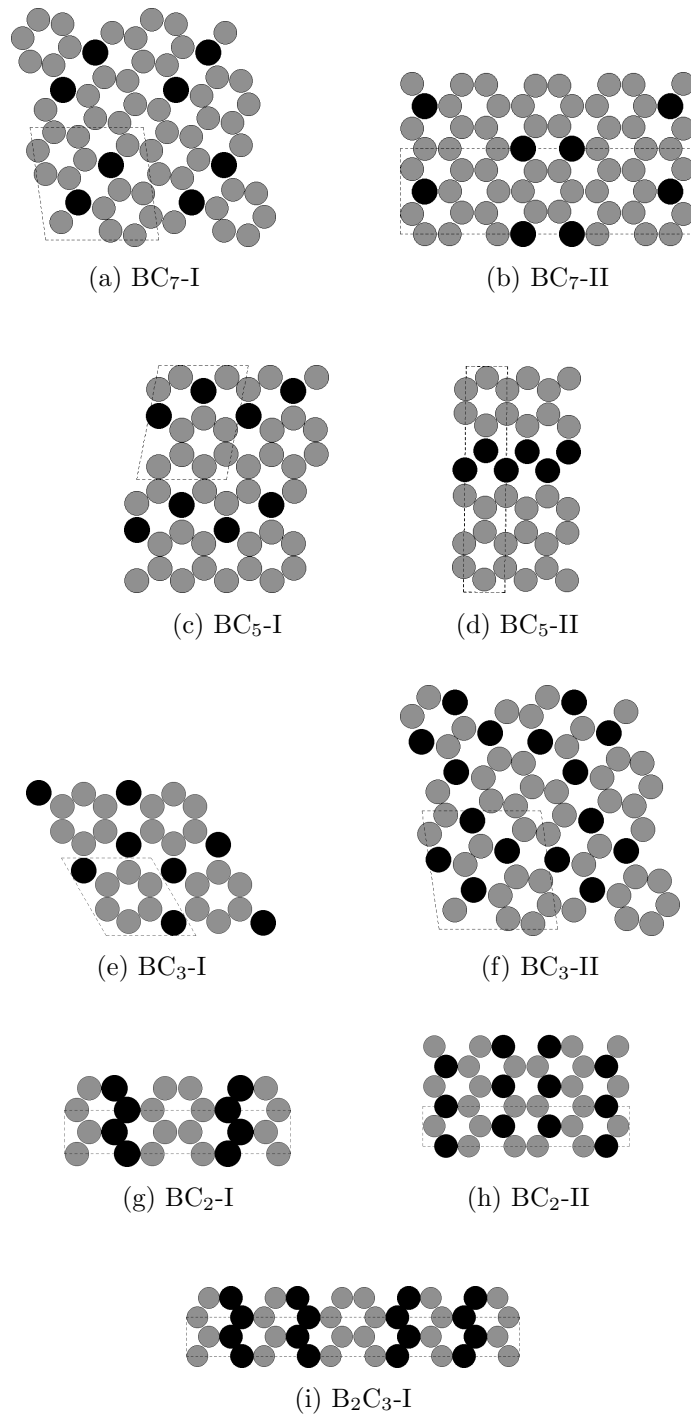


Figure 6.3: Boron graphene: low energy structures; boron represented by black spheres, carbon by grey ones.

For low B concentration, novel structures with 1,4-B-substituted six-membered units and aromatic-like carbon units have been found to be prevalent. At $\chi_B = 0.125$, two novel arrangements, namely BC₇-I (Figure 6.3a) and BC₇-II (Figure 6.3b) with relatively low formation energy have been predicted. This concentration was not taken into account in Luo's work.

For $\chi_B=1/6$, BC₅-I and BC₅-II are shown in Figures 6.3c and 6.3d respectively. BC₅-II is characterized by 1D zigzag boron chains, while BC₅-I is a novel structure having naphthalene-like units that are not completely isolated by boron atoms. The distance between carbon atoms connecting the naphthalene-like units is the longest C-C distance (1.489 Å). The others are in the range 1.400-1.451 Å. A longer distance denotes an improved single bond character. BC₅-II was predicted as the ground state at B:C 1:5 in Reference [95]. However the novel configuration BC₅-I is 12 eV lower in energy than BC₅-II.

At high B concentration, structures having 1D boron chains are prevalent. At $\chi_B=1/3$, the CE approach predicts the same low energy structure (BC₂-I) as the PSO method. BC₂-I is displayed in Figure 6.3g and presents chains of boron and carbon atoms. However a relatively energetically close structure, BC₂-II, is predicted in this work ($\Delta E_f=25$ meV). BC₂-II has 1,4-B-substituted six-membered units, Figure 6.3h. Because of the stoichiometry (high boron concentration), aromatic rings are not formed, however there is the presence of polyethylene-like and ethylene-like units.

At $\chi_B = 0.4$ a novel ground state is suggested, B₂C₃-I, Figure 6.3i, belonging to the family of structures having boron chain substructures. This concentration was not investigated by Luo et al. [95].

Summarising, in the boron concentration range $\chi_B = \{0.1250 - 0.2500\}$, low energy configurations are prevalently formed by aromatic units surrounded by boron atoms arranged in 1,4-substituted six-membered rings. While at higher boron concentrations, $\chi_B = \{0.3333 - 0.4000\}$, the typology proposed by Luo et al. [95] seem to be the most relevant. For ease of reference, results are reported in tabular form in Table 6.1.

Table 6.1: Formation energies of low-energy structures of the B-graphene system: ΔE_f is the formation energy referred to α -boron and graphene; $\Delta E_{(c.h.)}$ is the energy gap above the convex hull; the last column indicates the type of structure: “Z” 1D zigzag boron chain structure, “1,4-B” structure with 1,4-B-substituted six-membered rings.

Compound	χ_B	ΔE_f [eV/atom]	$\Delta E_{(c.h.)}$ [eV/atom]	type of configuration
BC ₇ -I	1/8	0.144	0.027	1,4-B
BC ₇ -II	1/8	0.164	0.046	1,4-B
BC ₅ -I	1/6	0.174	0.019	1,4-B
BC ₅ -II	1/6	0.186	0.031	Z
BC ₃ -I	1/4	0.234	0.000	1,4-B
BC ₃ -II	1/4	0.269	0.036	1,4-B
BC ₃ -III	1/4	0.280	0.046	Z
BC ₂ -I	1/3	0.363	0.023	Z
BC ₂ -II	1/3	0.388	0.048	1,4-B
B ₂ C ₃ -I	2/5	0.425	0.000	Z

Table 6.2: Bandgap calculated using HSE06 and B3LYP functionals of single-layer and bi-layer B-graphene compounds.

Compound	χ_B	HSE06 B.G. [eV]	B3LYP B.G. [eV]
single layer			
BC ₅ -I	1/6	0.323	0.439
BC ₃ -I	1/4	2.120	2.502
BC ₃ -II	1/4	1.257	1.599
double layer			
dl-BC ₃ -I	1/4	1.623	1.999

It is important to spend some words discussing the fact that some structures are not ground states but lie at reasonable energy levels above the convex-hull. While in metal alloy materials, such energy gaps could lead to phase separation, systems characterised by strong covalent bonding are difficult to re-arrange once they are formed. This is due to the reconstructive nature of the phase transformation process, that involves a high energy barrier. This concept has been widely underlined in the study of metastable carbon allotrope by Bucknum et al. [25]. Moreover low energy structures are important because they can partially describe the main bonding character at finite temperature, when some degree of disorder is added to the system.

6.3.2 Electronic properties

Using the hybrid functionals, HSE06 and B3LYP, described in Section 3.1.3, the electronic band structures for the configurations identified in the previous section have been calculated. The majority of compositions have a metallic band structure, in agreement with Luo et al. [95]. However, three particular compositions exhibit a bandgap at the Fermi level, indicative of semiconductors, namely BC₃-I, BC₃-II and BC₅-I. The phonon dispersion for these semiconducting structures has been calculated; no modes with nega-

tive eigenvalues have been identified, implying they are dynamically stable at 0 K [73]. Two of the semiconducting structures reported here, BC₃-II and BC₅-I, are entirely novel; Figures 6.4 and 6.5 show the phonon dispersion and electronic structure of these compounds.

The bandgaps for BC₃-I, BC₃-II and BC₅-I, calculated with both the HSE06 and B3LYP hybrid functionals are shown in Table 6.2. Note that the bandgaps calculated with B3LYP are systematically higher than those calculated with HSE06 functional, in agreement with the tendency of B3LYP to predict higher bandgap than HSE06 for graphene derivatives [162].

As argued in Section 6.3.1, BC₃-I and BC₃-II structures are characterized by the presence of aromatic-like and ethylene-like carbon units isolated by B atoms; BC₅-I by naphthalene-like units isolated by B atoms and C-C bonds bridging the naphthalene-like units.

To have a better understanding of this system, in particular the C-C bonding, a Mulliken population analysis [247] has been performed. The average overlap population of C-C bonds, that belong to aromatic-like or ethylene-like units, is 1.10 |e|, while the overlap population of C-C bond connecting the naphthalene-like units in BC₅-I is 1.00 |e|. The lowest overlap population, along with the longest bond length discussed in Section 6.3.1, indicates an enhanced single-bond character of the C-C bridging bonds in BC₅-I.

The calculated overlap population of B-C bonds is always lower than 0.98 |e|. The boron atoms have an associated charge of $\sim +0.56$ |e|, showing charge localization effect, as reported for related system (B-substituted single-wall carbon nanotubes) by Fuentes et al. [45].

The boron atoms are sp² hybridised with the three 2p electrons mainly participating to the formation of B-C σ -bonds. In author's opinion, the semi-conducting behaviour is therefore believed to be due to isolation of conducting carbon areas, prevalently aromatic, by bonds with partial single character.

It is important to underline that the absolute magnitude of bond population and the atomic charges calculated by population analysis have little physical meaning [248], because of the sensitivity to the atomic basis set. However, relative values have been shown to give useful information in identifying trends [249].

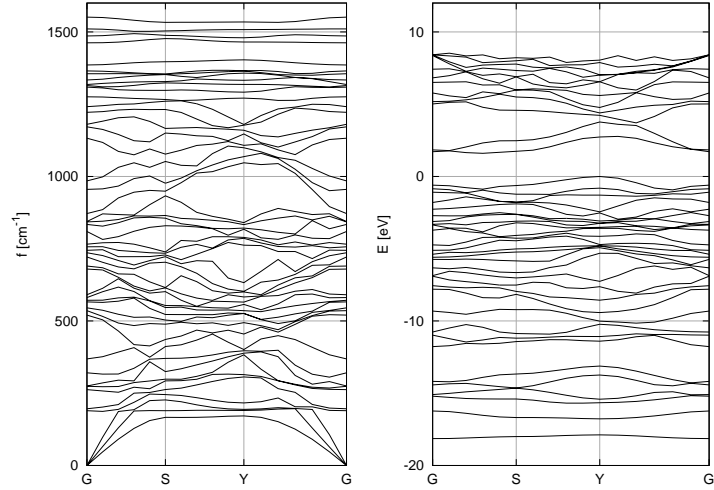


Figure 6.4: Phonon dispersion (left) and electronic band structure (right) of $\text{BC}_3\text{-II}$: no modes with negative eigenvalues are present, denoting a vibrationally stable structure. The band structure, calculated using B3LYP functional, shows a indirect bandgap of 1.599 eV.

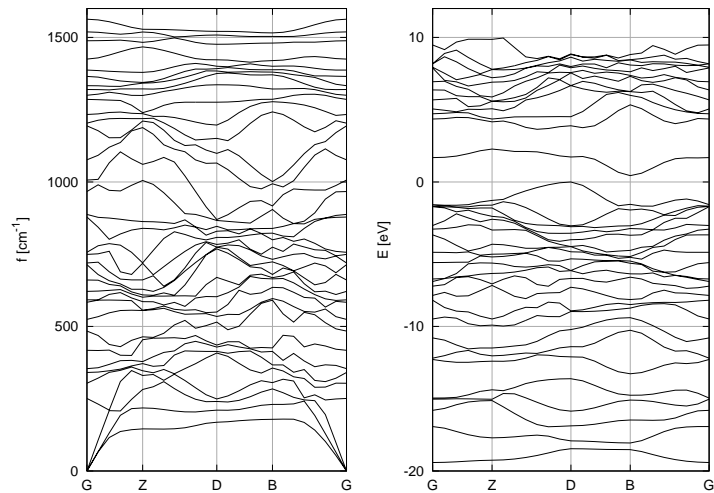


Figure 6.5: Phonon dispersion (left) and electronic band structure (right) of $\text{BC}_5\text{-I}$: No modes with negative eigenvalues are present, denoting a vibrationally stable structure. The band structure, calculated using B3LYP functional, shows a indirect bandgap of 0.439 eV.

6.4 Double-layered boron-substituted graphene

The electronic structure of pure graphene is affected by the local environment; the presence of a second layer of graphene, Section 2.3.1, or a supporting substrate [250] have both been shown to modify the electronics of the system. Graphene epitaxially grown on SiC substrate has ~ 0.26 eV bandgap due to graphene-substrate interactions. On the basis of these considerations, and the hypothesis that interlayer interactions will have an enhanced effect in systems with a non-uniform charge distribution, the effect of a second layer of B-C graphene is of particular interest; its investigation is the subject of the present section.

The effect on the electronic band structure of boron substituted graphene by addition of a second layer has been studied, using a simple model of two honeycomb layers stacked in the same fashion as hexagonal graphite [251]. The supercell is 13 Å in the out-of-plane direction. A CE search has been performed for 16 atoms per unit cell. Because of the complexity of the system, mainly due to interlayer interactions, it is not possible to converge to a low CV score. The best fit has a CV of 61 meV. Despite the high *uncertainty* the main result is reported because it can be supported by considerations based on chemical intuition.

A single ground state structure excluding the end-compounds, was identified. The structure has composition $\chi_B = 1/4$, and it is related to the single layered BC₃-I arrangement. Figure 6.6 displays several views of the structure, named here dl-BC₃-I (“dl” for double layer). The dynamical stability of dl-BC₃-I has been confirmed by calculation of the phonon mode dispersion, shown in Figure 6.7 on Page 114.

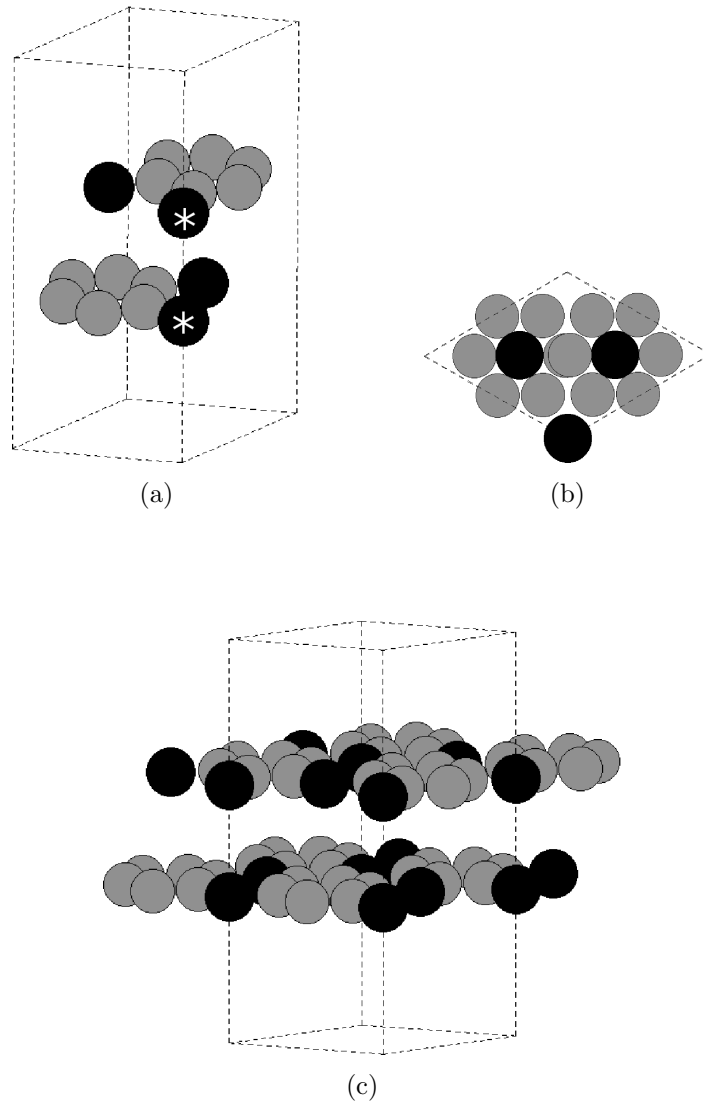


Figure 6.6: Double layer B-graphene, dl-BC₃-I, side view (a) and top view (b) 2×2 supercell view (c): for ease of comprehension, atoms lying at boundaries of the cell are not repeated. Boron atoms (black) are not equivalent: there are two different local environments: boron facing a benzene-like unit and boron facing boron on the opposite layer. In (a), the latter are marked with an asterisk.

In dl-BC₃-I, carbon atoms are crystallographically equivalent while boron atoms are placed in one of two different local environments. Considering the top layer, one subset of boron atoms, indicated with an asterisk in Figure 6.6a, is located directly above another boron atom in the bottom layer. The remaining boron atoms are located on top of a ring formed by carbon atoms. The calculated interlayer distance is 3.489 Å; the layers would be expected to experience interaction. In a unit cell, Figure 6.6a, there are two attractive interactions “B↔C-ring” and a repulsive interaction “B*↔B”. A Mulliken population analysis [247] has been performed. The charge associated with carbon atoms is $-0.18 |e|$. For of B* and B, the calculated charges are $+0.52 |e|$ and $+0.55 |e|$, respectively. This can be compared with the single layer BC₃ compound, where carbon atoms have an associated charge of $-0.19 |e|$ and the boron atoms, which are geometrically equivalent, have a charge of $+0.56 |e|$. In double layer systems, therefore, charge transfer is induced to compensate interlayer electrostatic interactions.

Comparing dl-BC₃-I with BC₃-I, the modified charge distribution infers a different electronic structure. The band structure of dl-BC₃-I calculated with B3LYP functional is displayed in Figure 6.7 on Page 114. The bandgap calculated with B3LYP and HSE06 functionals is 1.999 eV and 1.623 eV respectively; these values are included in Table 6.2. Interlayer interactions, due to presence of charged atoms distributed in ordered positions along the layers, strongly affect the bandgap. The bandgap of dl-BC₃-I is ~ 0.5 eV lower than the one of homologous single layer compound. This result is in agreement with early calculations of Tomanek et al. [43], showing that the metallic nature of BC₃ bulk material is due to the interlayer interactions, while a single layer of BC₃ was predicted to be semiconductor.

The small energy difference between the direct and the indirect gap, see Figure 6.7, should open the exciting possibility of producing light emitting/adsorbing devices with reasonable quantum efficiencies. It is likely that the bandgap could be tuned by changing the interlayer distance. This topic is a subject of on-going research.

Interestingly, dl-BC₃-I is only 0.004 eV/atom less stable than BC₃. This can be indicative of a tendency to avoid the folding and buckling that is typical of many 2-dimensional materials [252].

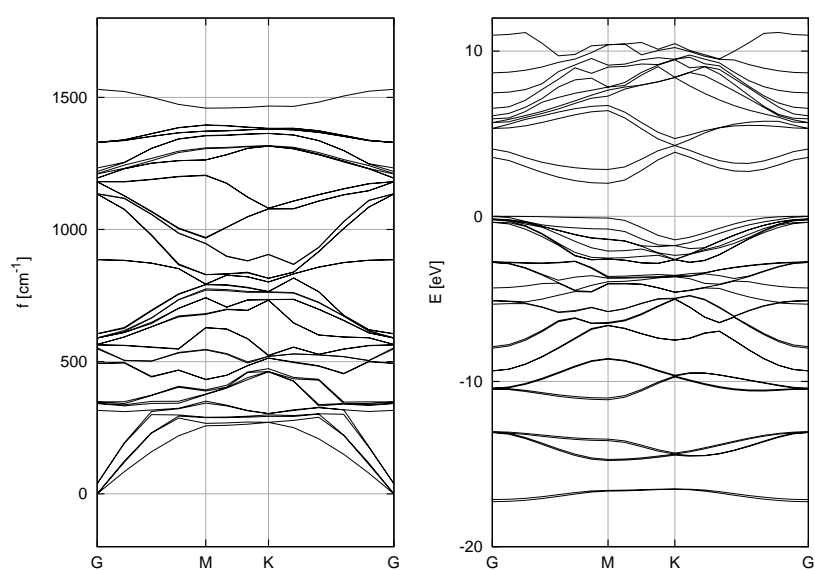


Figure 6.7: Phonon dispersion (left) and electronic band structure (right) of dl-BC₃-I: no modes with negative eigenvalues are present, denoting a vibrationally stable structure. The band structure, calculated using B3LYP functional, shows a indirect bandgap of 1.999 eV.

6.5 Chapter conclusions

On the basis of the present studies, it is suggested that boron substitution is an effective way to modify the bandgap of graphene related materials over a wide range of values. Novel metastable B-C semiconductor compounds have been identified at concentrations $\chi_B = 1/4$ and $\chi_B = 1/6$. The predominance of the 1,4-substitution in 6-membered unit has been confirmed by both the direct *ab initio* and the CE approaches. These structures have aromatic-like units isolated by single bonds (prevalently C-B bonds). In agreement with the important role of aromaticity in organic chemistry, structures having aromatic-like carbon units are the most stable energetically in a wide range of concentration. Fuentes et al. [45] reported a similar effect, related to band structure modification induced by substitution, in highly boron-substituted single-wall carbon nanotubes.

It would, perhaps, be counter-intuitive that the structures with 1D zigzag boron chains would be the most stable, as proposed by Luo et al. [95] These structures are, of course, prevalent at high boron concentration, when the formation of carbon units would imply the formation of extended areas of boron.

The effect of adding a second layer in modulating the bandgap has been demonstrated: dl-BC3-I has a bandgap some 0.5 eV lower than the one of the homologous single layered compound. This study strongly suggests that the bandgap at the Fermi level can be modulated over a wide range of values by changing the boron concentration and the local environment. This could be of fundamental importance for experimental researchers in successfully synthesising technologically useful semiconductor materials based on the carbon honeycomb structure for nano-electronics and energy-conversion applications.

The possibility of producing the structures proposed here is supported by the fact that the BC₃ honeycomb sheet has been grown epitaxially [118], and the BC₃ three-dimensional structure has already been synthesised [42]. It is possible that single-layer or few-layer materials could be produced by the

standard technique of exfoliation, widely used for producing graphene and other layered materials [253].

In terms of the computational methodology, the CE-DFT approach has been shown to find structures that have lower energies than the ones identified in the PSO method [95]. The CE approach allows a configurational search based on a particular parent lattice (topology) to be performed, while PSO takes into account a wider number of possible arrangements where the topology is changed. The PSO does not predict the correct ranking of structures, failing to take into account the dramatically increased number of possible combinations.

As a final point, it is perhaps worth mentioning that layered BC_3 compounds have been proposed as promising high-capacity Li inclusion compounds for use in Li-ion batteries [254].

Chapter 7

General discussion and conclusions

The main conclusions of the thesis are briefly outlined here:

- the tetragonal carbon allotrope, called glitter, is the only structure that is dynamically stable at 0 K among the ones that have been proposed for n-diamond; because of its stability, along with its metallic band structure and its consistency with the diffraction pattern of n-diamond [77], it is likely to describe the n-diamond arrangement;
- B, N, and Si substitutions in glitter are effective both for decreasing the formation energy and for opening a bandgap;
- boron substitutions in graphene are effective for opening a bandgap at the Fermi level; a number of entirely novel stable structures, some of them semiconducting, have been presented in this thesis: in the range $\chi_B = \{0.1250 - 0.2500\}$, the most stable configurations show two features: boron are arranged in 1,4-boron-substituted six membered ring, carbon prevalently forms isolated aromatic rings; at higher boron concentration $\chi_B > 1/3$, the structures with 1D zigzag boron chains, that have been proposed by Luo et al. [95], are the most prevalent;
- an extra layer of boron substituted graphene is effective for modifying the bandgap of the resulting material, giving a second way of modulating the bandgap.

7.1 On the methodology

On the side of the computational methods, there are two important considerations:

- *ab initio* lattice dynamics is of fundamental importance for testing the stability of novel predicted phases;
- cluster expansion is a powerful tool to predict novel configurations of carbon related materials, however the results must be carefully interpreted because it is difficult to achieve high accuracy; in the case of carbon substituted nets, CE is useful to drive the search; however results must be always confirmed by *ab initio* calculations and by a chemical understanding of the system.

I would like to underline that it is unlikely that configurations as complex as the ones reported in this work would be proposed on the basis of chemical intuition alone. Some of these structures, especially the ones with relatively large unit cell, are so complex that are difficult to be rationalised without the aid of computational tools.

It is however important to say that, although the configurational space has been investigated in a far wider region than in previous work, the configurational space that remains unexplored is vast. It is entirely possible that structures with larger unit cells, which are not considered here, would be relevant for a complete understanding of the systems. However, in my opinion, this is currently beyond the possibility of the computational tools now available, and remains the holy grail of computational materials research in substitutionally disordered crystalline systems.

Although *ab initio* calculations of phonons spectra have been widely employed to investigate phase stability and phase transition [27, 95, 255], it is well-known that several errors are introduced in the calculated force constants [217]: computational rounding and interpolation errors, errors due to the use of a finite basis set and a finite k -point set, errors in the finite

convergence of the structural parameters and errors related to the degree of anharmonicity. While the effects of the first three mentioned sources of errors can be mitigated by an accurate computing, anharmonicity is strongly dependent on the crystal structure. For instance, titanium and zirconium presents anharmonicity effect of thermal lattice vibrations [256]: bcc phases become unstable in the harmonic approximation [257, 258] revealing imaginary phonon frequencies. However these phases appear as high temperature phases, because they are stabilized by large vibrational and electronic entropy [258, 259, 260].

In closing, it is important to employ computational approaches being mindful of the limits of their validity in particular when predicting the stability novel structures in term of energy and dynamics.

7.2 Outlook

I would like to conclude by saying that working in the area of prediction of carbon-based structures has provided an extremely fascinating journey where I surely did not experience any lack of ideas for future investigations.

I am currently involved in writing additional publications to present fully the work of this thesis and I am hopeful in attracting further funding to answer the main open questions related to these fascinating systems:

Among the hypothetical carbon allotropes proposed in the literature, which ones are dynamically stable?

Is it possibly to find any definitive experimental evidence for glitter-like structures?

What is the effect of multi-element substitutions in graphene?

Are the novel structures stable at finite temperature?

List of Publications

Molecular-Level Characterization of Heterogeneous Catalytic Systems by Algorithmic Time Dependent Monte Carlo

N. Armata, **G. Baldissin**, G. Barone, R. Cortese, V. D'Anna, F. Ferrante,
S. Giuffrida, G. Li Manni, A. Prestianni, T. Rubino, Zs. Varga, D. Duca
Topics in Catalysis, 52 (2009) 431

Monte Carlo algorithms and codes, used to study heterogeneous catalytic systems in the frame of the computational section of the NANOCAT project, are presented along with some exemplifying applications and results. In particular, time dependent Monte Carlo methods supported by high level quantum chemical information employed in the field of heterogeneous catalysis are focused. Technical details of the present algorithmic Monte Carlo development as well as possible evolution aimed at a deeper interrelationship of quantum and stochastic methods are discussed, pointing to two different aspects: the thermal-effect involvement and the three-dimensional catalytic matrix simulation. As topical applications, (i) the isothermal and isobaric adsorption of CO on Group 10 metal surfaces, (ii) the hydrogenation on metal supported catalysts of organic substrates in two-phase and three-phase reactors, and (iii) the isomerization of but-2-ene species in three-dimensional supported and unsupported zeolite models are presented.

Structural and Kinetic DFT Characterization of Materials to Rationalize Catalytic Performance

N. Armata, **G. Baldissin**, G. Barone, R. Cortese, V. D'Anna, F. Ferrante,
S. Giuffrida, G. Li Manni, A. Prestianni, T. Rubino, D. Duca
Topics in Catalysis, 52 (2009) 444

This review shortly discusses recent results obtained by the application of density functional theory for the calculations of the adsorption and diffusion properties of small molecules and their reactivity on heterogenous catalytic systems, in the ambit of the Nanocat project. Particular focus has been devoted to palladium catalysts, either in atomic or small cluster form. Some protocols have been tested to obtain efficient ways able to treat the electronic and geometric influence of supports like zeolites and carbon nanotubes on the catalytic properties of palladium. The hydroisomerization of cis-but-2-ene is discussed as model reaction on supported and unsupported Pd clusters. Some preliminary results on the structural investigation of systems formed by a palladium clusters and block copolymers are also presented.

In situ powder neutron diffraction study of non-stoichiometric phase formation during the hydrogenation of Li_3N

D.J. Bull, N. Sorbie, **G. Baldissin**, D. Moser, M.T.F. Telling, R.I. Smith,
D.H. Gregory, D.K. Ross

Faraday Discussions, 151 (2011) 263

The hydrogenation of Li_3N at low chemical potential has been studied in situ by time-of-flight powder neutron diffraction and the formation of a non-stoichiometric $\text{Li}_{4-2x}\text{NH}$ phase and Li_4NH observed. The results are interpreted in terms of a model for the reaction pathway involving the production of Li_4NH and Li_2NH , which subsequently react together to form $\text{Li}_{4-2x}\text{NH}$. Possible mechanisms for the production of Li_4NH from the hydrogenation of Li_3N are discussed.

The pressure-temperature phase diagram of MgH₂ and isotopic substitution

D. Moser, **G. Baldissin**, D.J. Bull, D.J. Riley, I. Morrison, D.K. Ross,
W.A. Oates, D. Norus

Journal of Physics: Condensed Matter, 23 (2011) 305403

Computational thermodynamics using density functional theory ab initio codes is a powerful tool for calculating phase diagrams. The method is usually applied at the standard pressure of $p = 1$ bar and where the Gibbs energy is assumed to be equal to the Helmholtz energy. In this work, we have calculated the Gibbs energy in order to study the release temperature and phase modifications of MgH₂ at high pressures up to 10 GPa (100 kbar). The isotopic substitution of hydrogen with deuterium (or tritium) does not bring about any strong effects on the phase diagram. These considerations are of extreme importance for (i) the synthesis of novel substitutional magnesium based materials at high pressure and (ii) the determination of the correct reference states for the calculation of phase diagrams at high pressure. The calculated results are compared with experimental data obtained with an in situ neutron diffraction measurement.

n-Diamond: Dynamical stability of proposed structures

G. Baldissin, D.J. Bull

Diamond and Related Materials, 34 (2013) 60

A number of experimental works, mainly under extreme conditions, report a carbon phase with the same reflections as diamond but showing additional reflections that are forbidden for diamond. The crystal structure of this phase, called n-diamond by Hirai and Kondo (H. Hirai and K.-i. Kondo, *Science* 253 (1991) 772-774), remains unclear. By means of ab initio calculations based on density functional perturbation theory, the dynamical stability of the structures proposed to be n-diamond has been investigated up to a pressure of 30 GPa. According to the calculations, a tetragonal carbon allotrope, called glitter (M.J. Bucknum and R. Hoffman, *J. Am. Chem. Soc.* 116 (1994) 11456-11464), is the best candidate. The calculated electronic structure and bulk modulus of glitter are critically discussed.

Synthesis of Pure Lithium Amide Nanoparticles

G. Baldissin, N.M. Boag, C.C. Tang, D.J. Bull

European Journal of Inorganic Chemistry, 2013 (2013) 1993

Deprotonation of ammonia with n-butyllithium offers a facile synthetic route to produce pure lithium amide exhibiting fine granularity, which facilitates the complete thermal decomposition to lithium imide at a relatively low temperature of 600 K. Synthesised compounds were characterised by high-resolution synchrotron X-ray diffraction, and the particle morphology of lithium amide was studied by transmission electron microscopy. The proposed methodology readily affords the production of pure lithium amide nanoparticles at both bench-top and commercial scale.

Bibliography

- [1] G. Ceder. *Science*, 280(5366):1099, 1998.
- [2] S. M. Woodley and R. Catlow. *Nature Materials*, 7(12):937, 2008.
- [3] G. Ceder. *MRS Bulletin*, 35(09):693, 2010.
- [4] M. T. Yin and M. L. Cohen. *Physical Review Letters*, 45(12):1004, 1980.
- [5] D. de Fontaine, G. Ceder, and M. Asta. *Nature*, 343(6258):544, 1990.
- [6] S. Froyen and A. Zunger. *Physical Review Letters*, 66(16):2132, 1991.
- [7] W. A. Chalifoux and R. R. Tykwinski. *Nature Chemistry*, 2(11):967, 2010.
- [8] H.W. Kroto. *Angewandte Chemie International Edition*, 31(2):111, 1992.
- [9] S. Iijima. *Nature*, 354(6348):56, 1991.
- [10] K.S. Novoselov, A.K. Geim, S.V. Morozov, D. Jiang, M.I. Katsnelson, I.V. Grigorieva, S.V. Dubonos, and A.A. Firsov. *Nature*, 438(7065):197, 2005.
- [11] P. R. Wallace. *Physical Review*, 71(9):622–634, 1947.
- [12] K. S. Novoselov, A. K. Geim, S. V. Morozov, D. Jiang, Y. Zhang, S. V. Dubonos, I. V. Grigorieva, and A. A. Firsov. *Science*, 306(5696):666, 2004.
- [13] Nobelprize.org. The nobel prize in physics 2010, 2010.
- [14] K. Umemoto, S. Saito, S. Berber, and D. Tomnek. *Physical Review B*, 64(19):1934091, 2001.

- [15] R.H. Telling, C.P. Ewels, A.A. El-Barbary, and M.I. Heggie. *Nature Materials*, 2(5):333, 2003.
- [16] H. J. McSkimin and P. Andreatch. *Journal of Applied Physics*, 43(7):2944, 1972.
- [17] J.W. Klett, A.D. McMillan, N.C. Gallego, T.D. Burchell, and C.A. Walls. *Carbon*, 42(8-9):1849, 2004.
- [18] J. Klett, R. Hardy, E. Romine, C. Walls, and T. Burchell. *Carbon*, 38(7):953, 2000.
- [19] H.R. Karfunkel and T. Dressler. *Journal of the American Chemical Society*, 114(7):2285, 1992.
- [20] A.T. Balaban, D.J. Klein, and C.A. Folden. *Chemical Physics Letters*, 217(3):266, 1994.
- [21] I. Vlasov, O. I. Lebedev, V. G. Ralchenko, E. Goovaerts, G. Bertoni, G. Van Tendeloo, and V. I. Konov. *Advanced Materials*, 19(22):4058, 2007.
- [22] J.-K. Lee and P. John. *Thin Solid Films*, 519(2):625, 2010.
- [23] J.-K. Lee, P. John, S.-C. Kim, W.-S. Lee, and J.I.B. Wilson. *Diamond and Related Materials*, 17(710):1216, 2008.
- [24] M. J. Bucknum and R. Hoffmann. *Journal of the American Chemical Society*, 116(25):11456, 1994.
- [25] M. J. Bucknum, I. Stamatina, and E. A. Castro. *Molecular Physics*, 103(20):2707, 2005.
- [26] H. Hirai and K.-i. Kondo. *Science*, 253(5021):772, 1991.
- [27] H. J. Xiang, B. Huang, Z. Y. Li, S.-H. Wei, J. L. Yang, and X. G. Gong. *Physical Review X*, 2(1):011003, 2012.

- [28] M. M. Balakrishnarajan, P. D. Pancharatna, and R. Hoffmann. *New Journal of Chemistry*, 31(4):473, 2007.
- [29] C. F. Mabery. *Journal of the American Chemical Society*, 22(10):706, 1900.
- [30] A. Thomas, A. Fischer, F. Goettmann, M. Antonietti, J.-O. Müller, R. Schlögl, and J. M. Carlsson. *Journal of Materials Chemistry*, 18(41):4893, 2008.
- [31] Y. Zhang, H. Sun, and C. Chen. *Physical Review Letters*, 93(19):195504, 2004.
- [32] S. Chen, X. G. Gong, and S.-H. Wei. *Physical Review Letters*, 98(1):015502, 2007.
- [33] T. Komatsu, M. Samedima, T. Awano, Y. Kakadate, and S. Fujiwara. *Journal of Materials Processing Technology*, 85(13):69, 1999.
- [34] K. Yuge. *Journal of Physics: Condensed Matter*, 21(41):415403, 2009.
- [35] V. L. Solozhenko, D. Andrault, G. Fiquet, M. Mezouar, and D. C. Rubie. *Applied Physics Letters*, 78(10):1385, 2001.
- [36] M. O'Donoghue. *Synthetic, Imitation & Treated Gemstones*. Taylor & Francis, 1997.
- [37] A. Kraft. *International Journal of Electrochemical Science*, 2:355, 2007.
- [38] V. L. Solozhenko, O. O. Kurakevych, D. Andrault, Y. Le Godec, and M. Mezouar. *Physical Review Letters*, 102:015506, 2009.
- [39] P. V. Zinin, L. C. Ming, H. A. Ishii, R. Jia, T. Acosta, and E. Hellebrand. *Journal of Applied Physics*, 111(11):114905, 2012.
- [40] C. E. Lowell. *Journal of the American Ceramic Society*, 50(3):142, 1967.

- [41] B. M. Way, J. R. Dahn, T. Tiedje, K. Myrtle, and M. Kasrai. *Physical Review B*, 46(3):1697, 1992.
- [42] J. Kouvetakis, R. B. Kaner, M. L. Sattler, and N. Bartlett. *Journal of the Chemical Society, Chemical Communications*, (24):1758, 1986.
- [43] D. Tomanek, R. M. Wentzcovitch, S. G. Louie, and M. L. Cohen. *Physical Review B*, 37(6):3134, 1988.
- [44] W. K. Hsu, S. Firth, P. Redlich, M. Terrones, H. Terrones, Y. Q. Zhu, N. Grobert, A. Schilder, R. J. H. Clark, H. W. Kroto, and D. R. M. Walton. *Journal of Materials Chemistry*, 10(6):1425, 2000.
- [45] G. G. Fuentes, E. Borowiak-Palen, M. Knupfer, T. Pichler, J. Fink, L. Wirtz, and A. Rubio. *Physical Review B*, 69(24):245403, 2004.
- [46] W. Kaiser and W. L. Bond. *Physical Review*, 115(4):857, 1959.
- [47] K. Iakoubovskii, G. J. Adriaenssens, and Y. K. Vohra. *Journal of Physics: Condensed Matter*, 12(30):L519, 2000.
- [48] A. S. Barnard and M. Sternberg. *The Journal of Physical Chemistry B*, 109(36):17107, 2005.
- [49] H. Kanda, M. Akaishi, and S. Yamaoka. *Diamond and Related Materials*, 8(89):1441, 1999.
- [50] Z.Z. Liang, X. Jia, H.A. Ma, C.Y. Zang, P.W. Zhu, Q.F. Guan, and H. Kanda. *Diamond and Related Materials*, 14(1112):1932, 2005.
- [51] R.Z. Yu, H.A. Ma, Z.Z. Liang, W.Q. Liu, Y.J. Zheng, and X. Jia. *Diamond and Related Materials*, 17(2):180, 2008.
- [52] T. Matsui, M. Yudasaka, R. Kikuchi, Y. Ohki, and S. Yoshimura. *Materials Science and Engineering: B*, 29(13):220, 1995.
- [53] K. Ghosh, M. Kumar, T. Maruyama, and Y. Ando. *Journal of Materials Chemistry*, 20(20):4128, 2010.

- [54] R. Cheung. *Silicon carbide microelectromechanical systems for harsh environments*. Imperial College Press, London, 2006.
- [55] T. Muranaka, Y. Kikuchi, T. Yoshizawa, N. Shirakawa, and J. Akimitsu. *Science and Technology of Advanced Materials*, 9(4):044204, 2008.
- [56] R.C. Andrew, M. Braun, and N. Chetty. *Computational Materials Science*, 55(0):186, 2012.
- [57] F. Durand and J. C. Duby. *Journal of Phase Equilibria*, 20(1):61, 1999.
- [58] M. W. Dashiell, L. V. Kulik, D. Hits, J. Kolodzey, and G. Watson. *Applied Physics Letters*, 72(7):833, 1998.
- [59] K. Eberl, K. Brunner, and W. Winter. *Thin Solid Films*, 294(12):98, 1997.
- [60] K. H. Chung, J. C. Sturm, E. Sanchez, K. K. Singh, and S. Kuppurao. *Semiconductor Science and Technology*, 22(1):S158, 2007.
- [61] L. S. Palatnik, M. B. Guseva, V. G. Babaev, N. F. Savchenko, and I. I. Fal'ko. *Journal of Experimental and Theoretical Physics*, 60:520, 1984.
- [62] I. Konyashin, A. Zern, J. Mayer, F. Aldinger, V. Babaev, V. Khvostov, and M. Guseva. *Diamond and Related Materials*, 10(1):99, 2001.
- [63] M.J. Bucknum, C.J. Pickard, I. Stamatina, and E.A. Castro. *Journal of Theoretical and Computational Chemistry*, 5(2):175, 2006.
- [64] K. Yamada and A.B. Sawaoka. *Carbon*, 32(4):665, 1994.
- [65] M. Frenklach, R. Kematich, D. Huang, W. Howard, K.E. Spear, A.W. Phelps, and R. Koba. *Journal of Applied Physics*, 66(1):395, 1989.
- [66] J. M. Cowley, R. C. Mani, M. K. Sunkara, M. O'Keeffe, and C. Bonneau. *Chemistry of Materials*, 16(24):4905, 2004.

- [67] B. Wen, J. Zhao, T. Li, and C. Dong. *New Journal of Physics*, 8(5):62, 2006.
- [68] L.A. Bursill, A.L. Fullerton, and L.N. Bourgeois. *International Journal of Modern Physics B*, 15(31):4087, 2001.
- [69] L. Holland and S.M. Ojha. *Thin Solid Films*, 58(1):107, 1979.
- [70] B. Wen, J. J. Zhao, and T. J. Li. *International Materials Reviews*, 52(3):131, 2007.
- [71] P. Santiago, G. A. Camacho-Bragado, M. Marin-Almazo, J. Murgich, and M. J. Yacaman. *Energy & Fuels*, 18(2):390, 2004.
- [72] D. J. Kennett, J. P. Kennett, A. West, C. Mercer, S. S. Que Hee, L. Bement, T. E. Bunch, M. Sellers, and W. S. Wolbach. *Science*, 323(5910):94, 2009.
- [73] G. Baldissin and D. J. Bull. *Diamond and Related Materials*, 34:60, 2013.
- [74] A. F. Wells. *Three dimensional nets and polyhedra*. Wiley; Hoboken, New Jersey, 1977.
- [75] M. J. Bucknum. *Carbon*, 35(1):1, 1997.
- [76] C.J. Pickard, V. Milman, and B. Winkler. *Diamond and Related Materials*, 10(12):2225, 2001.
- [77] M. J. Bucknum and E. A. Castro. *Journal of Mathematical Chemistry*, 50:1034, 2012.
- [78] M. J. Bucknum, A. Ienco, and E. A. Castro. *Journal of Molecular Structure: THEOCHEM*, 716(13):73, 2005.
- [79] I. Stamatina, A. Dumitru, M. J. Bucknum, V. Ciupina, and G. Prodan. *Molecular Crystals and Liquid Crystals*, 417(910357744):167, 2004.

- [80] Y. Zhang, Y.-W. Tan, H. L. Stormer, and P. Kim. *Nature*, 438(7065):201, 2005.
- [81] A. H. Castro Neto, F. Guinea, N. M. R. Peres, K. S. Novoselov, and A. K. Geim. *Reviews of Modern Physics*, 81(1):109, 2009.
- [82] A. Bostwick, T. Ohta, T. Seyller, K. Horn, and E. Rotenberg. *Nature Physics*, 3(1):36, 2007.
- [83] J. Kedzierski, P.-L. Hsu, P. Healey, P.W. Wyatt, C.L. Keast, M. Sprinkle, C. Berger, and W.A. de Heer. *IEEE Transactions on Electron Devices*, 55(8):2078, 2008.
- [84] J.-H. Chen, C. Jang, S. Xiao, M. Ishigami, and M. S. Fuhrer. *Nature Nanotechnology*, 3(4):206, 2008.
- [85] S. V. Morozov, K. S. Novoselov, M. I. Katsnelson, F. Schedin, D. C. Elias, J. A. Jaszczak, and A. K. Geim. *Physical Review Letters*, 100(1):016602, 2008.
- [86] K. I. Bolotin, K. J. Sikes, Z. Jiang, M. Klima, G. Fudenberg, J. Hone, P. Kim, and H. L. Stormer. *Solid State Communications*, 910:351, 2008.
- [87] X. Zhou, J.-Y. Park, S. Huang, J. Liu, and P. L. McEuen. *Physical Review Letters*, 95(14):146805, 2005.
- [88] V. Perebeinos, J. Tersoff, and P. Avouris. *Physical Review Letters*, 94(8):086802, 2005.
- [89] F. Schwierz. *Nature Nanotechnology*, 5(7):487, 2010.
- [90] L. Britnell, R. M. Ribeiro, A. Eckmann, R. Jalil, B. D. Belle, A. Mishchenko, Y.-J. Kim, R. V. Gorbachev, T. Georgiou, S. V. Morozov, A. N. Grigorenko, A. K. Geim, C. Casiraghi, A. H. Castro Neto, and K. S. Novoselov. *Science*, 340(6138):1311, 2013.

- [91] L. Yang, C.-H. Park, Y.-W. Son, M. L. Cohen, and S. G. Louie. *Physical Review Letters*, 99(18):186801, 2007.
- [92] E. V. Castro, K. S. Novoselov, S. V. Morozov, N. M. R. Peres, J. M. B. Lopes dos Santos, J. Nilsson, F. Guinea, A. K. Geim, and A. H. Castro Neto. *Physical Review Letters*, 99(21):216802, 2007.
- [93] V. M. Pereira, A. H. Castro Neto, and N. M. R. Peres. *Physical Review B*, 80(4):045401, 2009.
- [94] V. Georgakilas, M. Otyepka, A. B. Bourlinos, V. Chandra, N. Kim, K. C. Kemp, P. Hobza, R. Zboril, and K. S. Kim. *Chemical Reviews*, 112(11):6156, 2012.
- [95] X. Luo, J. Yang, H. Liu, X. Wu, Y. Wang, Y. Ma, S.-H. Wei, X. Gong, and H. Xiang. *Journal of the American Chemical Society*, 133(40):16285, 2011.
- [96] M. Evaldsson, I. V. Zozoulenko, H. Xu, and T. Heinzl. *Physical Review B*, 78(16):161407, 2008.
- [97] L. Jiao, X. Wang, G. Diankov, H. Wang, and H. Dai. *Nature Nanotechnology*, 5(5):321, 2010.
- [98] F. Cervantes-Sodi, G. Csányi, S. Piscanec, and A. C. Ferrari. *Physical Review B*, 77(16):165427, 2008.
- [99] T. Ohta, A. Bostwick, T. Seyller, K. Horn, and E. Rotenberg. *Science*, 313(5789):951, 2006.
- [100] P. Gava, M. Lazzeri, A. M. Saitta, and F. Mauri. *Physical Review B*, 79(16):165431, 2009.
- [101] S. Ryu, M. Y. Han, J. Maultzsch, T. F. Heinz, P. Kim, M. L. Steigerwald, and L. E. Brus. *Nano Letters*, 8(12):4597, 2008.

- [102] H. J. Xiang, E. J. Kan, Su-Huai Wei, X. G. Gong, and M.-H. Whangbo. *Physical Review B*, 82(16):165425, 2010.
- [103] J. O. Sofo, A. S. Chaudhari, and G. D. Barber. *Physical Review B*, 75(15):153401, 2007.
- [104] M. H. F. Sluiter and Y. Kawazoe. *Physical Review B*, 68(8):085410, 2003.
- [105] H. J. Xiang, S.-H. Wei, and X. G. Gong. *Physical Review B*, 82(3):035416, 2010.
- [106] D. R. Dreyer, S. Park, C. W. Bielawski, and R. S. Ruoff. *Chemical Society Reviews*, 39:228, 2010.
- [107] K. A. Mkhoyan, A. W. Contryman, J. Silcox, D. A. Stewart, G. Eda, C. Mattevi, S. Miller, and M. Chhowalla. *Nano Letters*, 9(3):1058, 2009.
- [108] F. Withers, M. Dubois, and A. K. Savchenko. *Physical Review B*, 82(7):073403, 2010.
- [109] L. Kaufman. *Journal of Phase Equilibria and Diffusion*, 30(5):418, 2009.
- [110] K. S. Novoselov, V. I. Falko, L. Colombo, P. R. Gellert, M. G. Schwab, and K. Kim. *Nature*, 490(7419):192, 2012.
- [111] X. Wang, X. Li, L. Zhang, Y. Yoon, P. K. Weber, H. Wang, J. Guo, and H. Dai. *Science*, 324(5928):768, 2009.
- [112] L. Zhao, R. He, K. T. Rim, T. Schiros, K. S. Kim, H. Zhou, C. Gutierrez, S. P. Chockalingam, C. J. Arguello, L. Pálová, D. Nordlund, M. S. Hybertsen, D. R. Reichman, T. F. Heinz, P. Kim, A. Pinczuk, G. W. Flynn, and A. N. Pasupathy. *Science*, 333(6045):999, 2011.
- [113] D. Deng, X. Pan, L. Yu, Y. Cui, Y. Jiang, J. Qi, W.-X. Li, Q. Fu, X. Ma, Q. Xue, G. Sun, and X. Bao. *Chemistry of Materials*, 23(5):1188, 2011.

- [114] H. Liu, Y. Liu, and D. Zhu. *Journal of Materials Chemistry*, 21(10):3335, 2011.
- [115] S. Yu, W. Zheng, C. Wang, and Q. Jiang. *ACS Nano*, 4(12):7619, 2010.
- [116] M. Cattelan, S. Agnoli, M. Favaro, D. Garoli, F. Romanato, M. Meneghetti, A. Barinov, P. Dudin, and G. Granozzi. *Chemistry of Materials*, 25(9):1490, 2013.
- [117] H. Wang, Y. Zhou, D. Wu, L. Liao, S. Zhao, H. Peng, and Z. Liu. *Small*, 9(8):1316, 2013.
- [118] H. Yanagisawa, T. Tanaka, Y. Ishida, M. Matsue, E. Rokuta, S. Otani, and C. Oshima. *Physical Review Letters*, 93(17):177003, 2004.
- [119] C. J. Pickard and R. J. Needs. *Journal of Physics: Condensed matter*, 21(45):452205, 2009.
- [120] C. J. Pickard and R. J. Needs. *Nature Materials*, 9(8):624, 2010.
- [121] R. M. Martin. *Electronic structure: basic theory and practical methods*. Cambridge University Press; Cambridge, 2004.
- [122] I. N. Levine. *Quantum Chemistry*. Allyn and Bacon; Boston, 1974.
- [123] S. Muller. *Journal of Physics: Condensed Matter*, 15(34):R1429, 2003.
- [124] D. de Fontaine. Cluster approach to Order-Disorder transformations in alloys. In *Solid State Physics*, volume 47, 33. Academic Press; Waltham, Massachusetts, 1994.
- [125] A. V. Ruban and I. A. Abrikosov. *Reports on Progress in Physics*, 71(4):046501, 2008.
- [126] M. T. Dove. *Introduction to lattice dynamics*. Cambridge University Press; Cambridge, 1993.
- [127] B. Fultz. *Progress in Materials Science*, 55(4):247, 2010.

- [128] Nobelprize.org. The nobel prize in chemistry 1998, 1998.
- [129] C. Wolverton. Density functional calculations in the automotive industry: Catalyst supports and hydrogen storage materials. In *APS March Meeting Abstracts*, 5002, 2006.
- [130] Scopus.com. Sciverse scopus, 2013.
- [131] E. Schrödinger. *Physical Review*, 28(6):1049, 1926.
- [132] M. Born and R. Oppenheimer. *Annalen der Physik*, 389(20):457, 2006.
- [133] D.R. Hartree. *Proceedings of the Royal Society*, A113:621, 1928.
- [134] V. Fock. *Zeitschrift für Physik*, 61(1-2):126, 1930.
- [135] P. Hohenberg and W. Kohn. *Physical Review*, 136(3B):B864, 1964.
- [136] T. Kato. *Communications on Pure and Applied Mathematics*, 10(2):151, 1957.
- [137] M. Levy. *Physical Review A*, 26(3):1200, 1982.
- [138] W. Kohn and L. J. Sham. *Physical Review*, 140(4A):A1133, 1965.
- [139] P. Mori-Sánchez, Q. Wu, and W. Yang. *Journal of Chemical Physics*, 123(6):1, 2005.
- [140] A.D. Becke. *The Journal of Chemical Physics*, 98(7):5648, 1993.
- [141] J. P. Perdew and Y. Wang. *Physical Review B*, 45(23):13244, 1992.
- [142] J. P. Perdew, K. Burke, and M. Ernzerhof. *Physical Review Letters*, 77(18):3865, 1996.
- [143] J. P. Perdew, J. A. Chevary, S. H. Vosko, K. A. Jackson, M. R. Pederson, D. J. Singh, and C. Fiolhais. *Physical Review B*, 46:6671, 1992.
- [144] J. P. Perdew, J. A. Chevary, S. H. Vosko, K. A. Jackson, M. R. Pederson, D. J. Singh, and C. Fiolhais. *Physical Review B*, 48:4978, 1993.

- [145] F. Tran, R. Laskowski, P. Blaha, and K. Schwarz. *Physical Review B*, 75(11):115131, 2007.
- [146] B. S. Pujari, S. Gusarov, M. Brett, and A. Kovalenko. *Physical Review B*, 84:041402, 2011.
- [147] J. Hafner. *Journal of computational chemistry*, 29(13):2044, 2008.
- [148] J. P. Perdew and M. Levy. *Physical Review Letters*, 51(20):1884, 1983.
- [149] L. J. Sham and M. Schlüter. *Physical Review Letters*, 51(20):1888, 1983.
- [150] J. Perry, J. Tahir-Kheli, and W. Goddard. *Physical Review B*, 63(14):144510, 2001.
- [151] H. Xiao, J. Tahir-Kheli, and W. A. Goddard. *The Journal of Physical Chemistry Letters*, 2(3):212, 2011.
- [152] J. Muscat, A. Wander, and N.M. Harrison. *Chemical Physics Letters*, 342(34):397, 2001.
- [153] J. Heyd, J. E. Peralta, G. E. Scuseria, and R. L. Martin. *The Journal of Chemical Physics*, 123(17):174101, 2005.
- [154] J. Tao. *Journal of Chemical Physics*, 115(8):3519, 2001.
- [155] P.J. Stephens, F.J. Devlin, C.F. Chabalowski, and M.J. Frisch. *Journal of Physical Chemistry*, 98(45):11623, 1994.
- [156] A. D. Becke. *Physical Review A*, 38:3098, 1988.
- [157] S. H. Vosko, L. Wilk, and M. Nusair. *Canadian Journal of Physics*, 58(8):1200, 1980.
- [158] C. Lee, W. Yang, and R.G. Parr. *Physical Review B*, 37(2):785, 1988.
- [159] J. Heyd, G. E. Scuseria, and M. Ernzerhof. *The Journal of Chemical Physics*, 118(18):8207, 2003.

- [160] S. Park, B. Lee, S. H. Jeon, and S. Han. *Current Applied Physics*, 11(3):S337, 2011.
- [161] J. Heyd and G. E. Scuseria. *The Journal of Chemical Physics*, 121(3):1187, 2004.
- [162] V. Barone, O. Hod, J. E. Peralta, and G. E. Scuseria. *Accounts of Chemical Research*, 44(4):269, 2011.
- [163] V. Barone, J. E. Peralta, J. Uddin, and G. E. Scuseria. *The Journal of Chemical Physics*, 124(2):024709, 2006.
- [164] T. Nautiyal and S. Auluck. *Physical Review B*, 34:2299, 1986.
- [165] U. von Barth and L. Hedin. *Journal of Physics C*, 5(13):1629, 1972.
- [166] F. Bloch. *Zeitschrift für Physik*, 52(7-8):555, 1929.
- [167] J. C. Phillips. *Physical Review*, 112(3):685, 1958.
- [168] A. M. Rappe, K. M. Rabe, E. Kaxiras, and J. D. Joannopoulos. *Physical Review B*, 41(2):1227, 1990.
- [169] G. B. Bachelet, D. R. Hamann, and M. Schlüter. *Physical Review B*, 26:4199, 1982.
- [170] G. B. Bachelet, D. R. Hamann, and M. Schlüter. *Physical Review B*, 29:2309, 1984.
- [171] D. Vanderbilt. *Physical Review B*, 41(11):7892, 1990.
- [172] G. Kresse, and J. Hafner. *Journal of Physics: Condensed Matter*, 6(40):8245, 1994.
- [173] M.D. Segall, P.J.D. Lindan, M.J. Probert, C.J. Pickard, P.J. Hasnip, S.J. Clark, and M.C. Payne. *Journal of Physics: Condensed Matter*, 14(11):2717, 2002.

- [174] P. E. Blöchl. *Physical Review B*, 50:17953, 1994.
- [175] G.K.H. Madsen, P. Blaha, K. Schwarz, E. Sjöstedt, and L Nordström. *Physical Review B*, 64(19):195134, 2001.
- [176] C. Rostgaard. arXiv e-print 0910.1921, 2009.
- [177] E. Ising. PhD thesis, Mathematisch-Naturwissenschaftliche Fakultät der Hamburgischen Universität, Hamburg, 1924.
- [178] J. W. D. Connolly and A. R. Williams. *Physical Review B*, 27(8):5169, 1983.
- [179] J. M. Sanchez, F. Ducastelle, and D. Gratias. *Physica A*, 128(1-2):334, 1984.
- [180] M. Asta, V. Ozolins, and C. Woodward. *JOM*, 53(9):16, 2001.
- [181] G. Ceder, A. Van der Ven, C. Marianetti, and D. Morgan. *Modelling and Simulation in Materials Science and Engineering*, 8(3):311, 2000.
- [182] F. Ducastelle. *Order and Phase Stability in Alloys, Volume 3*. North Holland; Amsterdam, 1991.
- [183] A. Zunger. First principles statistical mechanics of semiconductor alloys and intermetallic compounds. In P.E.A. Turchi and A. Gonis, editors, *NATO ASI on Statics and Dynamics of Alloy Phase Transformation*, volume 319, 361, Plenum Press; New York, 1994.
- [184] E. Ising. *Zeitschrift für Physik*, 31(1):253, 1925.
- [185] L. Onsager. *Physical Review*, 65:117, 1944.
- [186] W. Weidlich. *British Journal of Mathematical and Statistical Psychology*, 24(2):251, 2011.
- [187] R. Phillips. *Crystals, Defects and Microstructures: Modeling Across Scales*, Cambridge University Press; Cambridge 2001.

- [188] P. D. Tepesch, G. D. Garbulsky, and G. Ceder. *Physical Review Letters*, 74(12):2272, 1995.
- [189] M. Stone. *Journal of the Royal Statistical Society: Series B*, 36:111, 1974.
- [190] A. van de Walle, M. Asta, and G. Ceder. *Calphad*, 26(4):539, 2002.
- [191] A. van de Walle and G. Ceder. *Journal of Phase Equilibria*, 23:348, 2002.
- [192] K.-C. Li. *Annals of Statistics*, 15(3):958, 1987
- [193] D. Lerch, O. Wieckhorst, G. L. W. Hart, R. W. Forcade, and S. Müller. *Modelling and Simulation in Materials Science and Engineering*, 17(5):055003, 2009.
- [194] A. van de Walle. *Calphad*, 33(2):266, 2009.
- [195] X. Gonze, B. Amadon, P.-M. Anglade, J.-M. Beuken, F. Bottin, P. Boulanger, F. Bruneval, D. Caliste, R. Caracas, M. Côté, T. Deutsch, L. Genovese, P. Ghosez, M. Giantomassi, S. Goedecker, D.R. Hamann, P. Hermet, F. Jollet, G. Jomard, S. Leroux, M. Mancini, S. Mazevet, M.J.T. Oliveira, G. Onida, Y. Pouillon, T. Rangel, G.-M. Rignanese, D. Sangalli, R. Shaltaf, M. Torrent, M.J. Verstraete, G. Zerah, and J.W. Zwanziger. *Computer Physics Communications*, 180(12):2582, 2009.
- [196] J. D. Gale. *Journal of the Chemical Society, Faraday Transactions*, 93(4):629, 1997.
- [197] M. Chakraborty, J. Spitaler, P. Puschnig, and C. Ambrosch-Draxl. *Computer Physics Communications*, 181(5):913, 2010.
- [198] K. Schwarz and P. Blaha. *Computational Materials Science*, 28(2):259, 2003.

- [199] S. R. Bahn and K. W. Jacobsen. *Computing in Science and Engineering*, 4(3):56, 2002.
- [200] I.D. Brown and B. McMahon. *Acta Crystallographica. Section B*, 58(1):317, 2002.
- [201] R.W. Grosse-Kunstleve. *Acta Crystallographica. Section A*, 55(2):383, 1999.
- [202] S. Baroni, P. Giannozzi, and A. Testa. *Physical Review Letters*, 58(18):1861, 1987.
- [203] W. Frank, C. Elsässer, and M. Fähnle. *Physical Review Letters*, 74:1791, 1995.
- [204] A. Quong and B. Klein. *Physical Review B*, 46(17):10734, 1992.
- [205] J.D. Verhoeven. *Steel metallurgy for the non-metallurgist*. ASM International, Materials Park, Ohio, 2007.
- [206] N. Govind, M. Petersen, G. Fitzgerald, D. King-Smith, and J. Andzelm. *Computational Materials Science*, 28(2):250, 2003.
- [207] G. Murrieta, A. Tapia, and R. de Coss. *Carbon*, 42(4):771, 2004.
- [208] C. Cab, G. Murrieta, G. Canto, G. Oskam, and R. de Coss. *Carbon*, 47(7):1637, 2009.
- [209] M. Born. *Proceedings of the Cambridge Philosophical Society*, 36(02):160, 1940.
- [210] P. Řehák, M. Černý, and J. Pokluda. *Journal of Physics: Condensed Matter*, 24(21):215403, 2012.
- [211] M. J. Bucknum, E. A. Castro, and B. Wen. *Journal of Mathematical Chemistry*, 50(8):2281, 2012.

- [212] M. J. Bucknum and E. Castro. *Journal of Mathematical Chemistry*, 39(3):611, 2006.
- [213] M. J. Bucknum, B. Wen, and E. A. Castro. *Journal of Mathematical Chemistry*, 48(3):816, 2010.
- [214] H. J. Monkhorst and J. D. Pack. *Physical Review B*, 13(12):5188, 1976.
- [215] B. G. Pfrommer, M. Côté, S. G. Louie, and M. L. Cohen. *Journal of Computational Physics*, 131(1):233, 1997.
- [216] R. P. Feynman. *Physical Review*, 56:340, 1939.
- [217] G. J. Ackland, M. C. Warren, and S. J. Clark. *Journal of Physics: Condensed Matter*, 9(37):7861, 1997.
- [218] B. Wen, R. Melnik, S. Yao, and T. Li. *Chemical Physics Letters*, 516(46):230, 2011.
- [219] S.M. Jarkov, Ya.N. Titarenko, and G.N. Churilov. *Carbon*, 36(56):595, 1998.
- [220] I. Konyashin, V. Babaev, M. Guseva, V. Khvostov, N. Savtchenko, and M. Fatow. *Vacuum*, 66(2):175, 2002.
- [221] B. Wen, J. Zhao, T. Li, C. Dong, and J. Jin. *Diamond and Related Materials*, 15(9):1323, 2006.
- [222] L. G. Ferreira, S.-H. Wei, and A. Zunger. *International Journal of High Performance Computing Applications* 5(1):34, 1991.
- [223] G. Baldissin, N. M. Boag, C. C. Tang, and D. J. Bull. *European Journal of Inorganic Chemistry*, 2013(12):1993, 2013.
- [224] L. Bellaiche and D. Vanderbilt. *Physical Review B*, 61(12):7877, 2000.
- [225] F. Fuchs, C. Wild, K. Schwarz, W. Müller-Sebert, and P. Koidl. *Applied Physics Letters*, 66(2):177, 1995.

- [226] K. Iakoubovskii and G.J. Adriaenssens. *Diamond and Related Materials*, 11(1):125, 2002.
- [227] C. Glover, M. E. Newton, P. M. Martineau, S. Quinn, and D. J. Twitchen. *Physical Review Letters*, 92(13), 2004.
- [228] B. Winkler, M. T. Dove, and M. Leslie. *American Mineralogist*, 76(3-4):313, 1991.
- [229] J. S. Lin, A. Qteish, M. C. Payne, and V. Heine. *Physical Review B*, 47(8):4174, 1993.
- [230] K. M. Merz, R. Hoffmann, and A. T. Balaban. *Journal of the American Chemical Society*, 109(22):6742, 1987.
- [231] G. Kresse and J. Furthmüller. *Physical Review B*, 54(16):11169, 1996.
- [232] G. Kresse and D. Joubert. *Physical Review B*, 59(3):1758, 1999.
- [233] A. B. Alchagirov, J. P. Perdew, J. C. Boettger, R. C. Albers, and C. Fiolhais. *Physical Review B*, 63(22):224115, 2001.
- [234] I. Stamatina, A. Dumitru, V. Ciupina, G. Prodan, and A. Morozan. The effect of silicon in the synthesis of the tetragonal structures: silicon dicarbide and glitter. In *The American Carbon Society, CARBON Conference 2004: Novel Forms, Chemical Modified Carbons*, 2004.
- [235] P.E. Blöchl, O. Jepsen, and O.K. Andersen. *Physical Review B*, 49(23):16223, 1994.
- [236] M. Hubáček and T. Sato. *Journal of Solid State Chemistry*, 114(1):258, 1995.
- [237] A.V. Kurdyumov, V.L. Solozhenko, M. Gubachek, N.I. Borimchuk, V.B. Zelyavskii, N.F. Ostrovskaya, and V.V. Yarosh. *Powder Metallurgy and Metal Ceramics*, 39(9-10):467, 2000.

- [238] A. J. V. Marwitz, M. H. Matus, L. N. Zakharov, D. A. Dixon, and S.-Y. Liu. *Angewandte Chemie International Edition*, 48(5):973, 2009.
- [239] A. M. Glazer. *Journal of Applied Crystallography*, 42(6):1194, 2009.
- [240] V.M. Vishnyakov, A.P. Ehiasarian, V.V. Vishnyakov, P. Hovsepian, and J.S. Colligon. *Surface and Coatings Technology*, 206(1):149, 2011.
- [241] J. Kennedy and R. Eberhart. In , *IEEE International Conference on Neural Networks, 1995. Proceedings*, volume 4, 1942, 1995.
- [242] K. Kim and K. D. Jordan. *The Journal of Physical Chemistry*, 98(40):10089, 1994.
- [243] M. J. van Setten, M. A. Uijttewaal, G. A. de Wijs, and R. A. de Groot. *Journal of the American Chemical Society*, 129(9):2458, 2007.
- [244] H. Tang and S. Ismail-Beigi. *Physical Review Letters*, 99(11):115501, 2007.
- [245] H. Tang and S. Ismail-Beigi. *Physical Review B*, 82(11):115412, 2010.
- [246] X. Wu, J. Dai, Y. Zhao, Z. Zhuo, J. Yang, and X. C. Zeng. *ACS Nano*, 6(8):7443, 2012.
- [247] R. S. Mulliken. *The Journal of Chemical Physics*, 23(10):1833, 1955.
- [248] E. R. Davidson and S. Chakravorty. *Theoretica Chimica Acta*, 83(5-6):319, 1992.
- [249] M. D. Segall, R. Shah, C. J. Pickard, and M. C. Payne. *Physical Review B*, 54(23):16317, 1996.
- [250] Zhou, S. Y., Gweon, G.-H., Fedorov, A. V., First, P. N., Heer, W. A. d., Lee, D.-H., Guinea, F., Neto, A. H. C., and Lanzara, A. *Nature Materials* **6**(10), 770–775 (2007).
- [251] Cousins, C. S. G. *Physical Review B* **67**(2), 024107 January (2003).

- [252] V. V. Ivanovskaya, P. Wagner, A. Zobelli, I. Suarez-Martinez, A. Yaya, and C. P. Ewels. Graphene edge structures: Folding, scrolling, tubing, rippling and twisting. In Luca Ottaviano and Vittorio Morandi, editors, *GraphITA 2011*, Carbon Nanostructures, 75. Springer Berlin Heidelberg, 2012.
- [253] E.-Y. Choi, W. S. Choi, Y. B. Lee, and Y.-Y. Noh. *Nanotechnology*, 22(36):365601, 2011.
- [254] Y. Liu, V. I. Artyukhov, M. Liu, A. R. Harutyunyan, and B. I. Yakobson. *The Journal of Physical Chemistry Letters*, 4(10):1737, 2013.
- [255] A. I. Lebedev. *Physics of the solid state*, 51(2):362, 2009.
- [256] K. Masuda-Jindo, S. R. Nishitani, and V. Van Hung. *Physical Review B*, 70:184122, 2004.
- [257] K. Persson, M. Ekman, and V. Ozolins. *Physical Review B*, 61(17):11221, 2000.
- [258] P. Souvatzis, O. Eriksson, M. I. Katsnelson, and S. P. Rudin. *Physical Review Letters*, 100:095901, 2008.
- [259] E. G. Moroni, G. Grimvall, and T. Jarlborg. *Physical Review Letters*, 76:2758, 1996.
- [260] C. Zener. Influence of entropy on phase stabilization. In P.S. Rudman, J. Stringer, and R.I. Jaffee, editors, *Phase Stability in Metals and Alloys*, 25, McGraw-Hill; New York, 1967.